Modeling the formation and evolution of secondary organic aerosol during CalNex 2010

Final Report
Contract 11-305

Prepared for:

California Air Resources Board and the
California Environmental Protection Agency
Research Division
P.O. Box 2815
Sacramento, CA 95812

Prepared by:

Principal Investigator: Jose-Luis Jimenez
Researchers: Patrick L. Hayes, Amber M. Ortega, Zhe Peng

Department of Chemistry & Biochemistry and
Cooperative Institute for Research in Environmental Sciences
University of Colorado
Boulder, CO 80309-0216

20-Oct-2015

Disclaimer

The statements and conclusions in this Report are those of the contractor and not necessarily those of the California Air Resources Board. The mention of commercial products, their source, or their use in connection with material reported herein is not to be construed as actual or implied endorsement of such products.

Acknowledgements

The authors thank the California Air Resources Board (Contract 11-305) for supporting this work. The authors would like acknowledge the numerous scientists who are involved the CalNex research effort. The authors thank Chris J. Hennigan (UMBC) and Allen L. Robinson (CMU) for providing the naphthalene and methylnaphthalene data; John S. Holloway (NOAA) for providing CO data; Roya Bahreini (University of California-Riverside) and Ann M. Middlebrook (NOAA) for providing OA data from the NOAA P3; Phil Stevens' research group (Indiana University) for use of OH reactivity data; Stuart A. McKeen (NOAA), Chris Cappa (UC-Davis) and multiple members of the Jimenez Group at CU-Boulder and the AMS and PAM user communities for helpful discussions. We are grateful to Jochen Stutz (UCLA), John Seinfeld (Caltech), and Jason Surratt (UNC-Chapel Hill) for co-organization of the CalNex Supersite, and to CARB for supporting the infrastructure at the site.

This Report was submitted in fulfillment of ARB contract 11-305, "Modeling the formation and evolution of secondary organic aerosol during CalNex 2010", by the University of Colorado under the sponsorship of the California Air Resources Board. Work was completed as of Oct. 2015.

Table of Contents

List of Figures

List of Tables

Glossary of Terms, Abbreviations, and Symbols

ΔCO	Enhanced CO concentration over background concentration
AMS	High Resolution Time-of-Flight Aerosol Mass Spectrometer
BBOA	Biomass Burning Organic Aerosol
BG-SOA	Background SOA
Caltech	California Institute of Technology
CalNex	California Research at the Nexus of Air Quality and Climate Change field campaign
CIOA	Cooking-Influenced Organic Aerosol
EC	Elemental Carbon
f_{55}, f_{57}, f_{60}	Fraction of the total organic signal at *m/z* 55, *m/z* 57, and *m/z* 60, respectively
GC-MS	Gas Chromatography Mass Spectrometry
GRI	Grieshop et al. (2009) parameterization for secondary organic aerosol formation from P-S/IVOCs
H:C	Atomic (molar) hydrogen to carbon ratio of OA
HOA	Hydrocarbon-like Organic Aerosol
IVOC	Intermediate volatility organic compounds
LA	Los Angeles
LOA	Local Organic Aerosol
LV-OOA	Low Volatility Oxygenated Organic Aerosol
NEI	National Emissions Inventory
nr	Non-Refractory
OA	Organic Aerosol
OC	Organic Carbon
O:C	Atomic (molar) oxygen to carbon ratio of OA
ODR	Orthogonal Distance Regression
OFR	Oxidation Flow Reactor
OA:OC	Ratio of organic aerosol mass to organic carbon mass
O_x	Odd-Oxygen ($O_3 + NO_2$)
PACO	Pasadena Aerosol Characterization Observatory
PAH	Polycyclic aromatic hydrocarbon
PAM	Potential Aerosol Mass Flow Reactor
PBL	Planetary Boundary Layer
PILS-IC	Particle-into-Liquid Sampling and Ion Chromatography
PM_1, $PM_{2.5}$	Particulate matter below 1 μm and 2.5 μm size cuts, respectively.
PMF	Positive Matrix Factorization
POA	Primary Organic Aerosol
	Primary semi-volatile and intermediate volatility organic compounds
PToF	Particle Time-of-Flight
PYE	Pye and Seinfeld (2010) parameterization for secondary organic aerosols formation from P-S/IVOCs
RH	Relative Humidity
rBC	Refractory Black Carbon
ROB	Robinson et al. (2007) parameterization for secondary organic aerosol formation from P-S/IVOCs

SMPS	Scanning Mobility Particle Sizer
SI-SOA	Secondary organic aerosol from primary semi-volatile and intermediate volatility organic compounds
SOA	Secondary Organic Aerosol
SOAR	Study of Organic Aerosol at Riverside Campaign
SVOC	Semi-volatile organic compounds
SP2	Single Particle Soot Photometer
SP-AMS	Soot Particle Aerosol Mass Spectrometer
SV-OOA	Semi-Volatile Oxygenated Organic Aerosol
TSI	Tsimpidi et al. (2010) parameterization for secondary organic aerosol formation from VOCs
UHSAS	Ultra-High Sensitivity Aerosol Spectrometer
VBS	Volatility basis set
VMT	Vehicle Miles Traveled
VOCs	Volatile organic compounds
V-SOA	Secondary organic aerosol formed from the oxidation of volatile organic compounds
WRF-CMAQ	Weather Research Forecasting – Community multiscale air quality model

Abstract

Field studies in polluted areas over the last decade have observed large formation of secondary organic aerosol (SOA) that is often poorly captured by models. Four parameterizations for urban secondary organic aerosol (SOA), frequently used in 3D models, are evaluated using a box model representing the Los Angeles Region during the CalNex 2010 field campaign. The model SOA formed only from the oxidation of VOCs (V-SOA) is insufficient to explain the observed SOA, even with parameterizations with multi-generation oxidation that produce much higher yields than have been observed in chamber experiments, or with increased yields to their upper limit estimates accounting for recently reported losses of vapors to chamber walls. The Community Multiscale Air Quality (WRF-CMAQ) model (v.5.0.1) underestimates the observed SOA mass by a factor of 25, which is consistent with many previous model-measurement comparisons for pre-2007 anthropogenic SOA modules in urban areas. Including SOA from primary semi-volatile and intermediate volatility organic compounds (P-S/IVOCs) improves model/measurement agreement for mass concentration. The results from 3 parameterizations show large differences and are not well constrained, underscoring the current uncertainties in this area. Our results strongly suggest that other precursors besides VOCs, such as P-S/IVOCs, are needed to explain the observed SOA concentrations in Pasadena. All the recent parameterizations over-predict urban SOA formation at long photochemical ages (~3 days). Reducing IVOC emissions by one-half in the model to better match recent IVOC measurements improves SOA predictions at these long photochemical ages. Measured polycyclic aromatic hydrocarbons (naphthalenes) contribute 0.7% of the modeled SOA mass. The amounts of SOA mass from diesel vehicles, gasoline vehicles, and cooking emissions are estimated to be 16 – 27%, 35 – 61%, and 19 – 35%, respectively, consistent with the observed fossil fraction of urban SOA, 71(±3)%. In-basin biogenic VOCs are predicted to contribute only a few percent to SOA, while there is likely a substantial contribution from regional biogenic SOA to the OA background. The percentage of SOA from diesel vehicle emissions is consistent with previous studies of the weekly cycle. However, the modeling work presented here suggests a strong anthropogenic source of modern carbon in SOA, due to cooking emissions, which was not accounted for in those previous studies, and which is higher on weekends. A simple two-parameter model successfully predicts SOA concentration, and the optimal parameter combination is very similar to that for Mexico City. This approach provides a computationally inexpensive method for predicting urban SOA.

An Oxidation Flow Reactor (OFR) was also deployed during CalNex. The reactor achieved equivalent atmospheric aging from hours up to several weeks. Enhancement of OA from aging showed a maximum net SOA production between 0.8–6 days of aging with net OA mass loss beyond 2 weeks. Reactor SOA mass peaked at night, in the absence of ambient photochemistry and correlated with trimethylbenzene concentrations. Reactor SOA formation was inversely correlated with ambient SOA and O_x, which along with the short-lived VOC correlation, indicates the importance of relatively reactive (τ_{OH} ~0.3 day) SOA precursors in the LA-Basin. Evolution of the elemental composition in the reactor was similar to trends observed in the atmosphere (O:C vs. H:C slope ~ -0.65). The ratio of OA in the reactor output to excess CO (ΔCO, ambient CO above regional background) vs. photochemical age is similar to previous studies at low to moderate ages and also extends to higher ages where OA loss dominates. A comparison of urban SOA formation in this study with a similar study of vehicle SOA in a tunnel supports the dominance of vehicle emissions in urban SOA. Pre-2007 SOA models underpredict SOA formation by an order of magnitude, while a more recent model performs better but overpredicts at higher ages.

Executive Summary

Background. Atmospheric aerosols (i.e., particulate matter or PM) have been the subject of intensive ongoing research due to their important impact on the radiative forcing of climate, which occurs through several mechanisms including the scattering and absorption of solar radiation as well as the alteration of the formation and properties of clouds. In addition, atmospheric aerosols reduce visibility and increase cardiac and respiratory disease in humans. The impact of aerosols on climate, the environment, and human health is determined, in part, by particle size and chemical composition. In many environments, including California, a large fraction (~50%) of the submicron aerosol mass in the lower portion of the atmosphere (i.e., the troposphere) is organic aerosol (OA). The sources, composition, and chemical processing of OA are not well understood, however. Generally, OA is comprised of thousands of individual compounds that are either directly emitted into the atmosphere ('primary' OA or 'POA') or are formed though chemical reactions involving gas phase precursors ('secondary' OA or 'SOA'). The multiple sources and complexity of molecular composition represent major challenges for understanding and prediction of SOA properties. Modeling studies of urban SOA using older models resulted in large underpredictions of the observed concentrations. More recent attempts predict higher concentrations of the order of those observed, but it is unclear if this is for the right reasons.

Methods. The California Research at the Nexus of Air Quality and Climate Change (CalNex) field campaign was conducted in Spring 2010, and was a multi-institution effort to address outstanding scientific questions regarding air quality and pollution over the state of California. A major scientific goal for CalNex was to improve scientific understanding of atmospheric aerosols in California, and specifically, characterize important SOA precursors and formation pathways. For CalNex the Pasadena ground site was uniquely equipped to characterize aerosols, and especially, organic aerosols. This report presents two complementary analyses aimed to quantitatively understand SOA formation in the LA Basin during CalNex. To achieve these goals the following approach is utilized: (1) Four parameterizations for urban secondary organic aerosol (SOA) frequently used in 3D models are evaluated using a box model representing the Los Angeles Region during the CalNex 2010 field campaign. We constrain the model predictions with measurements from several platforms and compare predictions with particle and gas-phase observations from the CalNex Pasadena ground site. That site provides a unique opportunity to study aerosol formation close to anthropogenic emission sources with limited recirculation. (2) A simple two-parameter model is adapted to predict SOA concentration and O/C from urban emissions. (3) An Oxidation Flow Reactor (OFR) was deployed to study SOA formation in real-time during the CalNex campaign in Pasadena, CA, in 2010. A high-resolution aerosol mass spectrometer (AMS) and a scanning mobility particle sizer (SMPS) alternated sampling ambient and reactor-aged air. The reactor produced OH concentrations up to 4 orders of magnitude higher than in ambient air, achieving equivalent atmospheric aging from hours up to several weeks in 3 minutes of processing. OH radical concentration was continuously stepped, obtaining measurements of real-time SOA formation and oxidation at multiple equivalent ages from 0.8 days–6.4 weeks of age. The OFR are extensively analyzed and compared to the models from approaches (1) and (2).

Results and Conclusions. The model SOA formed only from the oxidation of VOCs (V-SOA) is insufficient to explain the observed SOA concentrations, even when using SOA

parameterizations with multi-generation oxidation that produce much higher yields than have been observed in chamber experiments, or when increasing yields to their upper limit estimates accounting for recently reported losses of vapors to chamber walls. The Community Multiscale Air Quality (WRF-CMAQ) model (version 5.0.1) provides excellent predictions of secondary inorganic particle species but underestimates the observed SOA mass by a factor of 25 when an older VOC-only parameterization is used, which is consistent with many previous model-measurement comparisons for pre-2007 anthropogenic SOA modules in urban areas. Including SOA from primary semi-volatile and intermediate volatility organic compounds (P-S/IVOCs) improves model/measurement agreement for mass concentration. Our results strongly suggest that other precursors besides VOCs, such as P-S/IVOCs, are needed to explain the observed SOA concentrations in Pasadena. The results from the 3 parameterizations show large differences (e.g. a factor of 3 in SOA mass) and are not well constrained, underscoring the current uncertainties in this area. All the recent parameterizations over-predict urban SOA formation at long photochemical ages (~3 days) compared to observations from multiple sites, which can lead to problems in regional and especially global modeling. However, reducing IVOC emissions by one-half in the model to better match recent IVOC measurements improves SOA predictions at these long photochemical ages.

The amounts of SOA mass from diesel vehicles, gasoline vehicles, and cooking emissions are estimated to be 16 – 27%, 35 – 61%, and 19 – 35%, respectively, depending on the parameterization used, which is consistent with the observed fossil fraction of urban SOA, 71(±3)%. The relative contribution of each source is uncertain by almost a factor of 2 depending on the parameterization used. In-basin biogenic VOCs are predicted to contribute only a few percent to SOA. A regional SOA background of approximately 2.1 $\mu g\ m^{-3}$ is also present due to the long distance transport of highly aged OA, likely with a substantial contribution from regional biogenic SOA. The percentage of SOA from diesel vehicle emissions is the same, within the estimated uncertainty, as reported in previous work that analyzed the weekly cycles in OA concentrations. However, the modeling work presented here suggests a strong anthropogenic source of modern carbon in SOA, due to cooking emissions, which was not accounted for in those previous studies, and which is higher on weekends. The simplified 2-parameter model successfully predicts SOA concentration, and provides a computationally inexpensive method for predicting urban SOA in global and climate models.

Enhancement of OA from OFR aging showed a maximum net SOA production between 0.8–6 days of aging with net OA mass loss beyond 2 weeks. Reactor SOA mass peaked at night, in the absence of ambient photochemistry and correlated with trimethylbenzene concentrations. Reactor SOA formation was inversely correlated with ambient SOA and O_x, which along with the short-lived VOC correlation, indicates the importance of relatively reactive (τ_{OH} ~0.3 day) SOA precursors in the LA-Basin. Evolution of the elemental composition in the reactor was similar to trends observed in the atmosphere (O:C vs. H:C slope ~ -0.65). The ratio of OA in the reactor output to excess CO (ΔCO, ambient CO above regional background) vs. photochemical age is similar to previous studies at low to moderate ages and also extends to higher ages where OA loss dominates. A comparison of urban SOA formation in this study with a similar study of vehicle SOA in a tunnel supports the dominance of vehicle emissions in urban SOA. Pre-2007 SOA models underpredict SOA formation by an order of magnitude, while a more recent model performs better but overpredicts at higher ages. These results demonstrate the value of the reactor as a tool for *in situ* evaluation of the SOA formation potential and OA evolution from ambient air.

1. Introduction

Submicron aerosols impact regional to global climate (IPCC, 2013), visibility (Watson, 2002), and human health (Dockery and Pope, 1994). Quantification of the environmental and health impacts of atmospheric aerosols is difficult however, because of our incomplete understanding of aerosol physical and chemical properties. Atmospheric aerosols are typically a mixture of organic and inorganic matter, and the organic fraction is normally composed of hundreds or even thousands of compounds. Due to this complexity, accurate prediction of OA concentrations, as well as chemical properties is challenging (McKeen et al., 2007; Heald et al., 2011; Spracklen et al., 2011). This problem is especially important given that OA represents roughly half of the total tropospheric submicron aerosol mass in many environments including polluted urban regions (Murphy et al., 2006; Jimenez et al., 2009).

Given its complexity, OA is often categorized based on sources. Primary organic aerosols (POA) are emitted directly into the atmosphere from sources such as motor vehicles, food cooking, and wildfires. SOA is formed in the atmosphere by photooxidation and/or heterogeneous or cloud processing of gas-phase precursors. The gas-phase precursors for SOA potentially have many sources including vehicle emissions, the biosphere, biomass burning, and food cooking (e.g. Schauer et al., 1999; Hallquist et al., 2009; Hodzic et al., 2010b; Bahreini et al., 2012). A large portion of the submicron OA throughout the world can be classified as SOA (Zhang et al., 2007; Jimenez et al., 2009). Even in urban areas such as the Los Angeles Metropolitan Area, SOA is often found to be larger than POA, especially in the summer (Docherty et al., 2008; Hersey et al., 2011; Hayes et al., 2013).

Due to meteorological conditions (e.g. diurnal fluctuations in land-sea breeze patterns with weak synoptic forcing) and topography (e.g. the surrounding coastal mountain ranges) ventilation of air in the LA-Basin can be limited, historically resulting in high pollution levels. Several field campaigns have investigated SOA in the LA-Basin, including the 2005 Study of Organic Aerosol at Riverside (SOAR; Docherty et al., 2011) and the 2009 Pasadena Aerosol Characterization Observatory (PACO; Hersey et al., 2011). These studies identified SOA as a major fraction of total OA in the LA Basin in the summer, consistent with findings in previous urban field campaigns (Volkamer et al., 2006; de Gouw and Jimenez, 2009). This situation is in contrast to previous studies in this region which reported that primary OA was higher than SOA, other than during severe photochemical smog episodes; however, these estimates were likely affected by apportionment biases or the greatly underestimated SOA production of traditional models (Docherty et al., 2008). The 2010 California Research at the Nexus of Air Quality and Climate Change (CalNex) was a multiplatform large-scale field study, which utilized ground sites at Bakersfield and Pasadena, California, NOAA WP-3D and Twin Otter aircraft, and the research ship R/V Atlantis (Ryerson et al., 2013).

Traditional models for SOA formation use a semi-empirical approach wherein SOA formation is described in two steps: the gas-phase oxidation of VOC precursors resulting in the formation of semi-volatile organic compounds (SVOCs), followed by partitioning of the SVOCs to the particle phase. The parameters for these models (yields, saturation concentrations, etc.) are typically derived from smog chamber experiments on individual VOCs (Hallquist et al., 2009). Since about 2005, it has been shown in multiple publications from several field studies that traditional models under-predict observed SOA in urban areas by a large amount with a difference of up to a factor of 19. (Volkamer et al., 2006; de Gouw and Jimenez, 2009; Dzepina

et al., 2009; Hodzic et al., 2010a). A similarly large underestimate is typically not observed in areas dominated by biogenic SOA (Tunved et al., 2006; Chen et al., 2009; Hodzic et al., 2009; Slowik et al., 2010). In response, new precursors and pathways for SOA formation have been identified from measurements and incorporated into SOA models. The new formation pathways include SOA formation from primary semivolatile and intermediate volatility organic compounds (P-S/IVOCs) (Robinson et al., 2007), aqueous phase production in clouds (e.g. Lim et al., 2005) and aerosols (Ervens and Volkamer, 2010; Knote et al., 2014b), as well as the oxidation of VOCs such as isoprene, benzene, and acetylene that were previously thought to produce little or no SOA (Martin-Reviejo and Wirtz, 2005; Kroll et al., 2006; Volkamer et al., 2009).

The introduction of the volatility basis set (VBS) approach represents a conceptual advance for modeling OA (Donahue et al., 2006). This approach distributes organic species into logarithmically spaced volatility bins, which are used to calculate absorptive partitioning between the gas and particle-phases. Mass is transferred between the bins as photochemical oxidation proceeds and environmental parameters (i.e. temperature, dilution) change. The VBS approach has been applied to SOA from biogenic and anthropogenic VOCs as well as to P-S/IVOCs and the SOA formed from them (Robinson et al., 2007; Tsimpidi et al., 2010).

Although these updates have led to substantial reductions in the gaps between observed and predicted OA concentrations, major inconsistencies and uncertainties remain, and it is not clear that improved agreement is achieved for the right reasons. For instance, both Dzepina et al. (2011) and Hodzic et al. (2010a) reported that the Robinson et al. (2007) parameterization for the production of SOA from P-S/IVOCs contributed substantially to successful predictions of SOA concentration in a box and a regional model for the Mexico City region, but the predicted O/C values were approximately a factor of 2 too low. A different parameterization of SOA from P-S/IVOCs published by Grieshop et al. (2009) led to overpredicted total SOA concentration, but successfully reproduced the measured O/C values.

Complicating the picture further was the additional finding in Dzepina et al. (2011) that if the VBS with multi-generational aging was applied to VOCs following Tsimpidi et al. (2010), then all the SOA mass could be successfully predicted without considering P-S/IVOCs. A similar finding was observed in Tsimpidi et al. (2010) wherein the inclusion of P-S/IVOCs and an "aging VBS" treatment of VOC oxidation worsened over-prediction in the model during the afternoon. Thus, the relative importance of P-S/IVOCs versus VOCs in urban SOA production remains very uncertain. More generally, robust model/measurement closure – in which SOA chemistry is accurately represented – is an important step towards implementing effective particulate matter pollution controls in urban areas.

In order to characterize the SOA formation potential of urban emissions, an experimental technique is needed that is capable of rapid operation to allow examination of the variable potential of changing air masses. The "Potential Aerosol Mass" (PAM) oxidation flow reactor (OFR), was developed by Kang et al., (2007; 2011), and used in many laboratory experiments and recent field studies. It is a small flow reactor that exposes air samples to high oxidant levels (100-10,000 times atmospheric concentrations) with short residence time (<5 min). Recent work with the reactor has examined SOA yield, oxidation, and physicochemical changes using single precursors or simple mixtures in laboratory experiments, producing results similar to environmental chamber experiments (Massoli et al., 2010; Kang et al., 2011; Lambe et al.,

2011a; Lambe et al., 2011b; Bruns et al., 2015). SOA yields in the reactor are comparable or somewhat lower than for similar OH exposures in large environmental chambers, which has been suggested to be due to the short residence time of the reactor not being sufficient to allow complete condensation of semivolatiles (Lambe et al., 2015) or increased wall losses of gas-phase species due to the higher surface area to volume ratios of the reactor (Bruns et al., 2015). OH oxidation of alkane SOA precursors in the reactor show the effect of functionalization (oxygen addition) and fragmentation (carbon loss) reactions (Lambe et al., 2012). Recent reactor application to aging of biomass burning smoke showed that total OA after reactor oxidation was on average 1.42±0.36 times the initial primary OA (POA) with similar aging of biomass burning tracers to that observed in aircraft measurements (Cubison et al., 2011; Ortega et al., 2013). Aging measurements of vehicular exhaust using the reactor in a highway tunnel in Pittsburgh, PA indicated peak SOA production after 2.5 days of atmospheric equivalent photochemical aging (at OH = $3\sim10^6$ molec cm^{-3}) and concluded the chemical evolution of the OA inside the reactor appears to be similar to that observed in the atmosphere (Tkacik et al., 2014). Other studies also show that the reactor produces SOA with characteristics similar to that formed in the atmosphere for crude oil evaporation (Bahreini et al., 2012a; Li et al., 2013). The radical chemistry in the reactor has been recently characterized (Li et al., 2015; Peng et al., 2015). Thus, the reactor is useful for elucidating SOA formation processes under field conditions where utilizing large-scale environmental chambers is not practical and/or if higher aging is targeted.

Here we compare the results of a constrained SOA box model against measurements carried out at the Pasadena ground site during the California Research at the Nexus of Air Quality and Climate Change (CalNex) campaign. The use of a box model allows multiple state-of-the-art parameterizations to be tested. Once constrained by measurements, the box model facilitates the improved source apportionment of SOA in the Los Angeles Metropolitan Area. In particular, the amount of SOA formed from different precursors is quantitatively evaluated. The importance of diesel versus gasoline emissions as sources of SOA precursors – a topic that has received much recent interest – is discussed as well (Bahreini et al., 2012; Gentner et al., 2012; Hayes et al., 2013; Ensberg et al., 2014). Results are also compared to those of the 3-D WRF-CMAQ model. The CalNex field campaign, which took place in Spring/Summer 2010, provides a unique data set for evaluating gas-phase SOA models because of, in part, the large scope of the campaign, and the generally clear-sky conditions during the campaign that limited the effects of cloud chemistry. Specifically at the Pasadena ground site, which operated from May 15 2010 to June 15 2010, there were over 70 gas and particle phase measurements including cutting-edge techniques that provide new insights into SOA sources and chemistry. For example, highly time resolved 14C measurements with 3 – 4 h resolution are utilized in this work, whereas typically 12 h or lower resolution has been reported (Zotter et al., 2014). By comparing the CalNex dataset to recently proposed SOA models, the research described below aims to evaluate recently proposed SOA models and assess the importance of different SOA sources and formation pathways. During CalNex we measured submicron aerosol size and composition alternately for ambient air and for ambient air that had been aged in an oxidation flow reactor by systematically changing the OH exposure. This work is compared to the previous literature but extends beyond it with the new information provided by the in situ aging studies. By combining results from the ambient aerosol and aged ambient aerosol measurements, we provide a stronger test of current SOA models.

2. Materials and Methods

2.1. CalNex Field Campaign

The work in this study will focus on measurements from the Pasadena ground site during CalNex. The Pasadena site was located on the California Institute of Technology (Caltech) campus in Pasadena, CA (34.1406 N, 118.1225 W, 236 m above mean sea level); the location, airmass transport, and key measurements have been described in detail previously (Washenfelder et al., 2011; Hayes et al., 2013). The measurement period for our reactor study is 29 May–10 June 2010, hereafter referred to as the "sampling period." Meteorological conditions, including prevailing winds, boundary layer height, temperature, and relative humidity information are summarized by Washenfelder et al. (2011) and Hayes et al. (2013). Briefly, the site was located in the Caltech campus about 18 km northeast of downtown Los Angeles (34.1406 N, 118.1225 W). Pasadena lies within the South Coast Air Basin (SoCAB) and the Los Angeles metropolitan area. The prevailing wind direction during daytime in Pasadena was from the southwest, which brought air masses from the Santa Monica and San Pedro bays through Los Angeles to Pasadena. Thus, Pasadena during the daytime is predominately a receptor site for pollution emitted in the western Los Angeles metropolitan area that is then advected over a period of several hours (about 3 – 5 h). While more local emissions and background concentrations of atmospheric species must influence the site, the diurnal cycles of many primary species with anthropogenic sources (e.g. CO, black carbon (BC), and benzene) appear to be dominated by advection of pollution from the southwest. Specifically, CO, BC, and benzene concentrations display strong peaks around noontime as shown in Figure 2 of Hayes et al. (2013), which is due to a transport time of several hours until the emissions from the morning rush hour arrive in Pasadena. At nighttime, winds were weak and were most frequently from the southwest or southeast, which is illustrated in Hayes et al. (2013). The site was influenced at that time by more local emissions than by advection from downtown Los Angeles. Aged emissions from the prior daytime may have influenced the site as well during nighttime. An overview of the 2010 CalNex field campaign (Ryerson et al., 2013) and aerosol observations at the Pasadena Supersite (Hayes et al., 2013) can be found in previous publications. A gas-chromatography mass spectrometer (GC-MS) from NOAA was located at the same field site (Hayes et al., 2013; Warneke et al., 2013) and used for VOC measurements reported in this study. The NOAA WP-3D research aircraft sampled in situ meteorological, trace gas, and aerosol conditions aloft during CalNex (Bahreini et al., 2012b; Ryerson et al., 2013). Non-refractory submicron aerosol composition measurements aboard the NOAA WP-3D were made using an Aerodyne compact time-of-flight aerosol mass spectrometer (C-ToF-AMS, Drewnick et al., 2005). Details of operation, analysis, and quantification can be found in Bahreini et al. (2012b).

2.2. SOA box model

The models in this work are summarized in Table 1. The box model used here accounts for SOA formed from gas-phase oxidation of two sets of precursors: (1) VOCs (producing V-SOA), and (2) P-S/IVOCs (producing SI-SOA). Also included in the total model SOA is background SOA (BG-SOA), with a constant concentration of 2.1 $\mu g\ m^{-3}$ that is derived from observations as described later in Section 2.4. BG-SOA is considered non-volatile in the model, which is consistent with observations that very aged SOA has low volatility (Cappa and Jimenez, 2010). For the remainder of the SOA the equilibrium partitioning between the particle and gas-phases is calculated using the reformulation of Pankow Theory by Donahue et al. (2006). The particle-phase

fraction of species *i*, ξ_i, is calculated using its effective saturation concentration, C_i^*, and the total concentration of the organic material available for partitioning, *[OA]*.

$$\xi_i = \left(1 + \frac{C_i^*}{[OA]}\right)^{-1} \; ; \; [OA] = \sum_i [SVOC]_i \, \xi_i \qquad (1)$$

We note that there is ongoing scientific research examining if OA adopts a liquid or solid/glassy phase with potentially slow diffusion properties, and the conditions that result in equilibrium or kinetically-limited partitioning are not yet clear (e.g. Cappa and Wilson, 2011; Perraud et al., 2012). For the purpose of this study however, field measurements from CalNex strongly suggest that organic aerosols undergo equilibrium partitioning in Pasadena (Zhang et al., 2012). In particular, for water-soluble organic carbon, a surrogate for SOA, the partitioning coefficient was observed to be correlated with the OA mass. A similar observation was made at a rural site in Colorado, USA, and the lack of kinetic limitations to equilibrium may be attributable to the higher ambient relative humidity, mostly greater than 30%, in both Pasadena and Colorado compared to some studies that have reported kinetic limitations (Yatavelli et al., 2014). Furthermore, we note that the diurnally averaged relative humidity in Pasadena was always greater than 60%, which laboratory studies have suggested is above the ~30% threshold where particles form liquid phases (Renbaum-Wolff et al., 2013).

V-SOA in the box model includes products from the oxidation of 46 VOCs, and the V-SOA mass is distributed into a 4-bin VBS as shown Figure 1 (C^*=1, 10, 100, or 1000 μg m^{-3}). Furthermore, a Table with the names of each VOC as well as the relevant model parameters is provided in the Appendix A (Table A-1). The reaction rates for most of the VOCs are taken from Atkinson and Arey (2003) and, when not available there, Carter (2010). Three terpene compounds (α-pinene, β-pinene, and limonene) were lumped for this model, and the rate constant of this lumped precursor species is the weighted average – by ambient concentrations – of the individual rate constants (Atkinson and Arey, 2003). In addition, the rates for naphthalene, 1-methylnaphthalene, and 2-methylnaphthalene oxidation are taken from Chan et al. (2009). The SOA yields for the VOCs are taken from Tsimpidi et al. (2010). For naphthalene and the methylnaphthalenes the yields are from data presented in Chan et al. (2009), which have been re-fitted to obtain yields for the 4-bin VBS utilized in this work. V-SOA is also allowed to 'age' after the initial reaction, and the subsequent gas-phase oxidation (with a rate constant of 10^{-11} cm^3 $molec.^{-1}$ s^{-1}, which was erroneously reported as 4 times higher in Tsimpidi et al. (2010)) leads to a 10× decrease in volatility as well as a 7.5% increase in mass due to added oxygen for each generation. This parameterization for V-SOA is abbreviated as "TSI" in the text.

It is possible that the SOA yields used for V-SOA, which are based on the chamber experiment literature, are several-fold too low due to, for example, losses of gas-phase species to chamber walls (Matsunaga and Ziemann, 2010; Zhang et al., 2014). To investigate this possibility a model variation – named "4xV" – is run wherein the SOA yields from aromatics are increased by a factor of four, based on recent chamber studies in which higher concentrations of aerosol seed were utilized in order to suppress losses to chamber walls, and an upper limit of a factor of 4 increase in V-SOA yields was estimated (Zhang et al., 2014). The multi-generation aging of secondary species produced from VOCs is turned off in this variation, since otherwise the SOA yields would reach extremely unrealistic levels (~400%).

SOA from P-S/IVOCs (SI-SOA) is simulated utilizing three different parameter sets. No duplication of precursors is expected between the Tsimpidi et al. (2010) parameterization and the three P-S/IVOCs parameterizations, with the possible exception of the naphthalenes (Robinson et al., 2007; Dzepina et al., 2009; Dzepina et al., 2011). However, since the naphthalenes contribute a very small amount to the total SOA mass (see below), the impact of double-counting their SOA contribution is negligible. The first two P-S/IVOCs parameterizations are from Robinson et al. (2007), hereinafter "ROB", and an alternate set published by Grieshop et al. (2009), hereinafter "GRI". The differences between the two parameterizations are highlighted in Figure 1. When compared to ROB, primary and secondary species in GRI have a lower gas-phase reactivity (2×10^{-11} versus 4×10^{-11} cm^3 $molec^{-1}$ s^{-1}), a larger decrease in volatility per oxidation step (two orders of magnitude versus one), and more oxygen mass added to the products (40% versus 7.5% of the precursor mass). Furthermore, there are differences in the assumed enthalpies of vaporization, ΔH_{vap}, and molecular weights. Details of both parameterizations are given in Table A-2 in Appendix A.

The third parameterization utilized for SI-SOA is that published by Pye and Seinfeld (2010), hereinafter "PYE", which is also illustrated in Figure 1. In PYE the SOA from primary SVOCs and primary IVOCs follow different treatments. The primary SVOCs emitted are represented by two lumped species with C^*=20 and 1646 μg m^{-3} and relative concentrations of 0.51 and 0.49, respectively. The gas phase reactivity (2×10^{-11} cm^3 $molec^{-1}$ s^{-1}) and decrease in volatility per oxidation step (two orders of magnitude) are identical to GRI. However, only one oxidation step is allowed in PYE. The oxygen mass added to the products is 50% of the precursor mass, which is higher than that for ROB and GRI. Another difference in PYE is the enthalpy of vaporization for all organic species, which is 42 kJ/mol. Lastly, the molecular weight utilized here is 250 g mol^{-1}, the same as ROB, although this parameter is not specified in Pye and Seinfeld (2010). In PYE also the concentration of SOA from primary IVOCs is estimated by scaling-up the concentration of SOA from naphthalene by a factor of 66.

Heterogeneous uptake of glyoxal onto aerosols can be a relevant source of SOA under some conditions (Volkamer et al., 2007; Dzepina et al., 2009). Previously published work on the glyoxal budget for CalNex indicates that this compound contributes only a small fraction of the SOA mass in the LA basin, however (Washenfelder et al., 2011; Knote et al., 2014b), and we do not consider it further in this study. In Pasadena, the urban SOA peaked in the afternoons, which were generally clear and sunny during the campaign. This observation is consistent with the conclusion that reactions occurring in clouds did not play a major role in SOA production during CalNex. In addition, a comparison of OA/ΔCO for three days that were cloudy against the remainder of the campaign shows no apparent difference in the magnitude of the ratio or its evolution with photochemical age (Figure 2), which further supports the conclusion that SOA production from clouds can be neglected in this study.

The design of the model used here includes several more elements that are general for V-SOA and SI-SOA. Only oxidation by hydroxyl radical (•OH) is considered since in urban regions other oxidants such as ozone, nitrate radical, and chlorine radical are expected to be minor contributors to SOA formation from urban VOCs (Dzepina et al., 2009; Dzepina et al., 2011; Hayes et al., 2013). Additionally, the model is run using "high-NO_x conditions," which is consistent with previously calculated branching ratios for the RO_2 + NO, RO_2 + HO_2, and RO_2 + RO_2 reactions (Hayes et al., 2013) and the dominance of the RO_2 + NO pathway. The primary and secondary species are assumed to mix into a single organic phase. This assumption is based on

observations made off the coast of California that SOA condenses on primary particles (e.g., BC and POA) as indicated by the similar size distributions for these species across a range of photochemical ages (Cappa et al., 2012). In addition, the organic phase is taken to be separate from the inorganic phases, which is consistent with the relatively low O:C values observed during CalNex (Hayes et al., 2013) and previous studies demonstrating that organic/inorganic phase separation occurs when O:C is less than 0.7 (Bertram et al., 2011). It should be noted that this statement holds true even after applying the updated calibration for AMS O:C (Canagaratna et al., 2015).

The temperature dependence of C^* is calculated with the Clausius-Clapeyron equation.

$$C_i^* = C_{i,o}^* \frac{T_0}{T} \exp\left[\frac{\Delta H_{vap}}{R}\left(\frac{1}{T_o} - \frac{1}{T}\right)\right] \quad (2)$$

Where $C_{i,o}^*$ is the effective saturation concentration of condensable compound i at the reference temperature T_o (K), and R is the ideal gas constant. The ambient temperature, T, was taken to be 18°C, which represents the average campaign temperature during CalNex. A sensitivity test exhibited less than a 4% change in predicted mass at a given time-of-day when using 14°C and 24°C, which are the minimum and maximum temperatures for the diurnal cycle. The error in predicted mass over this temperature range is small compared to other uncertainties in SOA modeling, and therefore the use of a constant temperature of 18°C to calculate C^* should introduce negligible errors.

Table 1. *Summary of the SOA models and their major variants used in this work.*

Model Name	Variation	Notes	References	Figures
Box Model	1 (ROB + TSI)	VOCs: Tsimpidi et al. parameterization with aging. P-S/IVOCs: Robinson et al. parameterization, and all SOA treated within VBS framework.	Tsimpidi et al. *Atmos. Chem. Phys.* 2010, 525-546. Robinson et al. *Science* 2007, 1259-1262.	4,11,12,14,15,16, 17,18,23
	2 (GRI + TSI)	VOCs: Tsimpidi et al. parameterization with aging. P-S/IVOCs: Grieshop et al. parameterization, and all SOA treated within VBS framework.	Tsimpidi et al. *Atmos. Chem. Phys.* 2010, 525-546. Grieshop et al. *Atmos. Chem. Phys.* 2009, 1263-1277.	4,11,12,13,14,15, 16,17,18,23

	3 (PYE + TSI)	VOCs: Tsimpidi et al. parameterization with aging. P-S/IVOCs: Pye and Seinfeld parameterization.	Tsimpidi et al. *Atmos. Chem. Phys.* 2010, 525-546. Pye and Seinfeld *Atmos. Chem. Phys.* 2010, 4377-4401.	4,11,12,14,15,16, 17,18
	4 (ROB + 4xV)	VOCs: Tsimpidi et al. parameterization without aging and aromatic yield multiplied by 4. P-S/IVOCs: Robinson et al. parameterization, and all SOA treated within VBS framework.	Tsimpidi et al. *Atmos. Chem. Phys.* 2010, 525-546. Robinson et al. *Science* 2007, 1259-1262. Zhang et al. *PNAS* 2014.	11,12,14,15.16,1 7,18
	5	VOCs: Koo et al. and Ng et al. wherein SOA is treated in a lumped product parameterization.	Koo et al. *Atmos. Environ.* 2003, 4757-4768. Ng et al. *Atmos. Chem. Phys.* 2007, 3909-3922.	17
WRF-CMAQ	v5.0.1	4 anthropogenic VOC and 3 biogenic VOC precursors and GLY/MGLY. 12 semi-volatile partitioning species and 7 non-volatile SOA species	Carlton et al. *Environ. Sci. Technol.* 2010, 8553-8560.	19,20,21,22
SIMPLE	N/A	Single lumped precursor and single lumped, non-volatile SOA product.	Hodzic et al. *Geosci. Model Dev.* 2011, 901-917.	16,17,24,25
WRF-Chem	N/A	4-bin VBS framework with aging, 7 anthropogenic VOC classes and 4 biogenic VOC classes	Ahmadov et al. *J. Geophys. Res.-Atmos.* 2012, D06301.	6,7

Figure 1. *Schematic of the major SOA parameterizations used in the box model. The different regions of the volatility scale are indicated on the top axis: low-volatility organic compounds (LVOCs), semi-volatile organic compounds (SVOCs), intermediate volatility organic compounds (IVOCs), and volatile organic compounds (VOCs). The fraction in the particle phase, F_p (top panel), increases with decreasing volatility (i.e. C*) according to Equation 1. The campaign average OA concentration, 7 μg m^{-3}, has been used to calculate the partitioning. The parameterization of Tsimpidi et al. (2010) distributes the VOC oxidation products into four volatility bins, and subsequent oxidation reactions are allowed as indicated by the curved arrows. The two parameterizations for P-S/IVOC oxidation from Robinson et al. (2007) and Grieshop et al. (2009) are illustrated as well. Lastly, the parameterization of Pye and Seinfeld (2010) is shown in which SVOCs are treated as four lumped species (pink), and IVOCs are treated using the yields and volatility distribution for naphthalene oxidation (yellow). For clarity the arrows indicating IVOC aging are not shown.*

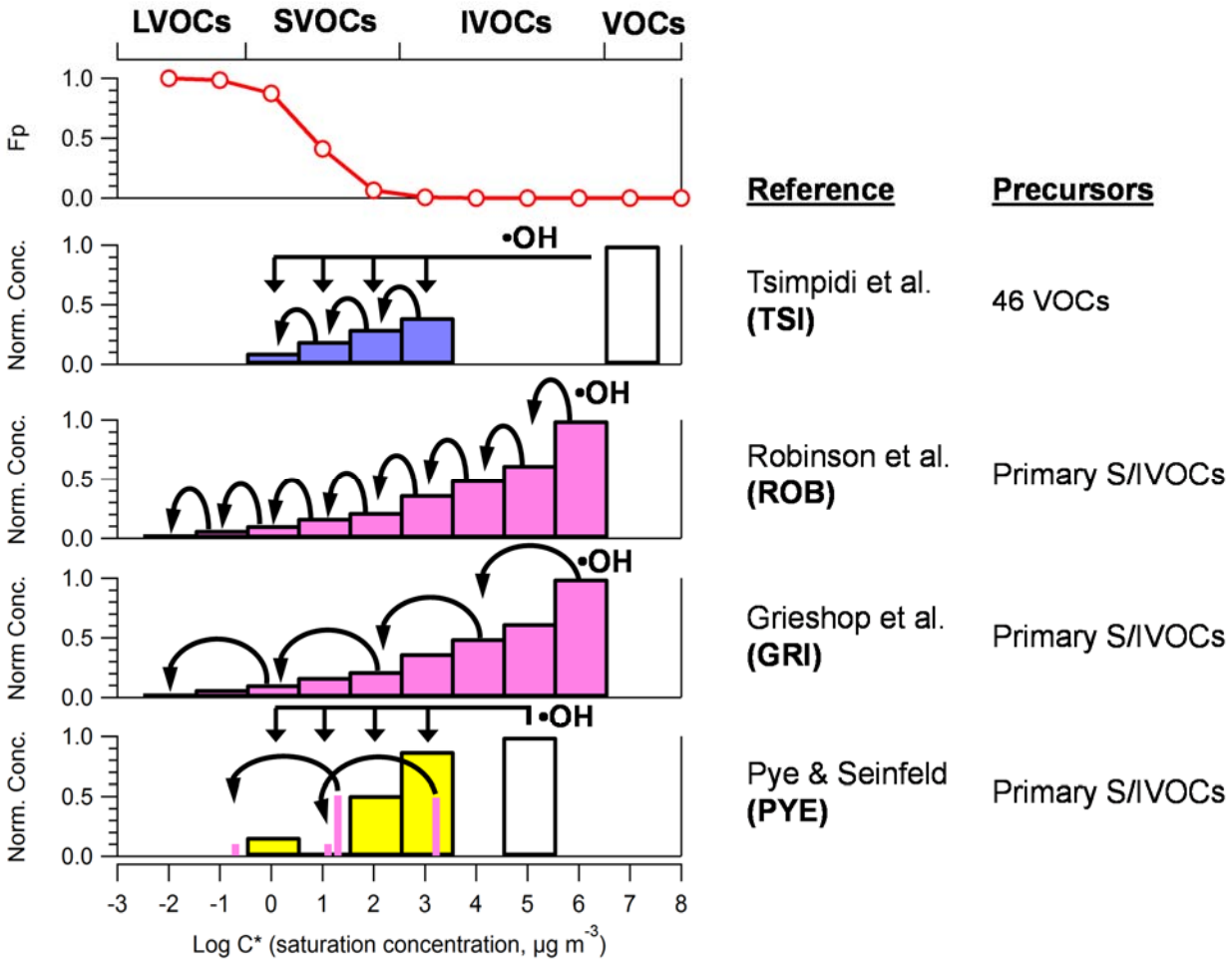

Figure 2. *The evolution of OA/ΔCO versus photochemical age for CalNex separated by cloudy days and mostly clear days. ΔCO is calculated as the difference of the ambient CO and the background CO (105 ppb) (Hayes et al., 2013). The cloudy days are 17 and 27 May 2010, as well as 11 June 2010. See p.15 for the specific calculation of photochemical age used here.*

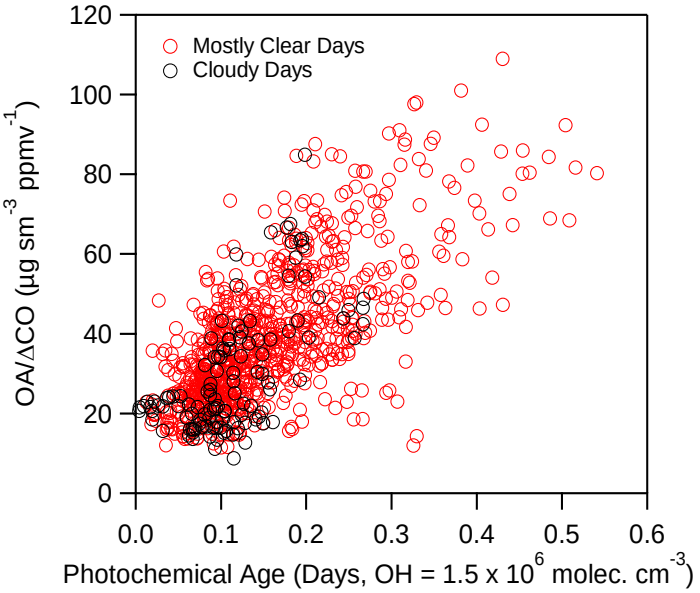

2.3. Model set-up

This work utilizes a box approach wherein the model calculates the evolution of organic species in an air parcel as it undergoes photochemical aging. A schematic of the model set-up is shown in Figure 3. The calculation is run 24 times to predict the average diurnal cycle for the entire campaign (15 May – 15 June). For each of the 24 repetitions, the calculation always starts at hour zero and then runs to 12 h of photochemical aging (Panel 2). Next, the model output at the same photochemical age as that observed at the Pasadena ground site for the given time-of-day is saved for comparison against measurements (Panel 3). The initial concentrations of VOCs in the air parcel are calculated by multiplying the background-subtracted CO concentrations measured at Pasadena by the emission ratios, ΔVOC/ΔCO, previously determined for CalNex, which are consistent with those for other US urban areas (Warneke et al., 2007; Borbon et al., 2013) (Panel 1). CO is an inert tracer of combustion emissions over these timescales and its formation from VOCs is very minor as well (Griffin et al., 2007). The CO background level represents the amount present from continental-scale transport and for which the co-emitted organic species have been lost by deposition (e.g. DeCarlo et al., 2010). The background was determined by examining CO measurements taken aboard the NOAA P3 aircraft off the Los Angeles coastline at altitudes less than 200 m as described in our previous paper (Hayes et al., 2013). Given that the model is set-up to predict the mean diurnal cycle of SOA during the entire CalNex-Pasadena measurement period, the mean diurnal cycle of the CO concentration is used for the calculation of the emissions. An important advantage of using CO as a conserved urban emissions tracer is that dilution of emissions in the air parcel is implicitly included in the model, since the reductions in CO concentration will lead to lower calculated initial precursor concentrations in that air parcel.

Figure 3. *Schematic of the SOA model set-up used in this work. Model inputs are indicated by hollow arrows whereas steps in the modeling process are indicated by solid arrow. All the steps in the dashed box are repeated for each hour of the day.*

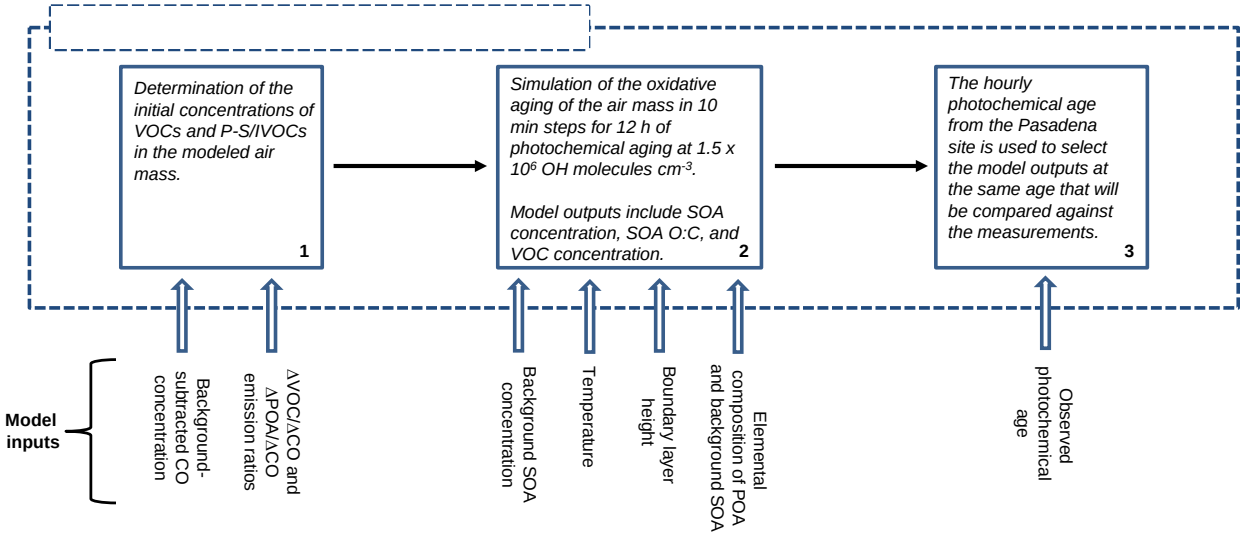

Figure 4. *Model/measurement comparisons of the diurnal cycles for selected VOC mixing ratios as well as for POA mass concentrations. POA is defined as the sum of Hydrocarbon-Like OA (HOA) and Cooking-Influenced OA (CIOA). Note that for the VOCs the GRI+TSI, ROB+TSI, PYE+TSI, ROB+4xV model variations give the same results.*

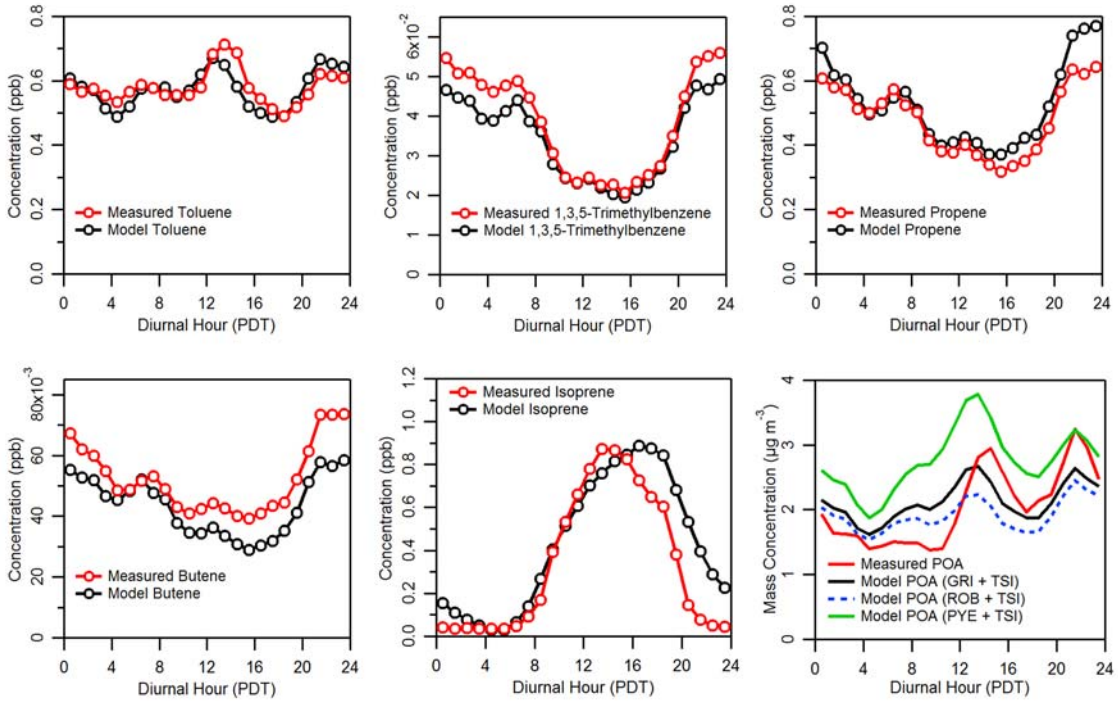

The biogenic VOCs are not expected to be emitted proportionally with CO, and therefore the approach described in the previous paragraph cannot be used to specify the biogenic VOC emissions. Rather, the emissions of biogenic VOCs were adjusted empirically to match the

observed concentrations of isoprene and terpenes, after accounting for anthropogenic isoprene using Δ(isoprene)/ΔCO (Borbon et al., 2013). Only ~4% of the daily average isoprene is from anthropogenic sources. In addition, the diurnal profile of emissions was assumed to be proportional to ambient temperature.

The model consistency with the VOC measurements, including for biogenic VOCs, is evaluated by comparing the measured and modeled diurnal cycles. Some of the cycles compared are given in Figure 4 as an example. It is observed that the model is generally consistent with the VOC measurements.

Figure 5. (Top) *Scatter plots for naphthalene, 1-methylnaphthalene, and 2-methylnaphthalene versus CO mixing ratios. Data includes only measurements from 00:00 – 06:00 (local time) to minimize the impact of photochemical oxidation on the PAH concentrations. Also shown in the top panels are the linear ODR analyses of the data with the y-intercept fixed at 105 ppb CO, which is the background CO concentration (Hayes et al., 2013). For more information on the methodology used to measure naphthalene and the methylnaphthalenes see Presto et al. (2011; 2012).* ***(Bottom)*** *Model and measurement diurnal cycles for naphthalene, 1-methylnaphthalene, and 2-methylnaphthalene.*

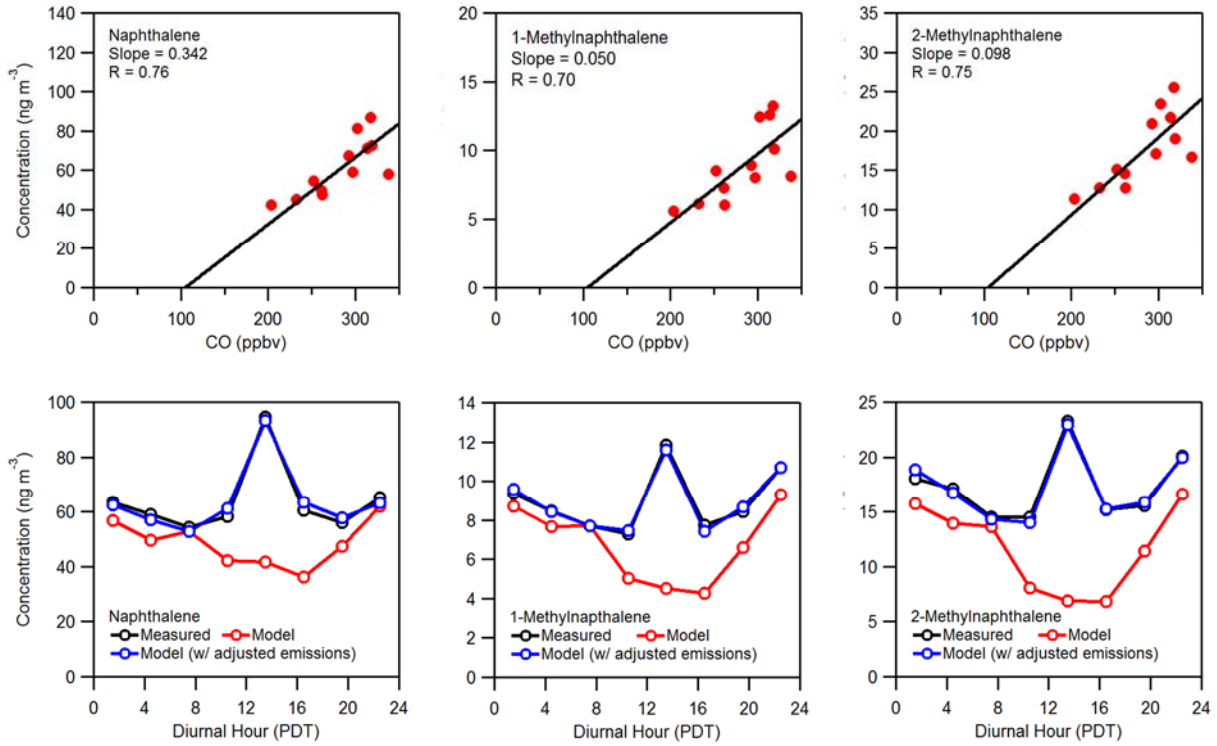

For naphthalene and its analogs, emission ratios are not available in the literature, to our knowledge. To obtain the emission ratios the concentrations of the polycyclic aromatic hydrocarbons were plotted versus CO, and a linear orthogonal distance regression (ODR) analysis was carried out. The data were filtered and include only periods from 00:00 – 06:00 (local time) to minimize depletion by photochemical processing (Figure 5). The slope from the regression analysis was then used as the emission ratio. However, as observed in Figure 5, the diurnal cycles for naphthalene and its analogs are not well-reproduced by the model during the daytime when using the early morning emission ratios. The sampling of these compounds was performed on a

tar roof, and it is possible that the local concentrations in the vicinity of roof may be elevated during daytime due to volatilization of the roofing tar and not representative of concentrations throughout the Los Angeles basin. The naphthalene and methylnaphthalene concentrations are well correlated with temperature. However, it is also possible that the volatilization occurs over a larger city scale, and thus a variation of the model is run wherein the emission ratios are changed empirically along the diurnal cycle so that the model reproduces the measured diurnal cycle for each speciated naphthalene (Figure 5). The increases in emissions range between 1 and 3.5 times the original value, and the implications for SOA are discussed in Section 3.1.3.

The calculation of the initial P-S/IVOC concentrations requires a somewhat different procedure compared to the VOCs. Instead, the amount of initially emitted POA is calculated from measured ΔPOA/ΔCO ratios and the measured CO concentration in Pasadena. Then the total concentration of P-S/IVOCs is set so that the particle-phase P-S/IVOC concentration matches the amount of initially emitted POA, while constraining the volatility distribution to that of the corresponding parameterization, as done in previous studies (e.g. Dzepina et al., 2009).

The model consistency with respect to the POA measurement is shown in Figure 4. The comparison for POA is adequate, and a linear ODR analysis yields a slope of 1.01 (R = 0.76) when the GRI+TSI parameterization is used. Of these three model variants, PYE+TSI shows a larger positive bias. This is likely due to the relatively large amount of primary SVOCs placed in the C*=20 bin compared to ROB+TSI and GRI+TSI, which will result in more partitioning to the particulate phase as the total OA mass is increased (e.g. by SOA formation)

The initial VOCs and P-S/IVOCs are then oxidized in the air parcel. The aging of the air parcel is simulated separately 24 times with each simulation using measured parameters (e.g. ΔCO, photochemical age, POA) corresponding to one hour during the mean diurnal cycle. Following Dzepina et al. (2009) the evolution of the different compounds in each of the 24 aging simulations is calculated by discretizing the rate equations using Euler's method.

The photochemical age of the urban emissions at each time of day is determined from the ratio of 1,2,4-trimethylbenzene to benzene as described previously (Parrish et al., 2007; Hayes et al., 2013). We note that the photochemical age estimated from NO_y/NO_x is very similar (Hayes et al., 2013), which is consistent with previous results from Mexico City for ages shorter than 1 day (C. A. Cantrell, Univ. of Colorado, personal communication, 2014). For some analyses the NO_y/NO_x age is used in this report, due to better temporal overlap with the subset of data being analyzed. There are three important considerations that must be evaluated when using VOC concentration ratios as photochemical clocks.

First, trimethylbenzene and benzene are predominately from anthropogenic sources, and thus the photochemical clock only applies to the evolution of anthropogenic emissions. Previous work by Washenfelder et al. (2011) estimated that most biogenic VOCs were emitted mostly in the last quarter of the trajectory of the air parcel arriving at Pasadena at 16:00 PDT. This estimate was based on the vegetation coverage observed in visible satellite images of the upwind areas, as well as on the ratio of isoprene to its first-generation products (methyl vinyl ketone and methacrolein). However, in this work, the photochemical age for biogenic VOCs is kept the same as for the anthropogenic VOCs. This approach will overestimate the amount of photochemical aging – and the SOA from in-basin biogenic emissions – during daytime. The modeled biogenic SOA should thus be considered an upper limit. As discussed below, the amount of SOA from in-basin biogenic VOCs is very small. Thus, our SOA model results are not

sensitive to the details of how SOA from biogenic VOCs emitted within the LA basin is modeled. We do not include oxidation of biogenic VOCs by O_3 or NO_3 in the box model, but these oxidants have only a minor role in SOA formation during the daytime when the peak for in-basin SOA concentration is observed. In particular, given the measured concentrations of oxidants (Hayes et al., 2013), oxidation of isoprene and terpenes by •OH is 37 and 5 times faster on average, respectively, than oxidation by O_3 during daytime.

The second consideration is that the purpose of using the ratio of VOC concentrations is to determine the •OH exposure for the air mass at the Pasadena site. (•OH exposure is the concentration integrated over time for an air parcel.) While the •OH exposure for the site is therefore well-constrained, the actual •OH concentration in the modeled air parcel as a function of time is not as well-constrained. Thus, the photochemical ages used here (Figure 6) are calculated using an average •OH concentration of 1.5×10^6 molec cm^{-3}, as described in our previous work (Hayes et al., 2013), and the model is run with the same concentration. Insofar as the model produces the same •OH exposure as determined from measurements, which is always the case in this modeling study, the actual concentration of •OH used in the model is not expected to substantially influence the results. In other words, while the concentration •OH in the model is assumed to be 1.5×10^6 molec cm^{-3}, the integral of the •OH concentration over time is constrained by the observed VOCs ratios. As expected, in the middle of the day the photochemical age will be longer than the transport age, and the opposite will be true during periods with low ambient •OH.

Third, photochemical age is a quantity developed as a metric for parcels of air arriving at a remote receptor site, and it is derived by assuming that the parcel is decoupled from fresh emissions as it is transported (Kleinman et al., 2007; Parrish et al., 2007). However, Pasadena is not a remote receptor site, and it is impacted by pollution that has been emitted recently as well as transported from more distant locations. The error in the calculated photochemical age that results from the mixing of nearby and far sources is evaluated in our previous work, and it may lead to underestimation of the actual photochemical age by ~10% (Hayes et al., 2013), which is relatively minor compared to the uncertainty in the OA measurement of ±30% (Middlebrook et al., 2012) and the possible biases in the different SOA parameterizations.

2.4. Model/measurement comparisons

The model is compared against the average diurnal cycles of various OA properties (e.g. concentration, O:C). The measurements utilized in this study are summarized in Table 2. In previous work the concentrations of five different OA components were determined using positive matrix factorization (PMF) of aerosol mass spectrometer (AMS) data, and the diurnal cycles of these components are shown in Figure 6 (Hayes et al., 2013). Hydrocarbon-like organic aerosol (HOA) and cooking-influenced organic aerosol (CIOA) are both thought to be dominated by POA. As discussed in Hayes et al. (2013), HOA is dominated by vehicle combustion emissions, and the CIOA is dominated by cooking sources. However, for the purpose of running the SOA model, HOA and CIOA are not treated separately, and instead their summed mass concentrations are used as the POA concentration. It should be noted however that the amount of SOA from HOA or CIOA associated P-S/IVOCs can still be calculated under certain assumptions as discussion in Section 3.1.2 below. Low volatility oxygenated organic aerosol (LV-OOA) is a surrogate for highly aged secondary organic aerosol, and it displays a flat diurnal profile. Furthermore, recent ^{14}C measurements show that this component is largely composed of non-fossil carbon (Zotter et al.,

2014). Both of these observations indicate that LV-OOA is transported into the Los Angeles Basin (Hayes et al., 2013).

Table 2. *Measurements acquired at the Pasadena ground site during CalNex and used in this study.*

Measurement	**Technique**	**Uncertainty**	**Reference**
Bulk aerosol mass concentrations for organics, nitrate, sulfate, and ammonium as well as the concentrations of organic aerosol components	High-resolution Aerosol Mass Spectrometry (AMS) and Positive Matrix Factorization (PMF) analysis	±30%	Hayes et al. 2013
Oxygen-to-carbon ratio	High-resolution Aerosol Mass Spectrometer (AMS) and Elemental Analysis (EA)	±30%	Hayes et al. 2013
Speciated VOCs	Gas chromatography – mass spectrometry	±5 – 25% (hydrocarbons) ±20 – 35% (oxygenates)	Borbon et al. 2013
CO	VUV Fluorescence	±4%	Hayes et al. 2013
Modern and fossil fraction of organic carbon	^{14}C	See text	Zotter et al. 2014
Concentration of SOA from specific precursor compounds	U.S. E.P.A. tracer method and measurement of oxygenates from filter samples using GC-MS	See text	Kleindienst et al. 2012
Concentration of naphthalene and its derivatives	Thermal desorption gas chromatography mass spectrometry	±30%	Presto et al. 2011 Presto et al. 2012

Figure 6. *(A) Average diurnal cycle of CO (red) and photochemical age (blue) for the Pasadena ground site during CalNex. Note: A background of 105 ppbv has been subtracted from the CO concentration. (B) Average diurnal cycle of the five OA components identified by PMF analysis, as well as the background SOA calculated from WRF-Chem. The five components are semi-volatile oxygenated organic aerosol (SV-OOA), cooking-influenced organic aerosol (CIOA), hydrocarbon-like organic aerosol (HOA), local organic aerosol (LOA), and low volatility organic aerosol (LV-OOA).*

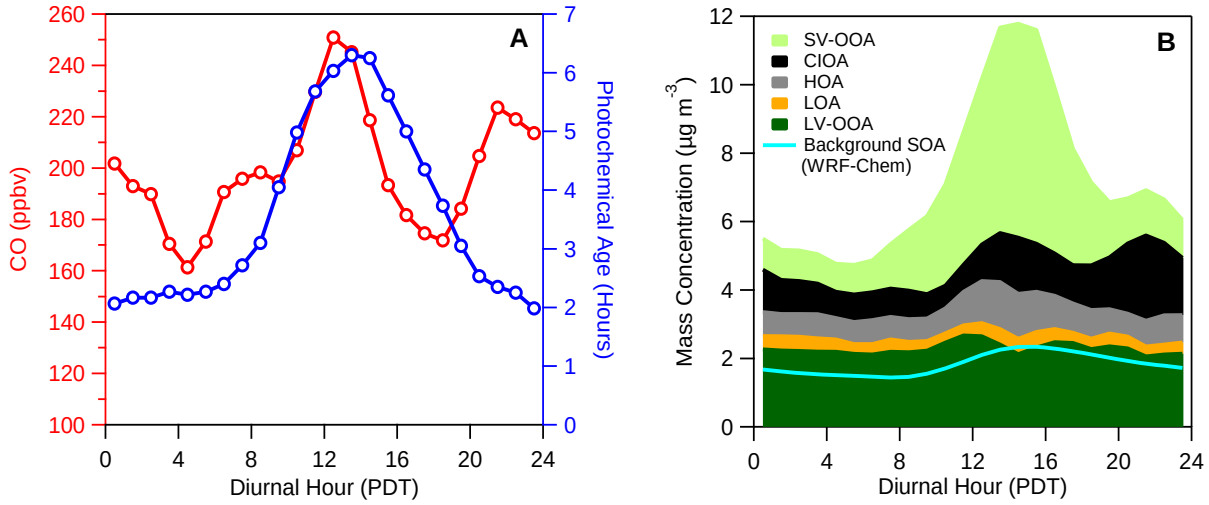

Figure 7. *Anthropogenic CO fluxes on a 12 km grid in Southern California that are used in the WRF-Chem simulation. The box indicates the region around and inside LA where the emissions of atmospheric species are set to zero in order to determine the concentration of background SOA.*

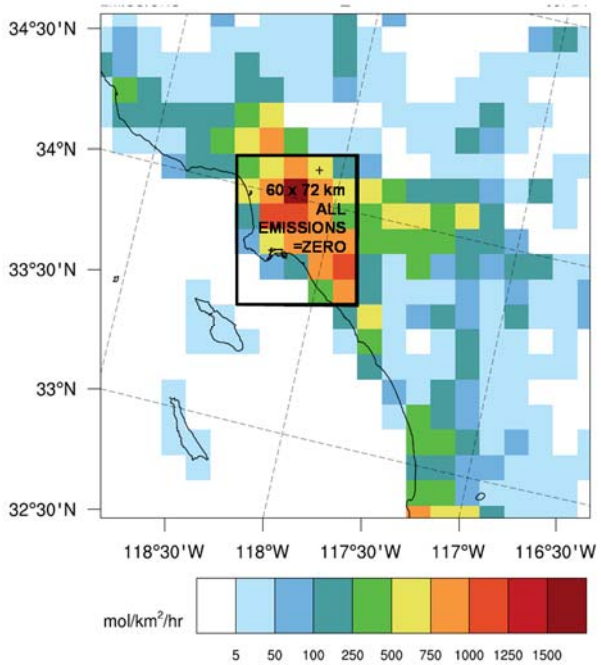

Results from 3-D WRF-Chem simulations were also used to evaluate the concentration of BG-SOA. These simulations determined the BG-SOA by removing all the emissions in the Los Angeles region as shown in Figure 7, and it was observed that there are both biogenic and anthropogenic emissions in California that contribute to the background OA. In addition, background marine OA is thought to be very low during the CalNex measurement period, since concentrations of OA were less than 0.2 μg m^{-3} over the open ocean west of California for regions with low pollution influence (P. K. Quinn, NOAA, personal communication, 2012). As shown in Figure 6B, the background SOA concentration from the WRF-Chem simulation is similar to the concentration of LV-OOA. Given these observations as well as the ^{14}C results discussed in the previous paragraph, we use the LV-OOA component to constrain the amount of BG-SOA, and specifically, set the amount of BG-SOA to be the minimum of LV-OOA observed in the diurnal cycle (2.1 μg m^{-3}). Heo et al. (2015) recently concluded that the background SOA in the LA basin has an important component from biogenic emissions over the Central Valley, which is consistent with our results.

In contrast, semi-volatile oxygenated organic aerosol (SV-OOA) displays a distinct diurnal profile that peaks at a similar time as photochemical age, which is consistent with this component being a proxy for freshly formed SOA from urban emissions. The ^{14}C measurements also indicate that SV-OOA is predominately, 71% (±3%), composed of fossil carbon. (Note: to obtain this percentage it is assumed that the OC/OM ratio is the same for fossil and non-fossil SV-OOA.) As described above, the box model designed here is specifically focused on SOA formation from precursors emitted within the Los Angeles basin, and the ^{14}C measurements and diurnal cycle strongly indicate that SV-OOA concentration is a better surrogate for total urban SOA than the total OOA concentration. Lastly, there is a fifth component displayed in Figure 6B, local organic aerosol (LOA) of primary origin and of uncertain sources, but this component comprises only ~5% of the aerosol mass. It is thought to be emitted very close to the site based on its very rapid time variations, and thus any co-emitted VOCs or S/IVOCs would have very little time to react and form SOA. Therefore, LOA is not considered further in this modeling study.

In principle, the box model could be run for multiple individual days. However, some datasets and published results used in this study are not available with sufficient time resolution for such an approach. In particular, the thermal desorption gas chromatograph mass spectrometry analysis for naphthalenes required adsorbent tube samples that were composited over several days. In addition, both the apportionment of the SV-OOA and LV-OOA components between fossil and non-fossil sources (Zotter et al., 2014) as well as the analysis of the diesel fraction of OOA (Hayes et al., 2013) required analyzing datasets from multiple days as a single ensemble. To facilitate incorporating these datasets and published results into this study, we have chosen to run the box model so that it simulates the average diurnal cycle during the campaign. The measurements used here (Table 2) all had excellent coverage during the CalNex campaign, with each instrument reporting data for more than 75% of the total campaign duration. Thus, the measurements are expected to be representative of conditions during the campaign.

An exception is the ^{14}C measurements, which were carried out on filters collected over 7 days. This limited sampling period is due to the time and resource intensive nature of the ^{14}C measurements (Zotter et al., 2014). In particular, the dates that the filters were collected were 30 May as well as 3, 4, 5, 6, 13, and 14 June 2010. Thus, these filters are more representative of the second half of the campaign that was more strongly influenced by pollution from the basin, compared to the first half of the campaign were regional advection played a more important role

(Ryerson et al., 2013). Given the cost of the ^{14}C analyses, these days were chosen on the basis of the larger urban influence determined from the real-time measurements and are therefore better suited to constrain urban sources (the subject of this report) than if the analyses had been performed on filters from randomly-chosen days. However, it is noted that the relative concentrations of the different components of the OA were similar when averaging the second half of the campaign or the entire campaign: 14% vs. 12% for HOA, 5% vs. 5% for LOA, 12% vs. 17% for COA, 28% vs. 34% for LV-OOA, 40% vs. 34% for SV-OOA. Thus, it appears reasonable to assume that the relative results from the ^{14}C analysis are representative of the entire campaign.

2.5. Modeling the SOA oxygen content

To simulate the oxygen-to-carbon ratio (O:C) of total OA, the box model utilizes the measured O:C for HOA, CIOA, and LV-OOA. The O:C values for HOA and CIOA are assumed to be constant because heterogeneous aging of primary aerosols is relatively slow, and thus the O:C should only vary by a relatively small amount due to this mechanism over the timescales considered here (Donahue et al., 2013). LV-OOA is predominately composed of aged background OA, and thus its O:C should not vary substantially either. The oxygen and carbon mass from HOA, CIOA, and LV-OOA are then added to the oxygen and carbon mass predicted in the model for freshly formed SOA.

The O:C of V-SOA is simulated using a modified version of the approach described in Dzepina et al. (2009). In that previous work the O:C of V-SOA was estimated to be 0.37 and constant. While this estimate is consistent with chamber experiments of aromatic precursors, it is conceptually difficult to reconcile with V-SOA aging wherein successive oxidation reactions are expected to reduce volatility and increase O:C. It is therefore assumed in the box model that O:C increases as follows: C* = 1000 μg m^{-3}, O:C = 0.25; C* = 100 μg m^{-3}, O:C = 0.30, C* = 10 μg m^{-3}; O:C = 0.40; C* = 1 μg m^{-3}, O:C = 0.60. This O:C distribution is taken from the first-generation distribution of Murphy et al. (2011), and in that work the O:C was simulated in a full 2-D VBS and depends on both volatility bin as well as oxidation generation. For the purpose of this study an intermediate approach is used wherein O:C depends on volatility bin only, and the first-generation distribution of Murphy et al. (2011) is applied to all oxidation generations of SOA. We note that only a small amount of V-SOA mass is from multi-generation oxidation (10 – 20%) for the relevant model conditions used for Pasadena. Thus, the O:C values predicted here will not be substantially different from a full 2-D VBS treatment.

The O:C ratio for SI-SOA is simulated following the approach described in Robinson et al. (2007). Conceptually, with each oxidation step the model adds 1 oxygen atom per 15 carbon atoms for ROB and 5.3 oxygen atoms per 15 carbons for GRI. This oxidation then gives an increase in mass of 7.5% or 40% for ROB and GRI, respectively, as discussed previously. (Note: It is assumed that H = 2×C + 2, which may not be strictly true, but an error of 1 or 2 hydrogen atoms per carbon does not substantially alter the calculated values for the mass increase.) With this relationship O:C can be calculated for each generation of oxidation. The organic aerosol to organic carbon ratio (OA:OC) ratio can be calculated as well using the relationship OA:OC = 1 + (16/12)×O:C + (1/12)×H:C, in which H:C = 2 – 0.54×O:C (Murphy et al., 2011; Hayes et al., 2013; Canagaratna et al., 2015). Then the OA:OC ratio is used to convert the OM mass concentration in each generation bin to OC mass concentration, and the O:C ratio is used to convert the OC mass in each generation bin to O mass concentration. Finally, the O mass and OC mass are each summed and subsequently divided to obtain O:C.

2.6. Correction for changes in partitioning due to emissions into a shallower boundary layer upwind of Pasadena

To account for changes in partitioning due to lower planetary boundary layer (PBL) heights, and thus, increased OA concentrations upwind of Pasadena, the concentrations of POA, V-SOA, and SI-SOA are increased upwind of Pasadena beyond the amount already simulated in the model. This correction is necessary because using CO as a conservative tracer of emissions does not account for how the shallow boundary layer over Los Angeles in the morning influences partitioning between the gas and particle phases. Specifically, during the afternoon Pasadena is a receptor site for pollution from downtown Los Angeles that was generally emitted into a shallower boundary layer during the morning. The reduced vertical dilution will lead to higher concentrations of POA as well as any urban SOA formed, which in turn leads to higher partitioning to the particle phase and less gas phase oxidation of primary and secondary S/IVOCs.

The correction of the partitioning mass is estimated using three different methods depending on the time-of-day. First, for air parcels measured at 00:00 – 07:00 local time when the PBL height is essentially constant for an extended period and emissions are dominated by local sources (Hayes et al., 2013), no correction needs to be made. Second, for air parcels measured between 07:00 – 16:00 when the PBL is increasing as the air parcels are advected, a correction is applied that assumes the PBL increases linearly from the height measured in the early morning hours to the height measured for a given time of day. Third, for air parcels after 16:00, it is assumed that a residual layer aloft is decoupled from the ground after 16:00, resulting in no subsequent dilution.

The correction for the partitioning calculation described in the previous paragraph is an approximation, and two sensitivity studies are carried out to estimate the magnitude of the possible errors introduced by this approximation. The first study follows the approach described above, except that instead of linearly increasing the partitioning mass upwind of Pasadena the correction follows a step-function and increases the partitioning mass to its maximum value immediately upwind of the ground site. This test should overestimate the amount of partitioning to the particle-phase, since such a dramatic change in PBL height is not expected. The second sensitivity study simply applies no correction factor to the partitioning mass, and thus it underestimates the partitioning to the particle-phase. For the model runs with the ROB+TSI and GRI+TSI parameterizations the resulting changes in average predicted mass for the sensitivity studies are +4/-12% and +6/-7%, respectively. These changes are small, which indicates that the description of the boundary layer dilution does not have a major influence on the results.

2.7. WRF-CMAQ model runs

The Community Multiscale Air-Quality Model (WRF-CMAQ) version 5.0.1 (https://www.cmascenter.org/cmaq/) was applied with 4 km horizontal grid resolution and 34 vertical layers extending from the surface (layer 1 height ~38 m) to 50 mb for the time period matching the CalNex field campaign. Aqueous phase chemistry includes oxidation of sulfur and methyglyoxal (Carlton et al., 2008; Sarwar et al., 2013), gas phase chemistry is based on Carbon-Bond 05 with updates to toluene reactions (CB05-TU) (Yarwood, 2010), and inorganic chemistry is based on the ISORROPIA II thermodynamic model (Fountoukis and Nenes, 2007). WRF-CMAQ estimates SOA yields from VOC precursors including isoprene, monoterpenes, sesquiterpenes, xylenes, toluene, benzene, and methylglyoxal (Carlton et al., 2010). Note that WRF-CMAQ contains the SOA precursor species alkanes and glyoxal, but these are not explicit

species in the CB05-TU gas phase mechanism (e.g., alkanes are mapped to "PAR", or paraffins). SOA species oligomerize to non-volatile organic carbon grouped by anthropogenic and biogenic origin (Carlton et al., 2010).

The Weather Research and Forecasting model (WRF), Advanced Research WRF core (ARW) version 3.1 (Skamarock et al., 2008) was used to generate gridded meteorological fields used for input to WRF-CMAQ and the emissions model. Surface variables, flow patterns, and daytime mixing layer heights are generally well characterized during this time period (Baker et al., 2013). Hourly solar radiation and surface layer temperature estimated by the WRF model are used as input for the Biogenic Emission Inventory System (BEIS) version 3.14 to estimate hourly speciated VOC and NO_x emissions (Carlton and Baker, 2011).

Stationary point source emissions are based on continuous emissions monitor (CEM) data for 2010 where available and otherwise the 2008 version 2 National Emission Inventory (NEI). Area source emissions are also based on the 2008 version 2 NEI. Mobile sector (on-road and off-road) emissions are interpolated between 2007 and 2011 totals provided by the California Air Resources Board. Emissions from other areas of the United States and other countries are included through time and space variant lateral boundary inflow. Hourly boundary inflow concentrations are taken from a coarser WRF-CMAQ simulation covering the continental United States that used inflow estimates from a global GEOS-CHEM (version 8.03.02) model (http://acmg.seas.harvard.edu/geos/) simulation. Additional details regarding model setup and evaluation are provided elsewhere (Kelly et al., 2014).

2.8. WRF-Chem model runs

Weather Research and Forecasting Model coupled to Chemistry (WRF-Chem) is a fully coupled meteorology-chemistry model. WRF-Chem simulations were performed for May and June 2010 on a 12 km resolution domain, which covers a large part of the western United States. The model simulations include meteorological, gas, and aerosol phase chemical processes. The SOA scheme used in this study is based on the VBS approach. The SOA parameterization and other model parameterizations are described in detail by Ahmadov et al. (2012). Here the main objective of the WRF-Chem simulation was to estimate the OA contribution of the emission sources located upwind of the Los Angeles basin. Thus, all the anthropogenic emissions and biogenic VOC fluxes were set to zero over an area of 60 x 72 km covering the Los Angeles basin (Figure 7) in our simulation. The WRF-Chem simulated OA concentrations for the Pasadena site therefore provide an estimate of the BG-OA at this site.

2.9. Oxidation Flow Reactor

To study SOA formation and OA aging in-situ, we deployed a Potential Aerosol Mass (PAM) oxidation flow reactor (Kang et al., 2007; Kang et al., 2011) at the Pasadena ground site. Fig. 8a shows a diagram of the operational setup. The reactor and ambient sample lines were located adjacent to one another, on the roof of the instrument trailer at 7.2 meters above ground (Fig. 8b). Ambient air was continuously sampled in an open flow-through configuration via a 14-cm diameter opening with coarse-grid mesh screen coated with an inert silicon coating (Sulfinert by SilcoTek, Bellefonte, PA). The mesh was designed to block debris and insects, as well as break up large eddies while allowing VOCs and oxidized gases to be sampled efficiently. This configuration, with no inlet, was chosen because of the observation of reduced SOA formation when any inlet and/or an inlet plate was used in a previous experiment (Ortega et al., 2013). The

reactor output was measured by an AMS (described below), a scanning-mobility particle sizer (SMPS, TSI Inc., Model 3936 with TSI 3010 CPC), and an O3 monitor (2B Technologies, Model 205). Fast switching valves were used to automatically alternate AMS and SMPS sampling between the reactor and unperturbed ambient sample line every 5 minutes. Bypass lines were used to maintain constant flow in both the reactor and ambient sample lines while instrumentation was sampling the other channel, to avoid artifacts due to particle or gas losses or re-equilibration that could occur if flow had been stagnant in the lines or modulated in the reactor. To maintain plug-like flow characteristics in the reactor, output flow was sampled from both a central stainless steel 1/4-inch OD tube at 2.0 lpm for aerosol measurements and a 3/8-inch OD PTFE Teflon perforated ring with 14-cm diameter for gas-phase measurements at 2.4 lpm. This setup allowed continuous measurements of both photochemically-aged and ambient aerosol.

Figure 8. (a) *Schematic of the oxidation flow reactor (OFR) coupled to an Aerodyne high-resolution time-of-flight aerosol mass spectrometer (AMS), scanning-mobility particle sizer (SMPS), and ozone (O_3) monitor. An ambient sampling line allowed for direct sampling of ambient air. Computer-controlled switching valves allowed for sampling in alternation from the reactor and ambient lines. Voltage supplied to UV lamps were varied via programmable computer control to step through oxidant concentrations in the reactor. Ring flow was via a PTFE Teflon line and was used for gas-phase measurements. Center flow was a copper line that continuously pulled the sample for aerosol analysis.* ***(b)*** *Photograph of the reactor with a sun / rain cover and of the ambient aerosol inlet (right, covered by foil insulation) on the trailer roof during CalNex.*

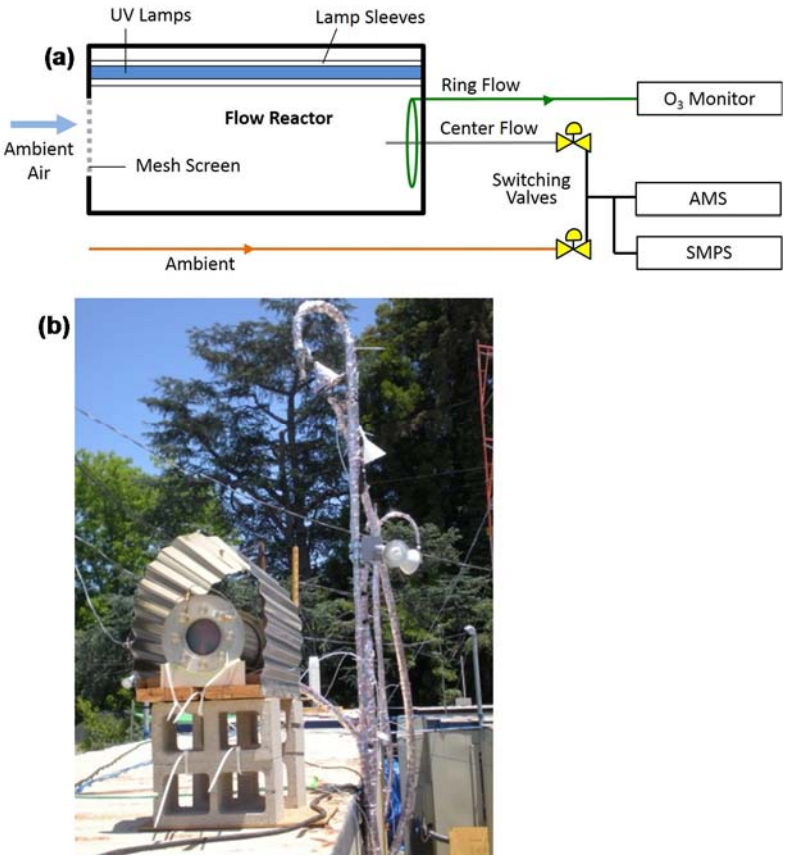

The total flow rate through the reactor was 4.4 lpm corresponding to a residence time of 3 min. The reactor was used to expose ambient air to high levels of OH and O3, produced when UV light from two low-pressure mercury lamps (model no. 82-9304-03, BHK Inc., with discrete emission peaks at 254 nm and 185 nm) initiated O2, H2O and O3 photochemistry. This mode of operation is referred to as OFR185 (Li et al., 2015). We use the term "aging" to refer to the combined effect of OH, O3, and light exposure in the flow reactor, although reactions in the reactor are understood to be dominated by OH under typical operating conditions (Peng et al., 2015). The intensity of aging was continuously stepped by computer-controlled lamp power supplies (custom made transformers from BHK Inc., controlled via Labview using a National Instruments analog output board NI USB-6501), resulting in systematic stepping of lamp input voltage from 50–110 VAC. This voltage stepping modulates the photon flux and consequently the OH concentrations in the reactor (Li et al., 2015).

Oxidant concentrations in the reactor were stepped in 20-minute intervals, through six levels (including lights off, i.e. no added oxidants) comprising a two-hour cycle (Fig. 9). Only data from the last five minutes of each 20-minute period are used, to avoid including reactor transient periods. As lamp intensity increased, O_3 and OH concentrations increased in the reactor, resultant OA concentrations were measured from the reactor after oxidant perturbation as seen in Fig. 9. To account for particle losses in the reactor, reactor AMS concentrations have been corrected by comparing particles measured through the ambient inlet (averaging two concurrent ambient measurements just before and after lights off measurement) to the levels during the last 5 minutes of each period with lights off. This correction is applied over the sample period, in a time varying way and accounting for variations in UV intensity, resulting in an average correction of +5.8%.

The OH exposure (OH_{exp}, OH concentration integrated over the reactor residence time) achieved in this study is primarily a function of lamp photon flux (at 185 and 254 nm), residence time, and ambient H_2O concentration and OH reactivity (Li et al., 2015; Peng et al., 2015). OH_{exp} was estimated using a calibration equation developed by multivariate fitting of the output from a kinetic model of reactor (OFR185) operation, and verified against data from several field and laboratory experiments including CalNex (Li et al., 2015). The equation (given in Li et al., 2015 and Peng et al., 2015) uses ambient H_2O concentration, reactor output O_3 concentrations, flow rate, and ambient OH reactivity from collocated measurements (data from the Stevens Group, Indiana University). According to this equation, internal OH_{exp} in the reactor typically ranged from 1.1×10^{11}–5.8×10^{12} molec. cm^{-3} s, 0.8 days–6.4 weeks of photochemical age assuming 24-hr average ambient OH concentrations of 1.5×10^{6} molec. cm^{-3} (Mao et al., 2009). "Total photochemical age" refers to the sum of ambient photochemical age and reactor internally-generated photochemical age, used throughout this work unless otherwise specified. Ambient photochemical age is calculated by the ratio of 1,2,4-trimethylbenzene to benzene (Borbon et al., 2013), using collocated gas-phase measurements as described in Hayes et al. (2013). Subsequent figures use total photochemical age in day-units applying the average OH concentration of 1.5×10^{6} molec. cm^{-3}. During CalNex, OH concentrations averaged up to 4×10^{6} molec. cm^{-3} during the daytime, from concurrent OH reactivity estimates. Since a significant part of SOA formation happens during the first few hours after emission, the 0.8 equivalent day minimum photochemical age would correspond to ~0.3 days at the peak OH observed during CalNex.

Figure 9. *A typical oxidant cycle showing steps in lamp intensity in the reactor. Top: reactor oxidant concentrations. Bottom: OA concentration for ambient and reactor output sampling.*

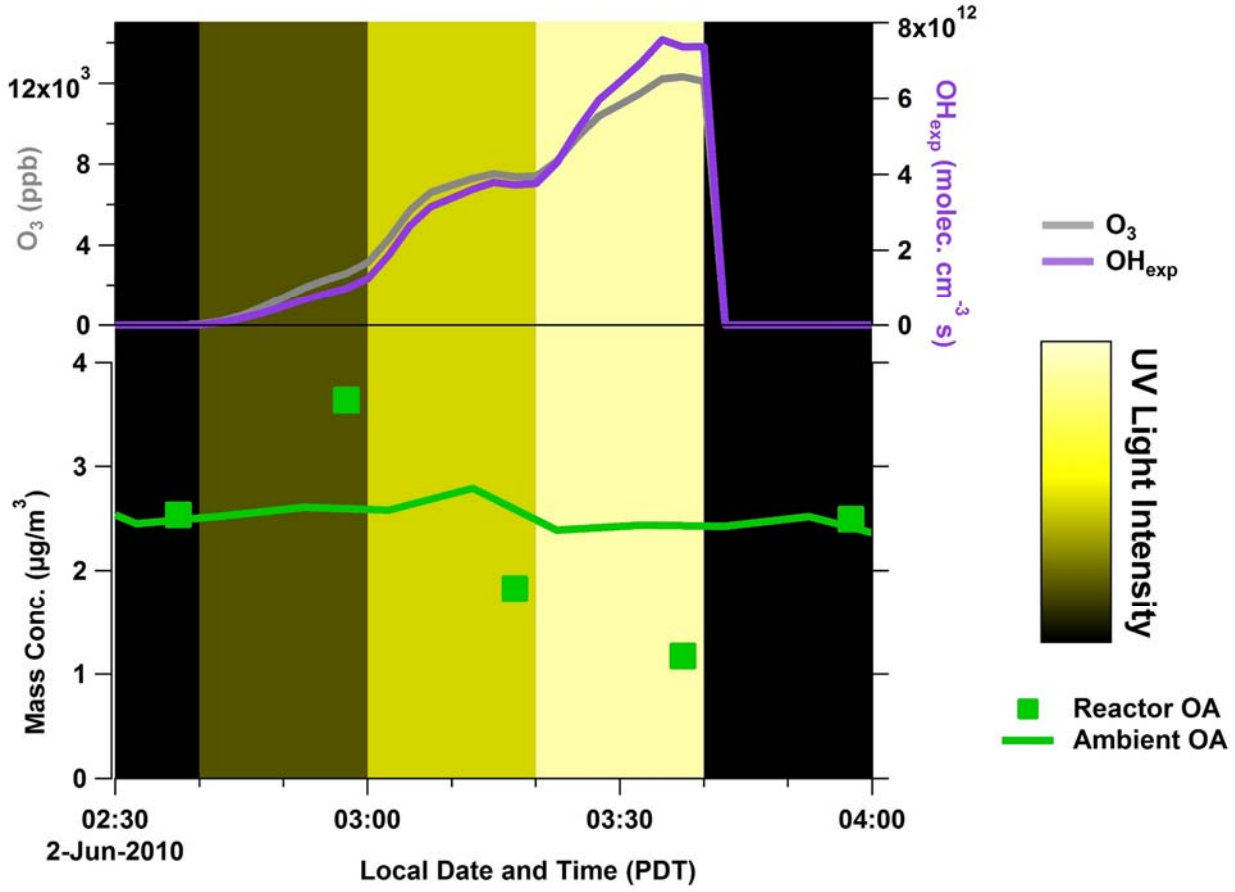

2.10. Particle Measurements Before and After the OFR

Particle concentration and composition were analyzed with a high-resolution time-of-flight aerosol mass spectrometer (HR-ToF-AMS, abbreviated as AMS hereafter; Aerodyne Research, Billerica, MA; DeCarlo et al., 2006; Canagaratna et al., 2007). The ambient measurement setup, instrument intercomparisons, scientific results, and their interpretation are reported in Hayes et al. (2013). he high-resolution (HR) fragmentation Table (Aiken et al., 2008) and peak fitting (DeCarlo et al., 2006) were applied to the reactor measurements with no additional adjustments beyond those performed for the ambient CalNex data by Hayes et al. (2013). The elemental analysis of OA (O:C, H:C) was performed using the "improved-ambient" method published by Canagaratna et al. (2015) for both reactor and ambient measurements, which increases O:C on average by 27% and H:C on average by 11% over the previous "Aiken ambient" method (Aiken et al., 2008). Details of the quantification of AMS reactor measurements (i.e. collection efficiency, inlet and particle lens losses) and intercomparison with the SMPS are discussed in Appendix B (Figs. B-1 to B-5). Hayes et al. (2015) performed a modeling study comparing the ambient AMS OA measurements with several box and 3-D SOA models. Here, we only discuss the modifications in post-processing and data analysis necessitated by the alternating sampling of the reactor output.

Figure 10. *Modeled fate of low volatility organic gases (LVOCs) formed in the reactor vs. OH_{exp} including wall loss, reaction with OH, condensation on aerosol, and exiting the reactor, with a fit for the fraction condensing on aerosols in the reactor. Lightly colored circles in the background are all individual 2.5-minute datapoints. Darker squares in the foreground are 6.7% quantiles of the data.*

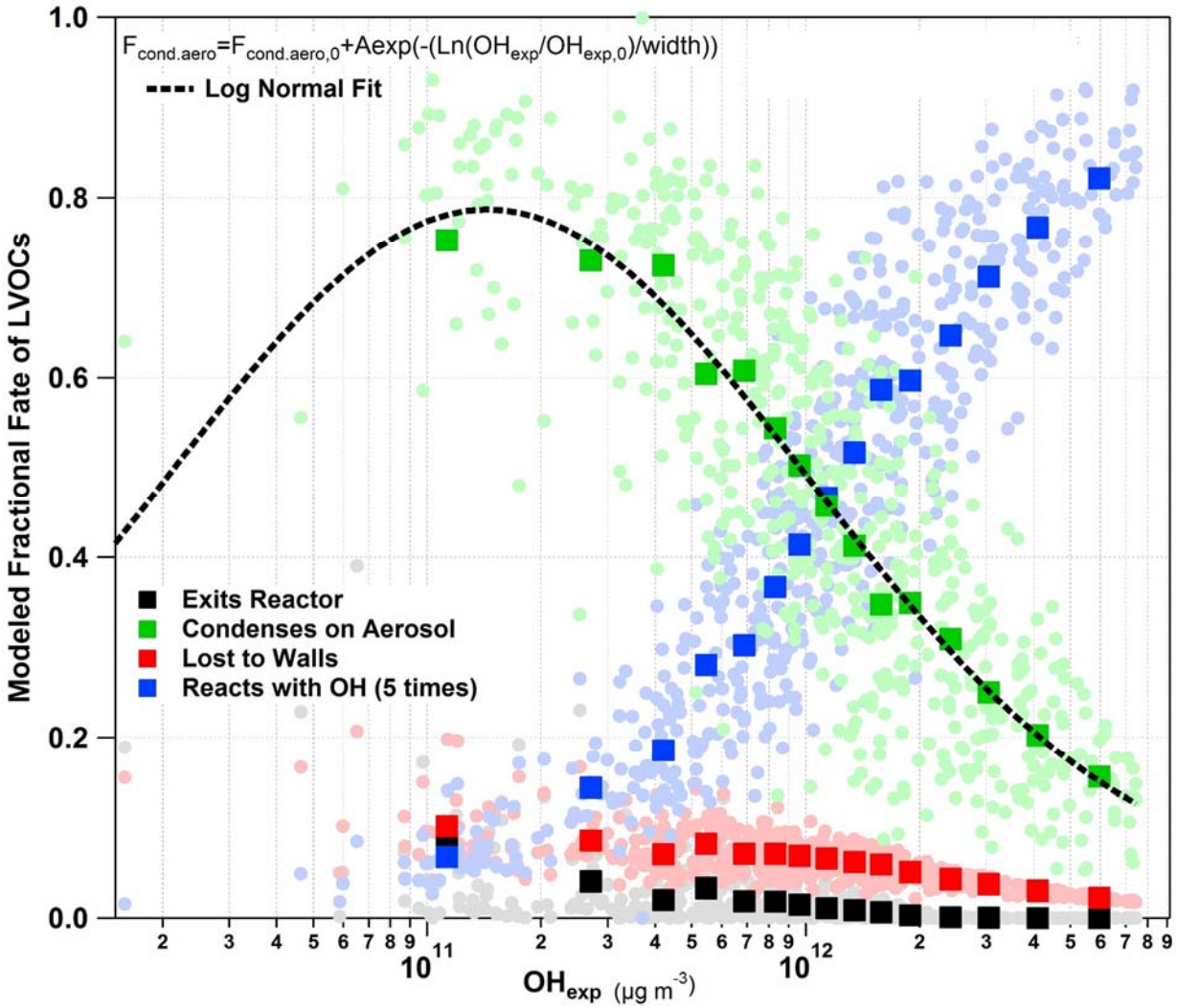

2.11. Fate of Low-Volatility Organic Gases in the Reactor

As organic gases are oxidized, they can form lower vapor pressure products, low-volatility organic compounds (LVOC). Semivolatile organic compounds (SVOC) will also be formed, but we focus this discussion on LVOC for simplicity. In the atmosphere, the dominant fate of these LVOC is condensation on aerosols, as OH lifetimes and dry deposition time scales are slower (Donahue et al., 2013; Knote et al., 2015). However, given the limited residence time, high surface/volume ratio, and the high oxidant concentrations in the OFR, other fates can be competitive. LVOC in the reactor can either condense on aerosols, be lost due to condensation on the reactor walls, react further with OH resulting in condensable or non-condensable products, or exit the reactor in the gas phase to condense on the sampling line walls.

Aerosol sampling instruments only measure the LVOC that condense on aerosols in the reactor. Given the short residence time and high OH_{exp} of the reactor, SOA formation could be underestimated due to these competing fates. To account for vapor losses, we follow the method detailed in Palm et al. (2015), using McMurry and Grosjean (1985) for wall loss estimation. The method of Pirjola et al. (1999) is used for estimating organic gas condensation to aerosols based on the measured SMPS size distributions with the Fuchs-Sutugin correction for gas diffusion in the transition regime (Seinfeld and Pandis, 1998). It is assumed that products after five oxidation steps with OH at $k_{OH} = 1 \times 10^{-11}$ molec cm^{-3} s^{-1} are lost (fragmented and too volatile to condense). This is used to simulate a typical C_{10} VOC oxidation in the reactor, and the results are not very sensitive to the number of oxidation steps used in the model (Palm et al., 2015). Parameters used include the measured surface-area-to-volume ratio (A/V) of the reactor (25 m^{-1}), a coefficient of eddy diffusion k_e approximated as 0.0036 s^{-1}, and a diffusion coefficient D = 4×10^{-6} m^2 s^{-1}, corresponding approximately to the diffusivity of a molecule with a mass of 200 g mol^{-1}.

At OH_{exp} lower than 1×10^{12} molec. cm^{-3} s (~10 days) the dominant LVOC fate is condensation to the aerosol (see Fig. 10). At higher OH_{exp}, the fate of organic gases is dominated by loss to reaction with OH rather than condensing on aerosol. LVOCs lost to the walls or exiting the reactor play only a small role under the conditions of this study, due to the relatively high ambient aerosol surface area. The amount of SOA formed in the reactor is corrected for the fraction of SOA that condense on the aerosol by fitting a line to the calculated fraction of LVOCs that condense on aerosol and dividing the measured SOA formed in the reactor by the fitted fraction of LVOCs that were lost by condensation on the aerosol (Fig. 10). This correction is a minimum at low to moderate ages, and highest at longest ages where net OA production is lowest. Thus, the maximum net SOA production was typically corrected by a factor of 1.2. At increasing ages, where OA loss due to heterogeneous oxidation begins to dominate over gas-phase oxidation, it becomes unfeasible to apply the correction, as the net OA enhancement in the reactor is negative. Thus, correction is applied when reactor-measured OA is greater than ambient OA ($ER_{OA}>1$, ΔOA Mass>0).

3. Results and Discussion

3.1. Modeling urban SOA mass concentration

3.1.1. Urban SOA concentration: model versus measurement comparisons

In Figure 11 the diurnal cycles of SV-OOA and urban SOA are shown. For all the model variations, the model V-SOA (light blue area) is substantially smaller than the observed SV-OOA concentrations (solid black line), even though the additional partitioning mass of SI-SOA is available for all model runs. Even in the model variation ROB+4xV where the V-SOA concentrations are substantially higher due to the higher VOC yields used, additional SOA precursors must be included to achieve model/measurement closure. This result is also true despite the inclusion of multi-generation V-SOA aging in ROB+TSI, GRI+TSI, and PYE+TSI, which increases the amount of SOA from VOCs to levels far beyond those observed in chambers, although over longer timescales than for the 4xV case. Previous work modeling SOA in Mexico City showed that either V-SOA aging or SI-SOA must be included in models to match observed SOA concentrations, but the inclusion of both resulted in an overprediction (Tsimpidi et al., 2010; Dzepina et al., 2011). In this study, the inclusion of aging only increases the concentration of V-SOA by 10 – 20% depending on the time of day due to the relatively low experimental photochemical ages. Thus, by testing models of SOA formation at short ages, our case study points towards the importance of additional SOA precursors such as P-S/IVOCs. Specifically, the contribution to total SOA from P-S/IVOCs in the box model is 65-75% (ROB+TSI), 80-87% (GRI+TSI), 80-92% (PYE+TSI), and 44-51% (ROB+4xV). The range indicates the variation in the contribution with the time-of-day. Thus, only in the ROB+4xV model variation is the estimated contribution to SOA from VOCs generally larger than or equal to that from the P-S/IVOCs. We note however these percentages include only the urban SOA and not the background OA, which is likely also SOA as discussed above.

When comparing the four parameterizations for SOA formation, it is apparent that the GRI+TSI and ROB+4xV variations best reproduce the observations. The predicted SOA mass using GRI+TSI lies within the measurement uncertainty most of the day. In contrast, the ROB+TSI variation does not produce high enough concentrations of SOA, and the model is consistently lower than the measurements even after considering the measurement uncertainties. The PYE+TSI variation tends to over predict SOA concentrations especially at nighttime and in the morning, and also exhibits larger discrepancies with respect to measured POA concentrations (Figure 4). Finally, the performance of the ROB+4xV variation is similar to GRI+TSI, highlighting the uncertainties about the dominant SOA precursors in urban areas (i.e. VOCs vs. P-S/IVOCs).

In general, the measurements peak one hour later than the model, which may be due to the simple treatment of sources and transport in the modeled air mass, but the overall correlation is excellent: R = 0.93 - 0.94 for ROB+TSI, GRI+TSI, PYE+TSI, and ROB+4xV. This study contrasts with an earlier comparison of the ROB and GRI parameterizations for SI-SOA in Mexico City, which showed that GRI produces more SOA than observed (Dzepina et al., 2011). Although the same modeling method was used to quantify the emissions and properties of P-S/IVOCs in both studies, the sources, composition, and SOA yields of P-S/IVOCs in urban areas are poorly characterized, and differences in those between the two urban areas may explain the differences in model performance for Pasadena and Mexico City.

Figure 11. *Model/measurement comparisons for urban SOA mass concentration plotted by time of day. The model results are shown for the* ***(ROB+TSI)****,* ***(GRI+TSI)****,* ***(PYE+TSI)****, and* ***(ROB+4xV)*** *variations. The model variations are described in Table 1. In all panels the SV-OOA determined from measurements at the Pasadena ground site is shown. The uncertainty for the AMS measurement used to determine the SV-OOA concentration is indicated by the dashed lines (Middlebrook et al., 2012).*

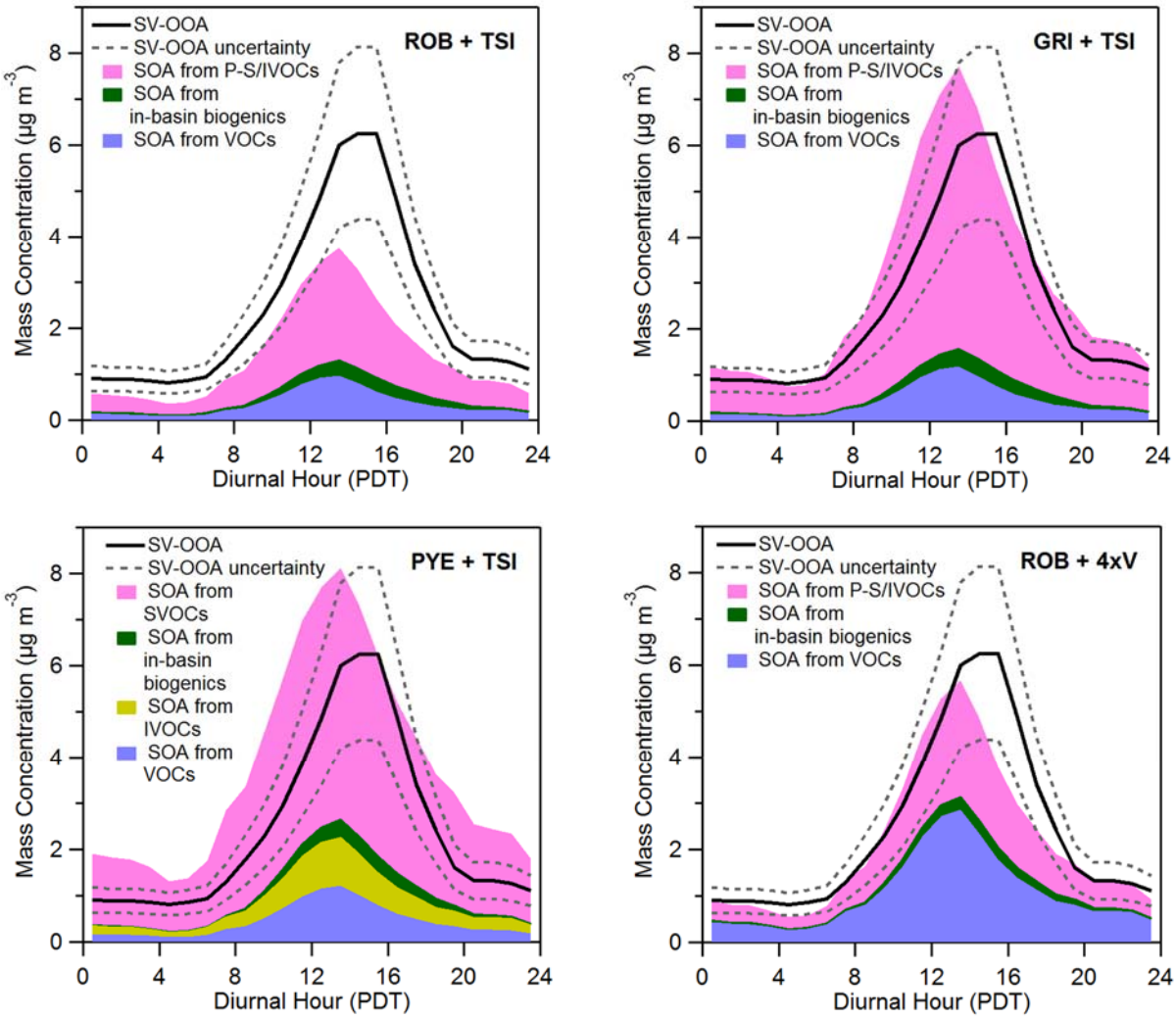

In addition, the effective SOA yields predicted in the box model for P-S/IVOCs can be compared against those determined in previous modeling and smog chamber studies. The effective yield is a function of photochemical aging, and thus for the purpose of this comparison we focus on the effective box model yields for 12:00 – 15:00 when there was a moderate amount of photochemical aging (5 h at an average •OH concentration of 1.5×10^6 molecules cm^{-3}) comparable to the degree of aging typically achieved in chambers. During this period the effective yields for P-S/IVOCs were 12%, 27%, and 36% for ROB+TSI, GRI+TSI, and PYE+TSI, respectively. Zhao et al. (2014) recently carried out a modeling study of SOA formed in Pasadena that was constrained with an extensive set of IVOC data and found an overall SOA yield for IVOCs of 29%, which falls within the range of effective yields for P-S/IVOCs that are predicted by the

box model for the three different parameterizations. Jathar et al. (2014) also recently estimated from chamber studies an effective SOA yield of 10 – 40% for unspeciated organic emissions from combustion sources, which is also consistent with the P-S/IVOC yields from our box model. For reference, the effective yields for the aromatic VOCs m-xylene, toluene, and benzene under high-NOx conditions in chamber studies range from 4 – 28% depending on the precursor identity and chamber conditions (Ng et al., 2007). Similar chamber studies on 12-carbon alkanes determined effective yields ranging from 11% – 160%, where the highest yield corresponded to a cyclic alkane (Loza et al., 2014). In general, it appears that the effective yields resulting from the box model for the lower photochemical ages used here are similar to those determined from other chamber and modeling studies.

It is also possible to compare the predicted IVOC concentrations in the box model versus the concentrations measured by Zhao et al. (2014). The comparison is summarized in Table A-3 of Appendix A. In total, the initial IVOC concentrations in the box model are two times higher compared to those determined from measurements (16 $\mu g\ m^{-3}$ versus 8(±1) $\mu g\ m^{-3}$). In addition, there is a larger difference for the $C^* = 10^3$ bin (2.5 $\mu g\ m^{-3}$ versus 0.2(±0.1) $\mu g\ m^{-3}$). At the same time, the model used by Zhao et al. to predict urban SOA is lower than the measurements by 50% on the urban scale, whereas as the box model used here does not exhibit such a low bias. Given these differences we have run two sensitivity studies to explore how the model predictions depend on the IVOC emissions that are discussed in the following sections. The first sensitivity study reduces the emission of P-S/IVOCs from cooking emissions to zero (Section 3.1.2), and the second sensitivity study reduces all IVOC emissions by one-half (Section 3.1.5). Both of these variations greatly improve the agreement between the modeled and measured IVOC concentrations.

3.1.2. Total SOA concentration: fossil vs contemporary carbon

As described above, on average 71(±3)% of the SV-OOA is composed of fossil carbon (Zotter et al., 2014), and it is important to evaluate whether this percentage is consistent with the model results. As shown in Figure 11, the V-SOA from in-basin biogenics is very small, and V-SOA is overwhelmingly from fossil carbon sources since it is dominated by aromatic precursors (see 3.1.3 below) and the main source of aromatic hydrocarbons in the Los Angeles basin is vehicle emissions (Borbon et al., 2013). For SI-SOA, two types of POA, and thus, primary P-S/IVOCs are included in this study. Since HOA is dominated by vehicle emissions, it is most likely composed of fossil carbon. On the other hand, CIOA will have a majority of modern carbon. In previous work we noted that 0 – 50% of the CIOA mass may be from non-cooking sources and, specifically, from vehicles (Hayes et al., 2013). Furthermore, recent results have shown that cooking emissions can form substantial amounts of SOA (El Haddad et al., 2012). If P-S/IVOCs emitted with HOA are 100% fossil carbon, P-S/IVOCs emitted with CIOA are 25(±25)% fossil, and both emission sources form SI-SOA with the same efficiency, then the corresponding amount of fossil urban SOA in the model would be 65(±9)%, 63(±12)%, 62(±12)%, and 78(±7)% for ROB+TSI, GRI+TSI, PYE+TSI, and ROB+4xV, respectively. It should be noted that these percentages do not include BG-SOA because the ^{14}C results from Zotter et al. (2014) correspond to SV-OOA. None of these predictions are significantly different from the ^{14}C measurements. An important caveat is that P-S/IVOCs from cooking sources are modeled using the same parameters as P-S/IVOCs from vehicle sources. It is possible that cooking and vehicle emissions do not exhibit the same SOA-forming properties, but it is not clear which would be a more potent SOA precursor as there are no parameterizations specific to cooking emissions available in the literature. Thus, the

ROB, GRI, and PYE parameterizations are used for all P-S/IVOCs regardless of their source, and the amount of SOA from HOA (or CIOA) associated P-S/IVOCs can be calculated as simply the product of the total SI-SOA and the ratio HOA/POA (or CIOA/POA), where the hourly HOA, CIOA, and SI-SOA concentrations are used. It should also be noted that in Los Angeles gasoline contains nearly 10% ethanol made from corn and thus modern carbon (de Gouw et al., 2012), but it is thought that ethanol and its combustion products are not incorporated into aerosols (Lewis et al., 2006).

Figure 12. *Model/measurement comparison of SOA mass concentrations after excluding from the model P-S/IVOC emissions, or in the case of the* ***PYE+TSI*** *variation, SVOC emissions from cooking-related activities. Otherwise the figure is identical to Figure 11.*

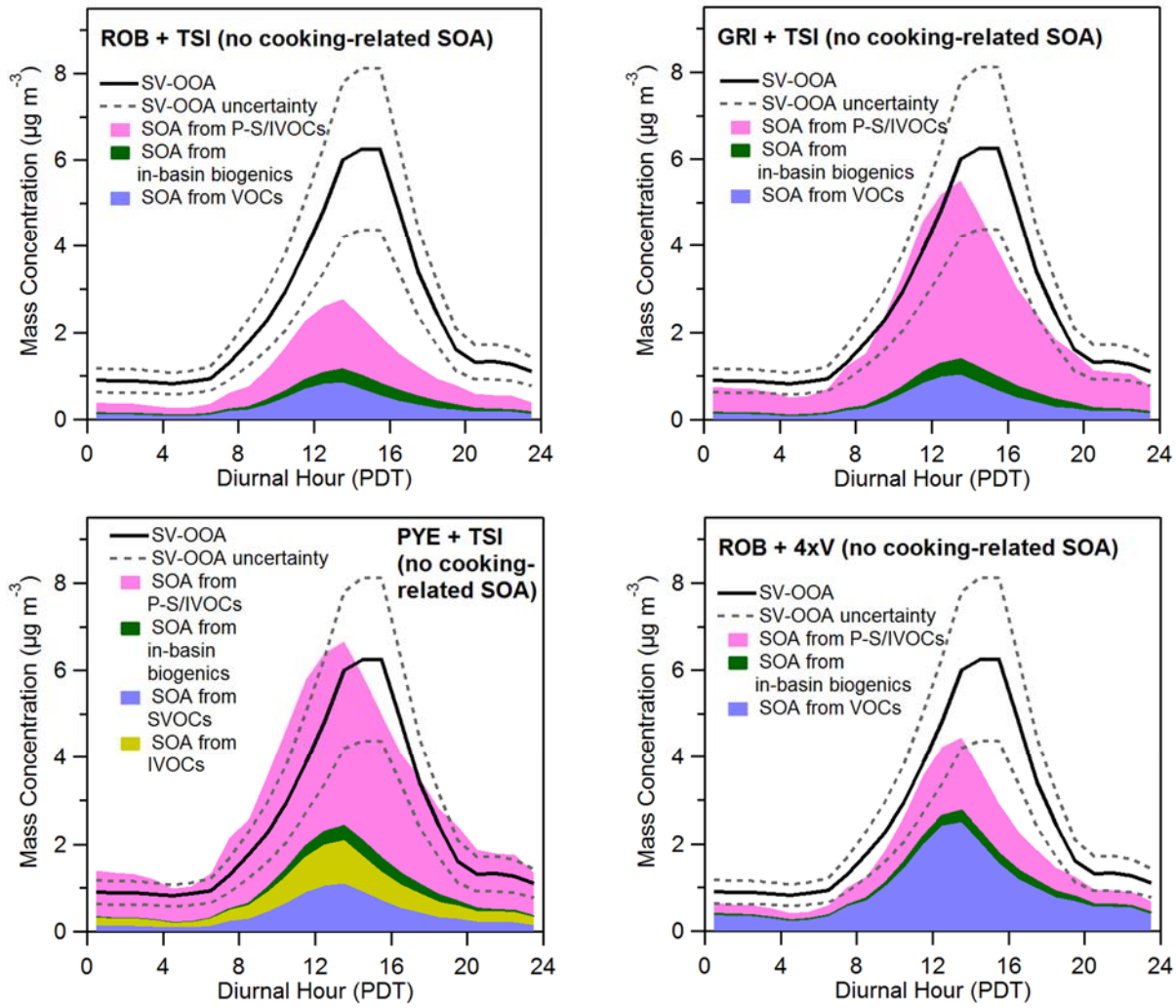

It should be noted that the fossil/modern split from the box model that is described above depends on the initial P-S/IVOCs concentrations and volatility distribution assumed in the model. These parameters are not well constrained for cooking emissions, as discussed in further detail in Section 3.1.4 below. In addition, as discussed in the previous section, the concentration of primary IVOCs in the box model is higher than that measured. Thus, as an extreme sensitivity study, the model variations were also run under the assumption that cooking sources did not emit any P-

S/IVOCs or, in the case of the PYE+TSI variation, any SVOCs (Figure 12). In this sensitivity study there is improved model/measurement agreement for the primary IVOCs as shown in Table A-3 of Appendix A. The GRI+TSI, PYE+TSI, and ROB+4xV variations reasonably reproduce the SV-OOA concentrations with some periods outside the measurement uncertainties. In contrast, the ROB+TSI variation without cooking-related P-S/IVOCs predicts concentrations that are too low. Regardless of the parameterization, a strong urban source of non-fossil SOA precursors, such as cooking emissions, must be included to obtain agreement with the ^{14}C measurements; otherwise the modeled SOA is overwhelmingly fossil. Clearly, there are still large uncertainties in SOA formation from cooking emissions. Further studies are needed to constrain models and to identify potential additional urban sources of non-fossil SOA, although our results suggest that cooking emissions are a potentially important source of anthropogenic non-fossil SOA.

Figure 13. *(A) Predicted SOA mass from precursor VOCs. For clarity only the five largest contributors to the SOA mass are shown. Note that SI-SOA from P-S/IVOCs is not included in this panel. (B) Campaign average concentrations of SOA from specific precursors as determined in the box model as well as by the U.S. EPA tracer method (Kleindienst et al., 2012). Comparisons are shown for methylbenzenes, naphthalenes, isoprene, and monoterpenes. For the naphthalenes the bar for "adjusted emissions" indicates the model variation where the naphthalene emissions are increased in order to match the measured concentrations in Pasadena as shown in Figure 5. The adjusted emissions are also used for the variation with a yield of 1.5 at C*=1. Note: The GRI parameterization is used to predict the SI-SOA for these results.*

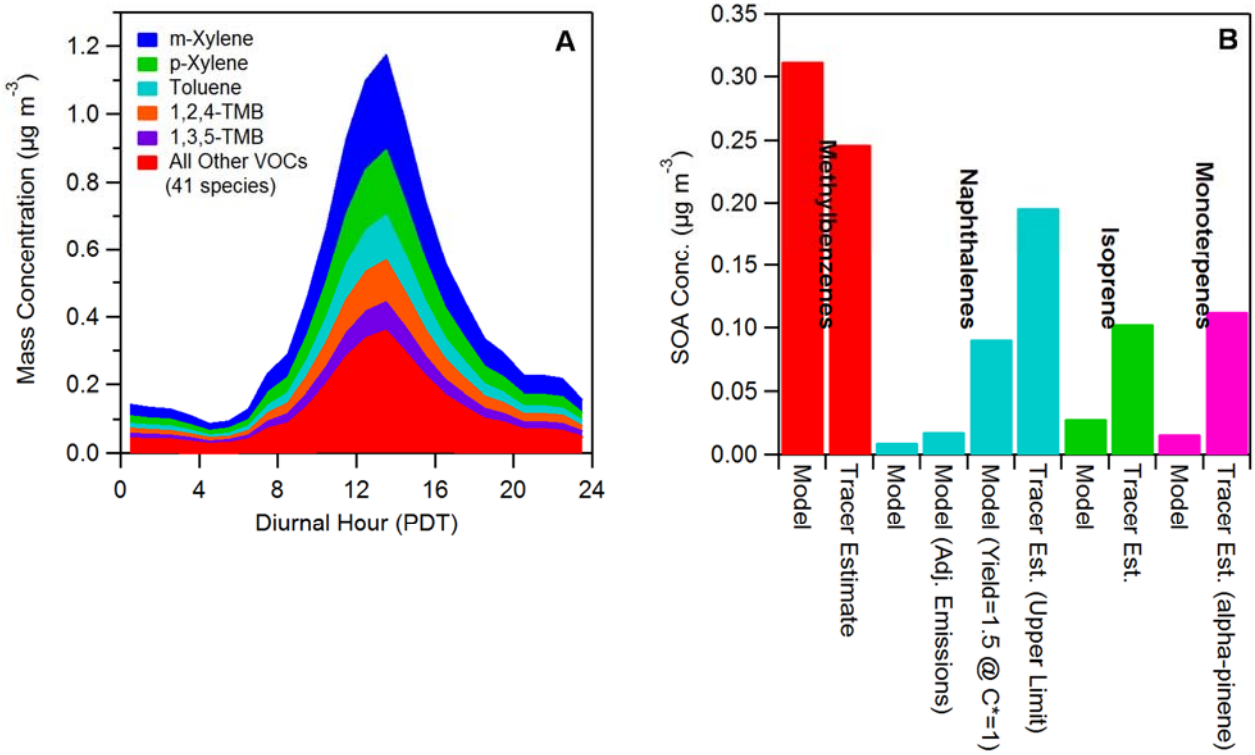

3.1.3. SOA concentration apportionment to precursor compounds

The diurnal cycles of V-SOA mass concentration produced from individual VOCs are shown in Figure 13A. Among the VOCs the five largest contributors to V-SOA are methyl-substituted aromatics such as xylenes, trimethylbenzenes, and toluene. When SOA concentrations peak, these compounds account for ~70% of the predicted V-SOA mass. In Figure 13B the precursor-specific model predictions are compared against results from a methodology developed by the U.S. EPA that apportions SOA to specific precursors using molecular tracers measured in ambient aerosol samples (Kleindienst et al., 2012). For methylbenzenes (i.e. aromatics containing one or more methyl substituents) the tracer molecule utilized is 2,3-dihydroxy-4-oxopentanoic acid, and for naphthalene, 1-methylnaphthalene, and 2-methylnaphthalene the tracer molecule is phthalic acid and its associated methyl-containing analogs. Several tracers are used for isoprene (Edney et al., 2005) and monoterpenes (Jaoui et al., 2005; Claeys et al., 2007; Szmigielski et al., 2007), and they are listed in Table A-4 of Appendix A.

For the methylbenzenes, the model/tracer comparison is good, indicating consistency between model predictions and ambient measurements. The similarity further validates the model, although it is noted that if V-SOA 'aging' is eliminated from the model the model/tracer comparison improves further and the difference becomes less than 5%. We note that this comparison cannot constrain whether chamber yields have been reduced by vapor losses, since the same effect would have occurred when measuring the yields included in the model and when measuring the SOA/tracer ratio used for the tracer estimate.

For the biogenic VOCs, isoprene and the monoterpenes, the tracer estimate indicates several-fold higher concentrations than predicted in the model. This difference is not surprising since the background SOA is thought to have a major contribution from isoprene and monoterpene oxidation in areas north of the Los Angeles Basin, and in the model BG-SOA from different VOCs is not resolved. In other words, the model results in Figure 13B represent only the in-basin biogenic SOA and are lower limits for total SOA from isoprene and monoterpenes. Moreover, the tracer estimates in Figure 13B are likely lower limits as well because the tracers may be lost by subsequent physical or chemical processes occurring in very aged aerosol transported to the measurement location (Hallquist et al., 2009). If the tracer molecule is oxidized or oligomerized, then it will be effectively lost with respect to the tracer method, even if its mass stays in the particle phase. If a semi-volatile tracer evaporates during atmospheric transport or from the filter after sampling, it is also lost from the point of view of the tracer method even though a chemical reaction has not occurred. It appears that the model/measurement comparison for the biogenic VOCs is qualitatively consistent given the known limitations of both approaches. However, the amount of SOA from biogenic VOCs as determined by the tracer method is only ~10% of the BG-SOA (0.22 versus 2.1 $\mu g\ m^{-3}$) even though the BG-SOA is predominantly biogenic as previously noted. The most likely explanation for the difference in mass concentration is the loss mechanisms described above. Other possible sources for the background such as biomass burning or marine OA are known to be very low at this location (Hayes et al., 2013), and more than 69% of the LV-OOA stems from non-fossil sources (Zotter et al., 2014).

Figure 13B also shows a comparison for the naphthalenes. The tracer estimates are over an order-of-magnitude higher than the model predictions when using the SOA yields from the literature (which are ~20% for the conditions of our study) and the emission ratios determined

from the regression analysis of nighttime measurements shown in Figure 5. The model is also run using the empirically adjusted emission ratios that better match the observed concentrations of the naphthalenes. The model for this variation is still much lower than the tracer estimate. As an additional sensitivity study, we also run the model with the adjusted emissions and a yield of 150% that places all the oxidized mass in the C^*=1 μg m^{-3} volatility bin. This last variation represents an upper limit estimate of SOA from naphthalenes, in which nearly all of the mass plus the added oxygen partitions to the particle phase, which is much higher than laboratory observations. The tracer estimate, however, is still about a factor of two higher than the model. It is known that the tracer estimate is an upper limit, because the tracer compound, phthalic acid, may not be a unique tracer, and it potentially could be emitted from primary sources (Kleindienst et al., 2012). However, there may be other alkylated or functionalized PAHs that are not explicitly accounted for in the box model, and some of them might produce this tracer.

The best estimate from the model with the adjusted emissions results in 0.7% of the predicted SOA being formed from the measured naphthalenes. Utilizing the upper limit of the model results for the PAHs, including that from the parameterization with a purposefully high yield, it is apparent that naphthalene, 1-methyl naphthalene, and 2-methyl naphthalene account for less than 4% of the SOA mass. While previous work has suggested that PAHs are important precursors for SOA in the Los Angeles Basin (Hersey et al., 2011) these earlier findings were qualitative and based on the observation of phthalic acid in samples. The work presented here, both the modeling results as well as the tracer results, quantitatively demonstrates that SOA from identified PAHs is relatively small but not negligible when compared to the total SOA concentration. An upper limit for the contribution of this group of precursors is 8(±3)% of the SOA. This percentage is calculated using the tracer method in which the SOA concentration from PAHs is higher than in the box model and a 30% uncertainty for the SV-OOA concentration. Lastly, we note that no suitable tracers for alkane oxidation have been identified yet, which prevents carrying out similar model/tracer comparisons with respect to the P-S/IVOCs, since these compounds are thought to be composed primarily, although not exclusively, of alkanes.

3.1.4. SOA concentration apportionment to gasoline vehicles, diesel vehicles, cooking activities, and in-basin biogenic sources

In addition to apportioning the amount of SOA formed from individual compounds there is also considerable recent interest in the apportionment of SOA between diesel and gasoline vehicle emissions as well as other urban sources (Bahreini et al., 2012; Gentner et al., 2012; Hayes et al., 2013; Ensberg et al., 2014). The SOA model developed here can be used to address this important problem, and in Figure 14 the urban SOA mass calculated in the model is apportioned between diesel vehicles, gasoline vehicles, cooking sources, and in-basin biogenic emissions. The SOA mass is apportioned to each source using the following method, which can be described in five steps. First, the background is set to 2.1 μg m^{-3}. Second, the in-basin biogenic SOA is calculated as described in the methods section. Third, for the diesel contribution, since it was previously estimated that 70(±10)% of the vehicle OA (surrogated by the measured HOA here) is emitted from diesel vehicles (Hayes et al., 2013), it is assumed in the model that 70% of the P-S/IVOCs co-emitted with HOA are from diesel vehicles as well. The remaining 30% of the measured HOA is assumed to be emitted by gasoline vehicles. For both diesel and gasoline emissions the amount of P-S/IVOC emitted is estimated with the approach discussed in p.15 and illustrated in Fig. 3.

While VOCs emissions from diesel vehicles are low (Warneke et al., 2012) in the Los Angeles Basin, VOCs have still been measured in diesel fuel. Specifically, using the measurements of Gentner et al. (2012) given in Tables S9 and S10 of that paper, the percentage of each VOC included in our model emitted from diesel vehicles is calculated. The precursor-specific SOA concentrations, as shown in here in Figure 13, are then multiplied by these percentages to determine the fraction of V-SOA attributable to diesel emissions, which is 3%. It should be noted that for all the VOCs included here except 1,3-butadiene, styrene, and anthropogenic isoprene, the corresponding concentrations in gasoline and diesel fuel are published in Gentner et al. (2012). Fourth, the cooking contribution is calculated by assuming that 75% of the P-S/IVOCs co-emitted with CIOA are from cooking activities. This percentage is chosen since it lies halfway between 50 and 100%, which is the current constraint from measurements on the amount of CIOA from cooking sources as discussed above and in Hayes et al. (2013). Fifth, the gasoline fraction is taken to be the SOA formed from all the remaining VOCs as well as the remaining P-S/IVOCs.

Figure 14. *The estimated fractional contribution to SOA mass concentration from gasoline vehicles, diesel vehicles, cooking emissions, and in-basin biogenic emissions. The results for the four model variations are displayed as pie charts as well as a bar chart. The bar chart also shows the percentage of SOA that is from fossil or modern sources as determined by Zotter et al. (2014). The modern sources are indicated by hollow bars and fossil sources are indicated by solid bars. Background SOA is not included in this figure, but the analogous figure with background SOA is given in Figure 15.*

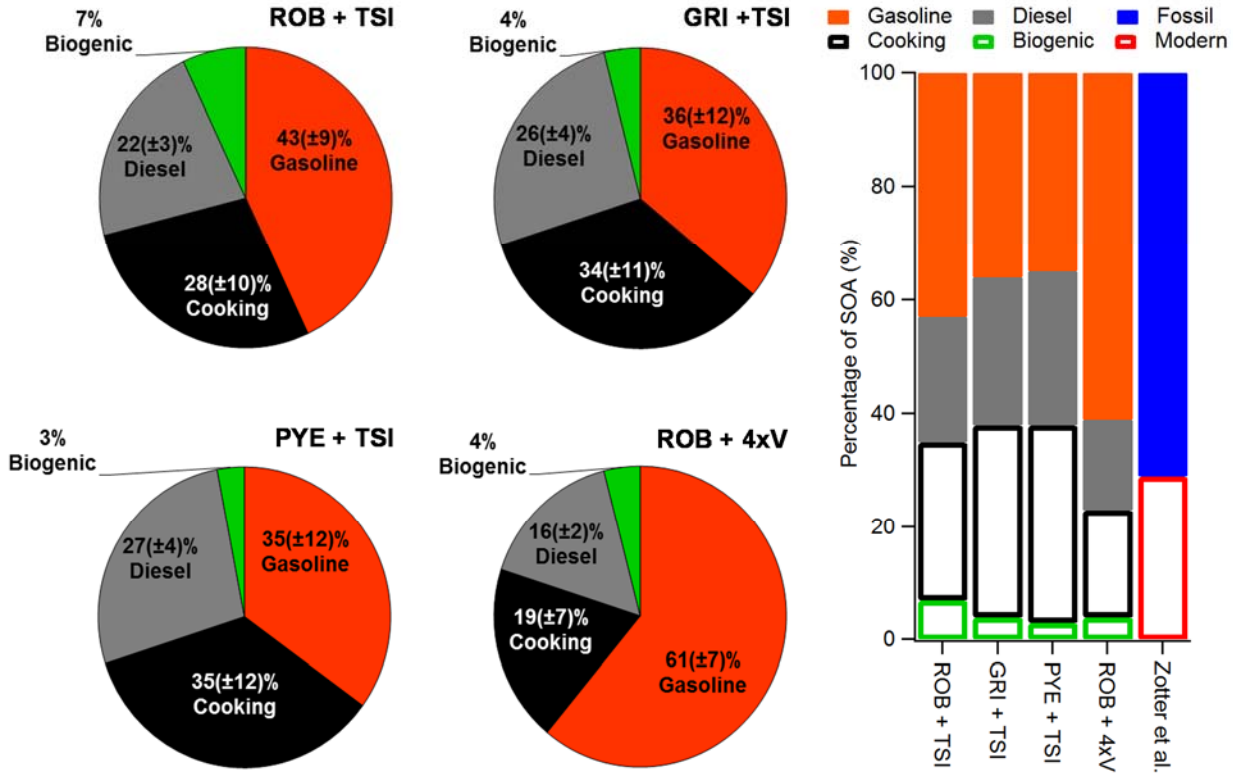

As can be seen in Figure 14, for the urban SOA (i.e. excluding the background OA) diesel, gasoline, and cooking emissions all contribute substantially to SOA formation, with the sum of

gasoline and cooking being much larger than diesel for all model variants. In contrast, the in-basin biogenic contribution is small. The analogous results when the background is included are shown in Figure 15. The formation of SOA from diesel emissions accounts for 16 – 27% of the urban SOA in the model depending on the variant used. This result is very similar to the percentage reported in our previous work, 19(+17/-21)%, which was determined using measurements of OOA weekly cycles (Hayes et al., 2013). In addition, the existence of a diesel contribution in the model is consistent with PMF analysis of FTIR spectra of OA filter samples collected in Pasadena, in which, one SOA component exhibited relative peak intensities in the C-H stretching region that suggest some contribution from diesel emissions (Guzman-Morales et al., 2014), although the percentage of SOA from diesel could not be determined in this previous work. The results of our work stand in contrast to those of Gentner et al. (2012) however, wherein the contribution of diesel and gasoline to vehicular SOA were estimated to be 70% and 30%, respectively. This discrepancy may be due to the assumption used by Gentner et al. that effectively all vehicle emissions are unburned fuel, whereas recent experiments have indicated that important SOA precursors exist in gasoline vehicle emissions that are not present in unburned gasoline when after-treatment devices such as catalytic converters are used (Jathar et al., 2013).

Also shown in Figure14 is a bar graph summarizing the result from each parameterization grouped by fossil and non-fossil sources as well as the fossil fraction of SV-OOA determined by Zotter et al. (2014). The results of the two studies are consistent, with cooking and in-basin biogenic SOA accounting for between 23 – 38% of the in-basin SOA mass in the models. These two sources represent the modern fraction in the box model.

The uncertainties shown in Figure 14 (in parentheses) are calculated by propagating the uncertainty in the amount of HOA from diesel sources, as well as the uncertainty in the amount of CIOA from cooking sources under the assumption that the P-S/IVOCs co-emitted with these primary aerosols have similar uncertainties. It is also noted that another source of uncertainty is the selection of the ROB+TSI, GRI+TSI, PYE+TSI, or ROB+4xV model variation. The model variant used has an important impact on the apportionment, but the greatest amount of urban SOA formed from diesel emissions when considering all the uncertainties described in this paragraph is still only 31%.

The uncertainties in Figure 14 do not however account for certain assumptions that were made in order to perform the source apportionment. In particular, it was assumed that the P-S/IVOCs to POA ratio as well as the volatility distribution of P-S/IVOCs is the same for all sources, which is likely not the case. However, to our knowledge there is insufficient information in the literature to prescribe different volatility distributions for different sources.

Lastly, the percentage of SOA attributed to cooking emission in this work also requires discussion. Compared to gasoline or diesel vehicles there is relatively little data on the SOA forming potential of cooking emissions, but nevertheless there is both direct and indirect data supporting the SOA forming potential of cooking emissions. First, it is clear from numerous source apportionment studies that cooking emissions are a source of organic matter in the atmosphere (e.g. Robinson et al., 2006; Mohr et al., 2011; Hayes et al., 2013). Second, molecular speciation of cooking emissions has demonstrated that cooking activities emit a variety of volatile and semi-volatile compounds that are known SOA precursors (Schauer et al., 1999, 2002). Third, chamber studies have demonstrated SOA formation from cooking emissions. The latter results have been presented at several major conferences, but have not yet been published in the peer-reviewed

literature (El Haddad et al., 2012). Thus, it is reasonable to conclude that SOA models should include the SOA resulting from chemical processing of cooking emissions, but there is a lack of chamber yields that could be used to develop specific SOA parameterizations. We have therefore assumed that SOA from cooking emission can be described using the same parameterizations as used for SOA from vehicular P-S/IVOCs. The amount of emitted P-S/IVOC from cooking is estimated with the same method used for vehicle emissions (p.15), and thus the fraction of these precursors emitted from cooking is proportional to the measured CIOA/(HOA+CIOA). We have also performed a sensitivity study where we assume that cooking emissions do not produce any SOA. Ultimately, the percentage of SOA from cooking emissions reported here should be considered a first-order estimate that should be updated when additional data regarding SOA from cooking emissions becomes available.

Figure 15. *The estimated relative concentration of SOA from gasoline vehicles, diesel vehicles, cooking emissions, in-basin biogenic emissions, and the regional background.*

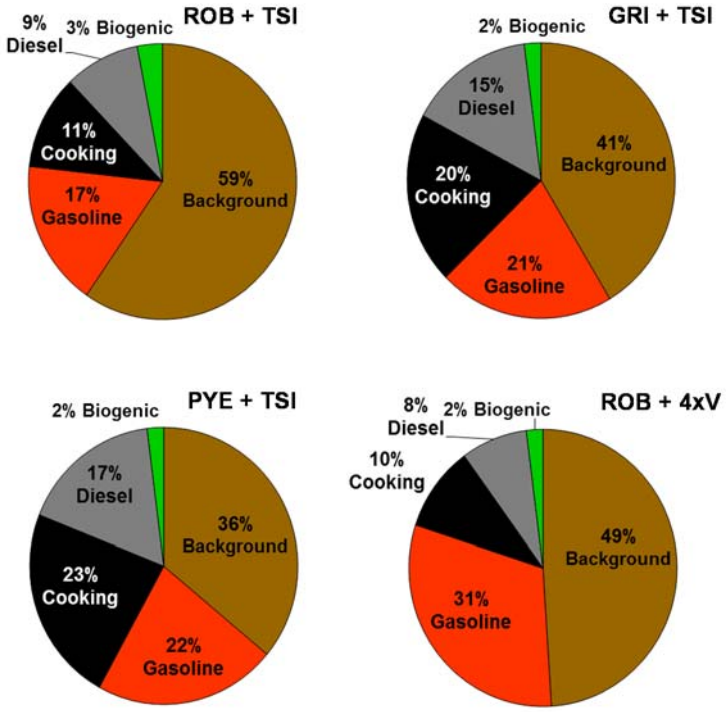

3.1.5. Evolution of SOA concentration for 3 days

It is of high interest to explore the evolution of the different parameterizations discussed here at greater photochemical ages than those observed at the Pasadena site, since this behavior can lead to different results in regional and global modeling studies, and since similar combinations of parameterizations were found to overpredict regional SOA downwind of Mexico City (Dzepina et al., 2011). To explore this question, the evolution of SOA concentration was simulated for 3 days using each of the four major variations (ROB+TSI, GRI+TSI, PYE+TSI, ROB+4xV). The same simulation was carried out for the SIMPLE model and it is discussed below in Section 3.3. The results are shown in Figure 16, and in order to facilitate comparisons the SOA concentrations are normalized to the CO concentration, after subtracting the CO background (DeCarlo et al., 2010). These simulations are for continuous aging at a reference •OH concentration of 1.5×10^{6}

molec cm^{-3}, and thus, they do not attempt to simulate a diurnal variation in the amount of photochemical aging. This approach is used because it facilitates the comparison against field measurements described below. Furthermore, the box model does not account for how dilution downwind of Los Angeles may increase SOA evaporation and thus the rate of oxidation via increased partitioning to the gas phase. However, this phenomenon would only lead to small changes in total model SOA, and that should not change the conclusions discussed in this section (Dzepina et al., 2011). Also shown in Figure 16 is the same ratio, SOA/ΔCO, determined previously from measurements at the Pasadena site (Hayes et al., 2013). At photochemical ages less than 0.25 days, GRI+TSI and ROB+4xV perform the best (Table 3), which is consistent with the comparisons against the diurnal average of SOA since the diurnal photochemical age peaks at about 0.25 days (Figure 6A). However, for higher photochemical ages between 0.25 and 0.5 days the performance of ROB+TSI improves.

Figure 16. *SOA concentration predicted by the ROB+TSI, GRI+TSI, PYE+TSI, and ROB+4xV parameterizations for up to 3 days of photochemical aging at a reference •OH concentration of 1.5×10^{6} molec cm^{-3}. Also shown in the four panels is the same result for the SIMPLE model using the optimized parameters. Note that the SOA concentrations have been normalized to the background subtracted CO concentration to account for changes in emission strengths, and the processed data are identified by the symbol SOA/ΔCO. In addition, the SOA/ΔCO data determined for the Pasadena site from the measurements of Hayes et al. (2013) are shown as well as similar airborne measurements for the Los Angeles basin outflow performed by Bahreini et al. (2012) aboard the NOAA P3 (black marker). The Bahreini et al. data corresponds to an average of all data between 1 – 2 days of photochemical aging. The OA/ΔCO ratio reported by de Gouw and Jimenez (2009) is also indicated (gray box) as an estimate of SOA/ΔCO in highly aged air masses.*

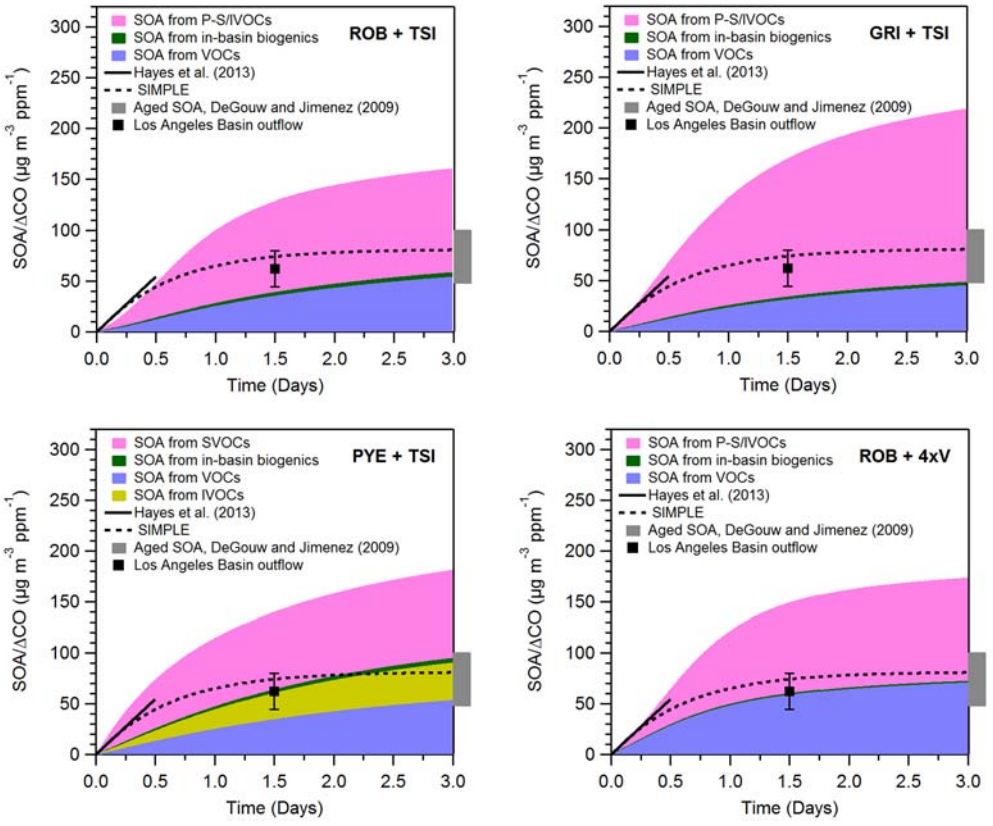

Table 3. *Slope of SOA/ΔCO as reported by Hayes et al. (2013), and as predicted in the four major box model variations. For the box model, the slopes are obtained by performing a linear ODR analysis on the data shown in Figure 16.*

Variation	**SOA / ΔCO slope between 0 and 0.25 Days**	**SOA / ΔCO slope between 0.25 and 0.5 Days**
Observed (Hayes et al. 2013)	108 μg m^{-3}	
ROB + TSI	69 μg m^{-3} $ppmv^{-1}$	88 μg m^{-3} $ppmv^{-1}$
GRI + TSI	110 μg m^{-3} $ppmv^{-1}$	130 μg m^{-3} $ppmv^{-1}$
PYE + TSI	168 μg m^{-3} $ppmv^{-1}$	153 μg m^{-3} $ppmv^{-1}$
ROB + 4xV	105 μg m^{-3} $ppmv^{-1}$	123 μg m^{-3} $ppmv^{-1}$

We also note that all of the parameterizations used in this section produce SOA/ΔCO ratios substantially larger (by factors of 2 or more) than those observed globally for aged air masses (i.e. photochemical ages greater than one day at an average OH concentration of 1.5×10^6 molec cm^{-3}). For reference the range of OA/ΔCO ratios reported by de Gouw and Jimenez (2009) for aged urban SOA across multiple sites is indicated by the gray regions in Figure 16. This OA/ΔCO ratio includes both POA and SOA, but POA is a small contributor to OA/ΔCO for very aged air. Also shown in Figure 16 is the SOA/ΔCO ratio observed by Bahreini et al. (2012) from the NOAA P3 aircraft in the Los Angeles Basin outflow where air masses were aged from 1 – 2 days. This ratio is similar to the range taken from de Gouw and Jimenez (2009). The differences between the modeled and the measured SOA/ΔCO at higher photochemical ages may be important for regional and global models as they suggest an overestimation of urban SOA downwind of polluted regions. One possible explanation for the higher predicted values is the lack of a fragmentation mechanism in the parameterizations, which would reduce the SOA mass by producing higher volatility products. Indeed, decreases in SOA concentration at high photochemical ages have been observed in flow-tube studies, although typically at photochemical ages much longer than 3 days (George and Abbatt, 2010). Also dry deposition in the regional models may decrease over-prediction depending on how it is implemented (Knote et al., 2014a).

A third explanation is the potential overestimation of IVOC emissions in the box model. As discussed in Section 3.1.1, the initial concentration of primary IVOCs in the model is a factor of 2 higher than the values determined from field measurements by Zhao et al (2014). To investigate this possibility, a sensitivity study was run in which the initial concentrations of primary IVOCs in the volatility bins C*= 10^3, 10^4, 10^5, and 10^6 were decreased by one-half. The results of this sensitivity study are shown in Figure 17. In general, ROB+TSI, GRI+TSI, PYE+TSI, and ROB+4xV all show better agreement with measurements at long photochemical ages, although all four variants still overestimate the measurements. For shorter photochemical ages (in the urban scale) ROB+TSI under-predicts the SOA concentration, whereas GRI+TSI and ROB+4xV both predict SOA/ΔCO ratios that are not significantly different from the measured values (Hayes et al., 2013), and lastly PYE+TSI overestimates the SOA concentration. Thus, IVOCs emissions that

are too high in the box model may be responsible for some, but not all, of the overestimation of SOA concentrations at long photochemical ages.

Figure 17. *SOA concentration predicted by the ROB+TSI, GRI+TSI, PYE+TSI, and ROB+4xV parameterizations for up to 3 days of photochemical aging at a reference •OH concentration of 1.5×10^6 molec cm^{-3}. These predictions correspond to the sensitivity study in which the concentration of IVOCs in the volatility bins $C^*=10^3 – 10^6$ were reduced by one-half. Also shown in the three panels is the same result for the SIMPLE model using the optimized parameters (see Section 3.3 for further discussion). Note that the SOA concentrations have been normalized to the background subtracted CO concentration to account for changes in emission strengths, and the processed data are identified by the symbol SOA/ΔCO. In addition, the SOA/ΔCO data determined for the Pasadena site from the measurements of Hayes et al. (2013) are shown (black line) as well as similar airborne measurements downwind of Pasadena performed by Bahreini et al. (2012) aboard the NOAA P3 (black marker). The Bahreini et al. point corresponds to an average of all LA Basin outflow data between 1 – 2 days of photochemical aging. The OA/ΔCO ratio reported by de Gouw and Jimenez (2009) is also indicated (gray box) to serve as an estimate of SOA/ΔCO in highly aged air masses.*

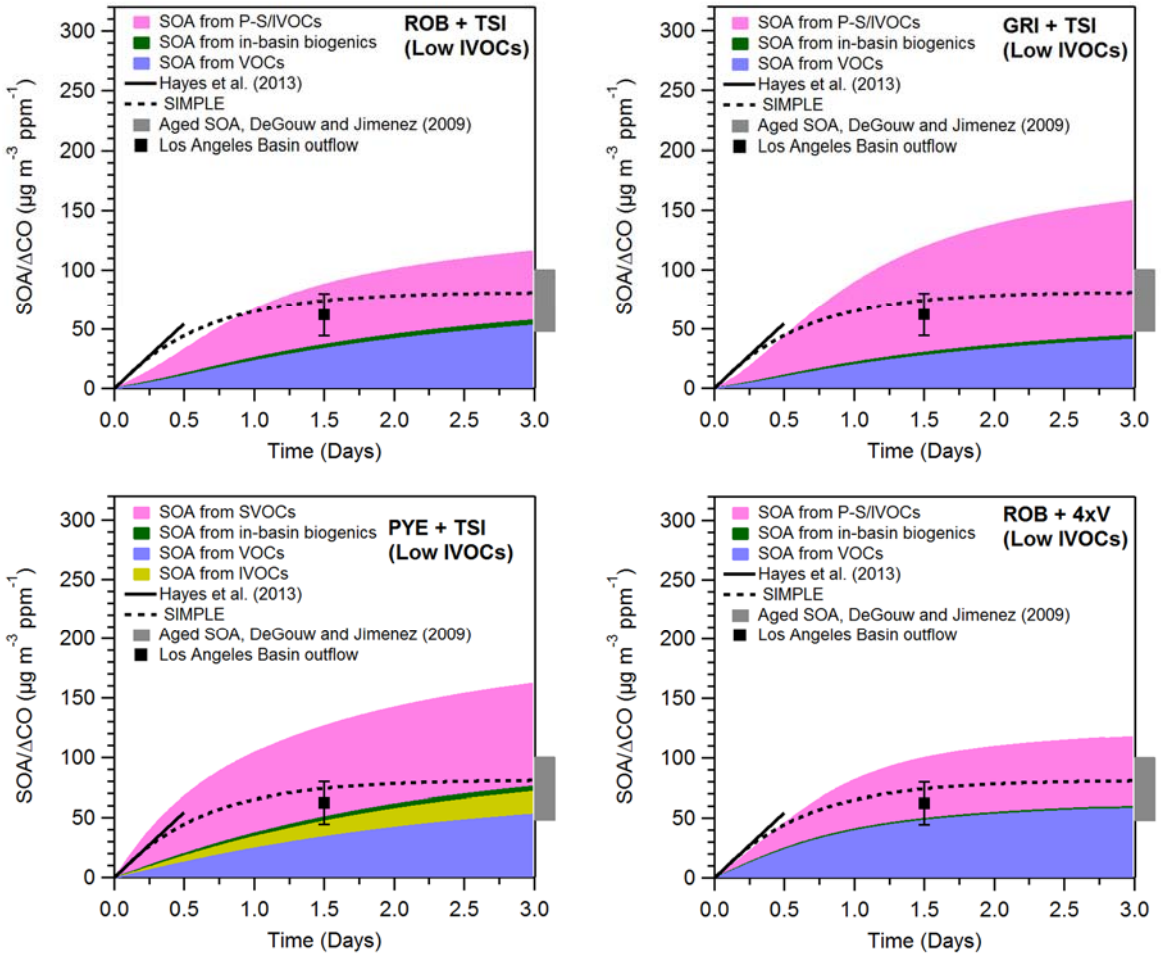

Figure 18. *Model/measurement comparison of SOA mass concentration after reducing the emission of IVOCs in the model by one-half. Otherwise the figure is identical to Figure 16.*

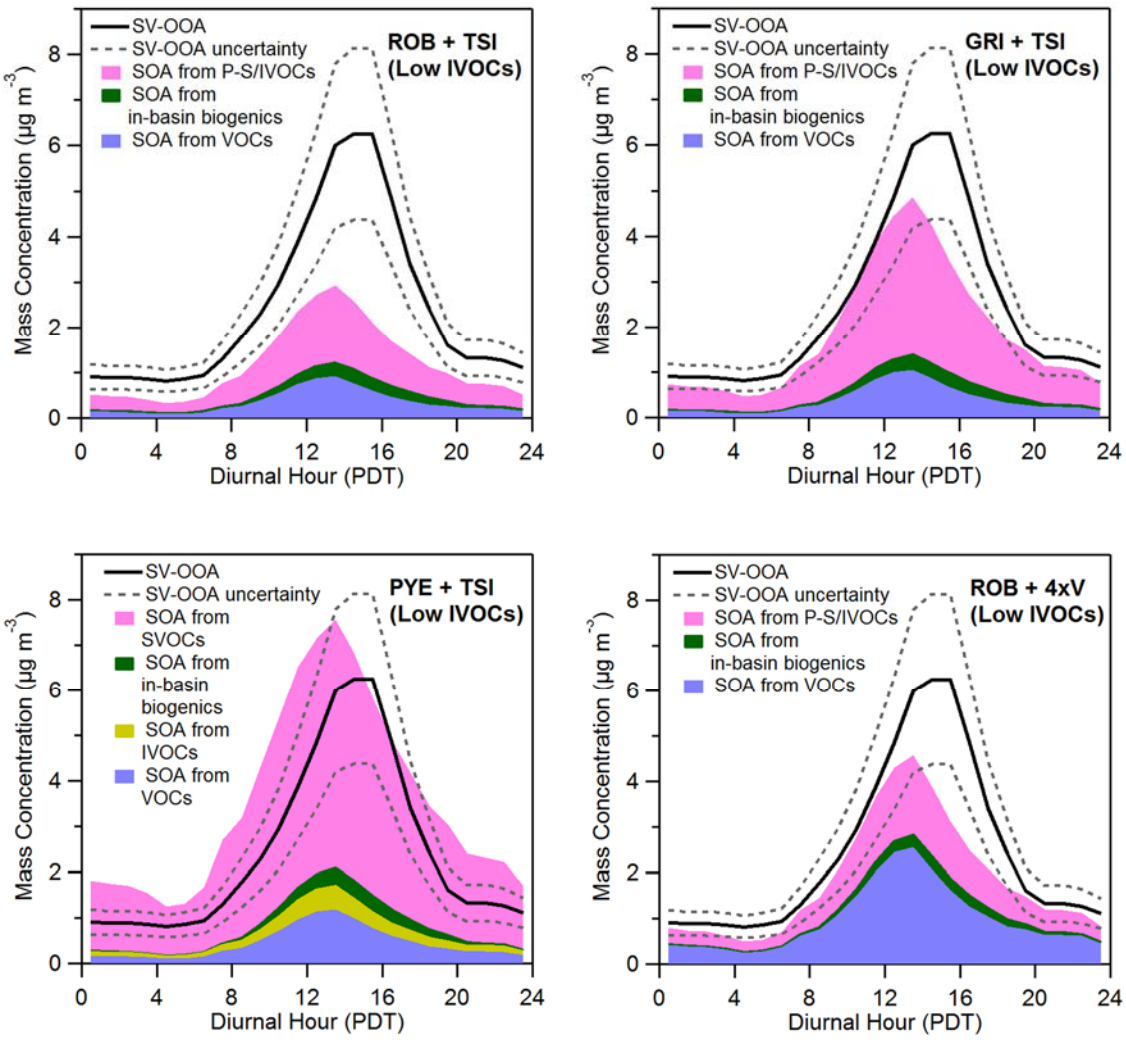

For reference, we note that when the IVOC concentrations are halved the four variations all predict less SI-SOA for the Pasadena ground site (Figure 18), but the contribution of P-S/IVOCs to SOA formation remains important: 59 – 73% (ROB+TSI), 72 – 80% (GRI+TSI), 79 – 92% (PYE+TSI), 38 – 48% (ROB+4xV). Furthermore, all four variations still predict a fossil fraction of urban SOA consistent with the ^{14}C measurements at the Pasadena site: 66(±9)%, 64(±10)%, 61(±12)%, 78(±6)%, respectively. Note that in calculating these fossil fractions the IVOCs emissions from cooking and gasoline/diesel were reduced by the same amount (i.e. one-half).

3.1.6. Comparison of WRF-CMAQ versus measurements and box model

The comparison of the SOA predicted for Pasadena by the WRF-CMAQ model is shown in Figure 19A. Unlike the box model, the 3-D WRF-CMAQ model simulates the production and transport of SOA both within and outside the Los Angeles Basin. It is therefore most appropriate to compare the WRF-CMAQ model output with OOA (SV-OOA + LV-OOA) rather than just SV-OOA as is done for the box model that focused only on the urban area. The WRF-CMAQ SOA is

well correlated with the measured OOA (R= 0.73), but the SOA mass concentration in the model is ~25 times lower than the observed amount. This discrepancy is observed despite the fact that the VOCs show reasonable agreement (Fig. 20, Panels A – C). The difference of a factor of 25 in the SOA concentrations is also observed consistently across different photochemical ages (Fig. 20, Panel D). Furthermore, the performance of WRF-CMAQ is good for the inorganic aerosol species (Fig. 21 and 22) as well as for elemental carbon and different meteorological parameters (Baker et al., 2013; Kelly et al., 2014). These comparisons indicate that while the model appears to be accurately simulating the transport to Pasadena and photochemical aging, the amount of SOA formed from urban precursors is greatly underestimated by WRF-CMAQ. Given the importance of P-S/IVOCs as SOA precursors in the box model, the lack of these species in WRF-CMAQ explains a substantial fraction of the difference between the models.

Figure 19. *(A) Scatter plot of SOA predicted by the WRF-CMAQ model versus the OOA determined from measurements at the Pasadena ground site. Also shown in this panel is an ODR linear regression analysis of the data with the y-intercept fixed to zero. (B) SOA diurnal cycles from the WRF-CMAQ and box model. The box model was run using an empirical two product parameterization (i.e., Model Variant 5 in Table 1) wherein the oxidized products cannot undergo aging (Dzepina et al., 2009).*

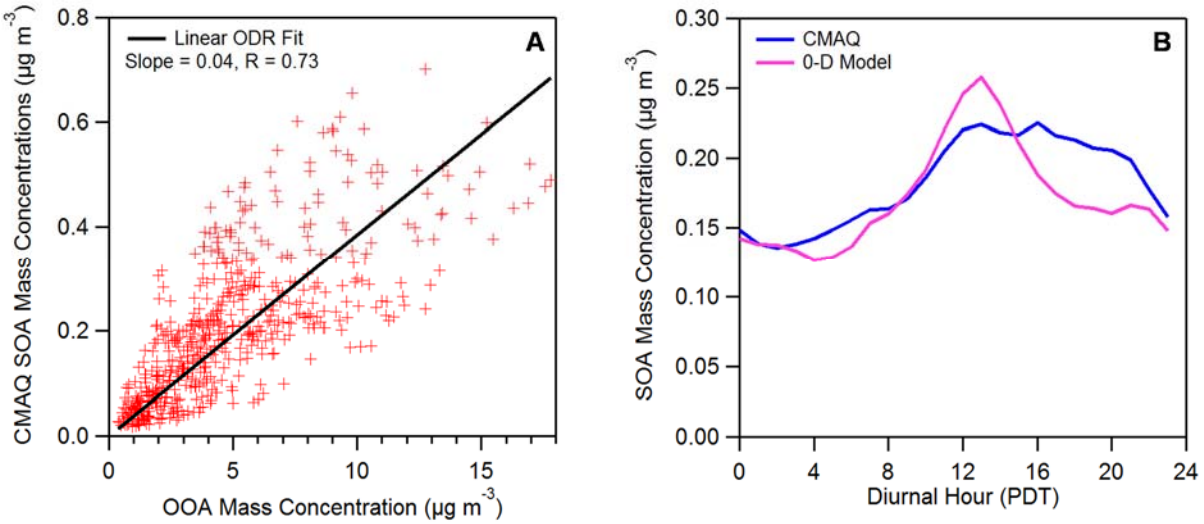

To further examine both WRF-CMAQ and the box model results, we modify the SOA module of the box model to be similar to the treatment of urban SOA in WRF-CMAQ as described by Carlton et al. (2010). First, for the box model P-S/IVOCs are not included, since these species are not in WRF-CMAQ. Second, the BG-SOA in the box model is adjusted to 0.1 µg m^{-3} so that the concentrations of SOA in the two models are similar in the early morning hours when the background dominates. Third, the box model uses a different approach for simulating V-SOA identical to that described by Dzepina et al. (2009). Briefly, instead of the VBS, an empirical 2-product parameterization wherein the oxidized products cannot undergo aging is used (Koo et al., 2003).

$$VOC + \bullet OH \rightarrow \alpha_1(SVOC_1) + \alpha_2(SVOC_2) \quad (3)$$

Figure 20. *Scatter plots of* ***(A)*** *benzene,* ***(B)*** *low-yield aromatic VOCs, and* ***(C)*** *high-yield aromatic VOCs measured by GC-MS against the concentration predicted by WRF-CMAQ. The*

low-yield aromatics correspond to the family ARO1 and the high-yield aromatics to the family ARO2 in Table A1. Also shown for reference are the 5:1, 1:1, and 1:5 lines. ***(D)*** *SOA/ΔCO as a function of photochemical age as determined by measurements (black circles) and predicted by WRF-CMAQ (red squares). The left and right axes are plotted on different scales for clarity. Photochemical age is estimated from the ratio of NO_Y to NO_X (Hayes et al., 2013).*

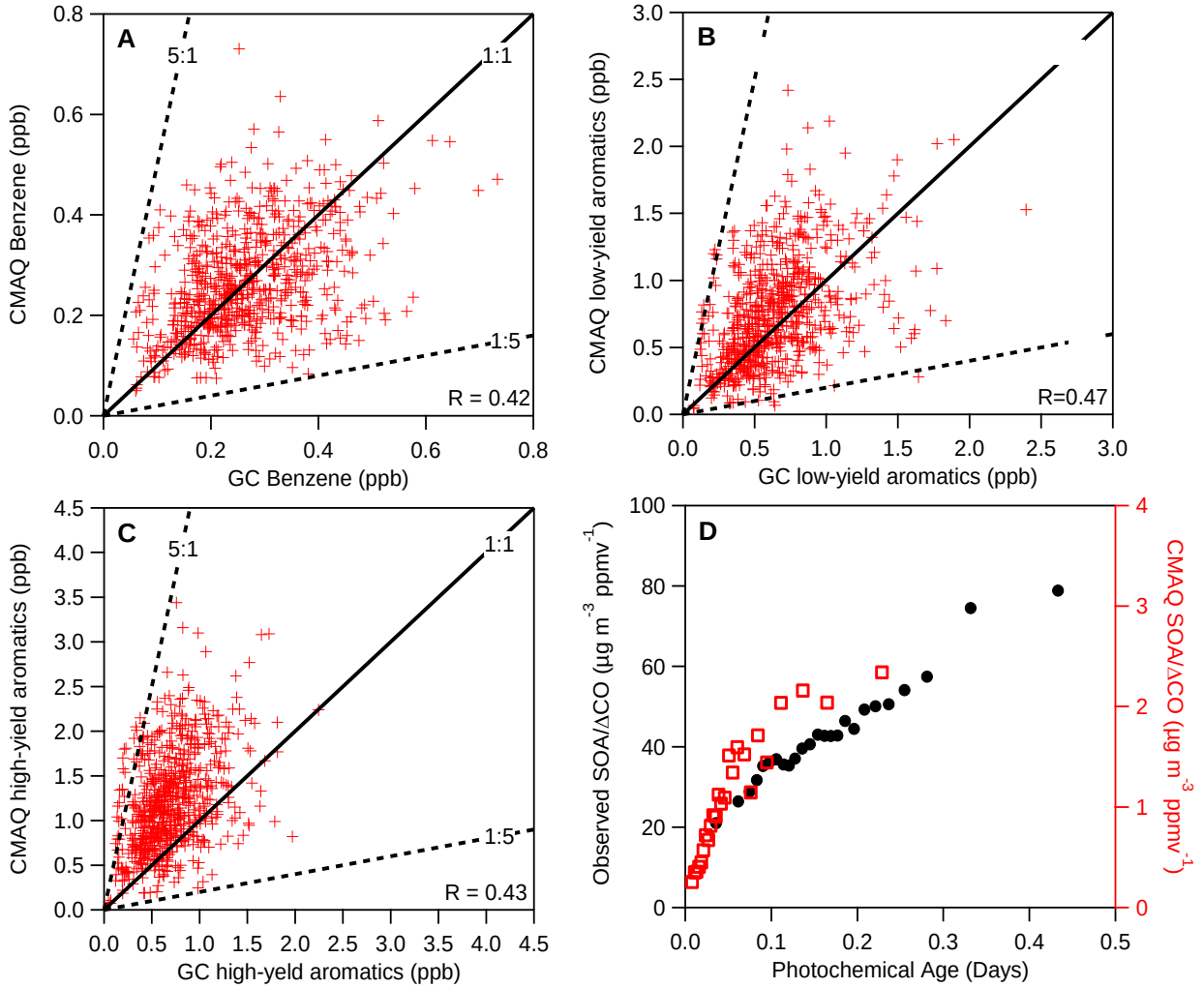

The effective saturation concentration for each lumped product, *SVOC*, is then used to calculate the equilibrium partitioning between gas- and particle-phases as shown earlier in Equation 1. Also, in Equation 3, α is the yield for each VOC. Note that the Koo et al. (2003) parameterization produces substantially lower V-SOA yields than the Tsimpidi et al. (2010) parameterization used in the rest of this work. The latter parameterization was updated using more recent chamber results (with higher yields) such as those of Ng et al. (2007). The use of the older Koo et al. (2003) parameterization for this specific comparison was motivated by the fact that the parameterization for urban SOA in the version of CMAQ used here is based on the same older data and does not contain the higher updated yields in, for example, Tsimpidi et al. (2010).

Figure 21. *Time series of inorganic and organic aerosols at the Pasadena ground site during CalNex measured by an AMS or modeled by WRF-CMAQ. For SOA, the concentration was determined using positive matrix factorization analysis of the AMS measurements. The AMS measurements have a PM_1 size cut, and the WRF-CMAQ model results are the sum of the Aiken and accumulation modes, which corresponds to $PM_{2.5}$. (Note: In WRF-CMAQ all SOA species are assigned to the accumulation mode.)*

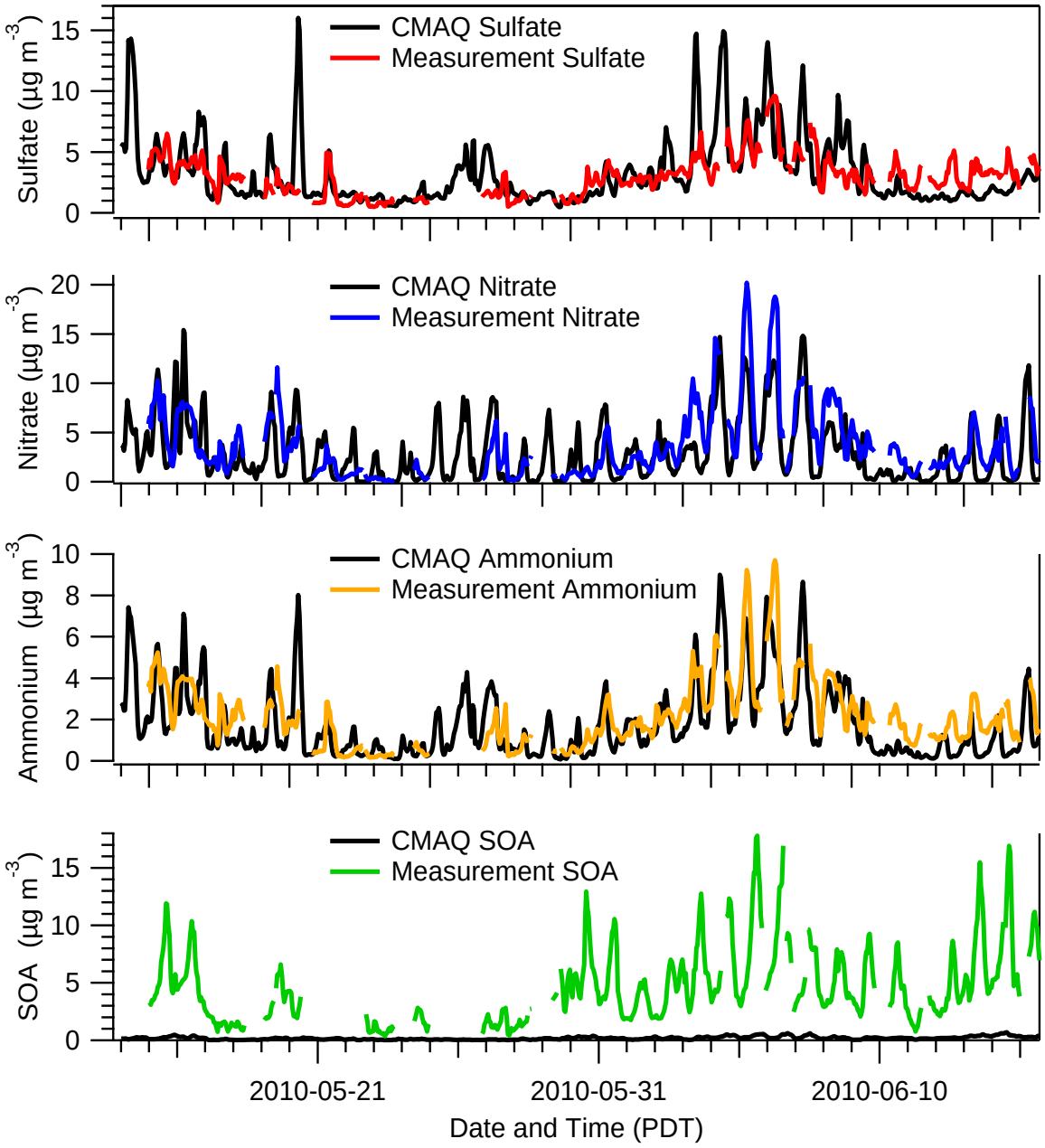

The results of the comparison of WRF-CMAQ with the modified box model are shown in Figure 19B. With those modifications the results are very similar. This good agreement indicates that the differences between the default box model and WRF-CMAQ are not due to differences in transport or another variable, but rather the intrinsic differences in the SOA modules. In addition,

the comparison between the two models suggests that 3-D air quality models need to include either SOA from P-S/IVOCs, additional precursor sources, and/or increased V-SOA yields to accurately predict SOA concentrations in the Los Angeles Basin and other urban areas.

Figure 22. *Scatter plots of the inorganic aerosol measurements from an AMS against the modeled concentrations from WRF-CMAQ. The data shown are the same as in Figure 21. Also shown are the corresponding linear ODR analyses and corresponding fit parameters.*

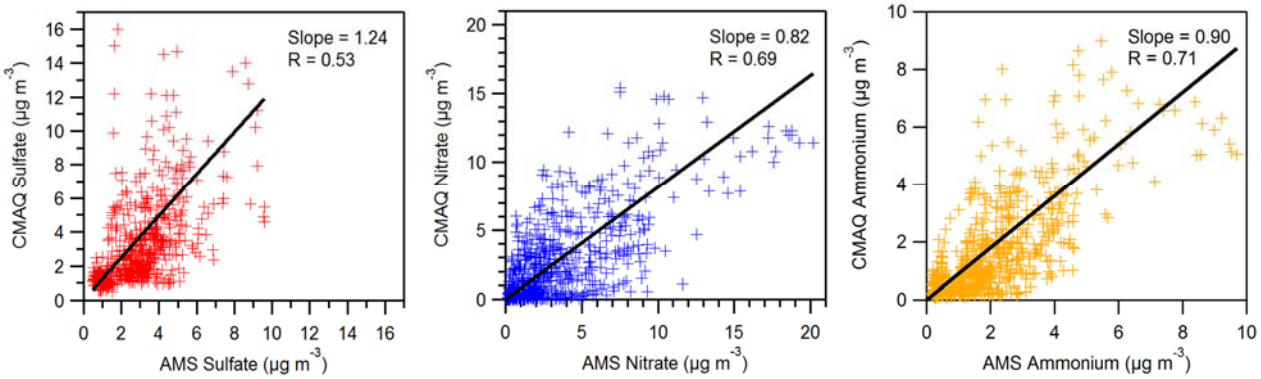

Figure 23. *Model/measurement comparison for O:C of total OA versus time of day. The left panel contains the results when using the ROB+TSI model variation, whereas the right panel contains the results when using the GRI+TSI model variation. In both panels the O:C of OA measured at the Pasadena ground site is shown along with the O:C uncertainty. Shown in both panels is the model O:C when including only the SOA from VOCs (blue line), and the model O:C when including the SOA from both VOCs and P-S/IVOCs (pink line).*

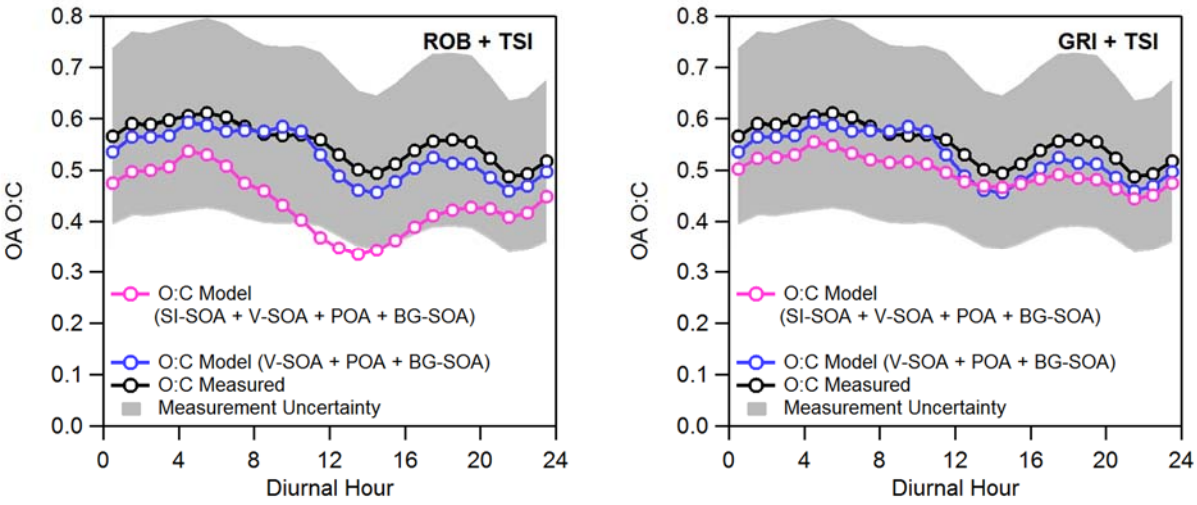

3.2. Comparison of predicted and measured SOA oxygen content

The diurnal cycle of O:C of total OA is shown in Figure 23, along with the estimated ±30% uncertainty of the O:C determination (Aiken et al., 2007; 2008). A recent re-evaluation of the AMS elemental analysis has found an underestimation of oxygen content for multi-functional oxidized organics (Canagaratna et al., 2015). Thus, the updated calibration factors have been used in the work here, and they increase the measured O:C and H:C by factors of 1.28 and 1.1, respectively.

The model predictions of O:C are shown for both the ROB+TSI and GRI+TSI variations. The measured O:C is similar or higher than the models, and exhibits only small changes during the day. The minimum after noon in the measured O:C is due to the arrival of POA above Pasadena as well as the production of fresh SOA. The second minimum in the evening is due to emissions of CIOA, which has relatively low oxygen content.

When the model is run with the ROB+TSI variation for O:C evolution in SOA the model diurnal cycle is generally lower than the field data. Similar to the comparison of mass concentration, the GRI+TSI model variation better reproduces the O:C observations. As a control the model is also run without SI-SOA, which, interestingly, also does an excellent job of reproducing the observations. Two conclusions can be drawn from the results shown in Figure 23. First, the SI-SOA in the ROB parameterization appears to be not sufficiently oxidized, which drives down the predicted O:C, and, in general, SOA production and oxidation in Pasadena is very rapid and is therefore best described by the GRI parameterization. Second, both SI-SOA from the GRI parameterization and V-SOA have an O:C of ~ 0.45, which is not very different from the weighted mean of HOA, CIOA, and LV-OOA (O:C ~ 0.6), and, as a result, the total OA O:C is relatively constant for the different times of day. This consideration also explains why O:C does not change substantially when the SI-SOA is included or excluded in the model.

Lastly, we note that there are large uncertainties in the parameters used to predict O:C such as the distribution of O:C values as a function of volatility for V-SOA or the amount of oxygen mass added to the SI-SOA for each oxidation reaction. It is therefore not very meaningful to conclude from this study that one parameterization performs better than another. Rather, it is apparent that when using several different previously published SOA parameterizations (i.e. ROB+TSI, GRI+TSI, and TSI alone) it is possible to reproduce the observed O:C at the Pasadena ground site.

3.3. A simple parameterization for SOA formation in polluted urban regions

While medium-complexity parameterizations of SOA formation and evolution such as those used above represent some important details of SOA chemistry and properties, there is a need for very computationally inexpensive SOA parameterizations that still retain good accuracy for use in regional, global, and climate models. Such a parameterization was recently reported by Hodzic and Jimenez (2011), and was designed to predict properties of urban SOA in global and climate modeling studies (referred to as the "SIMPLE" parameterization hereinafter). The model represents SOA precursors as a single surrogate lumped species, termed here 'VOC*', which is emitted proportionally to anthropogenic CO. The model converts VOC* to SOA by reaction with •OH with a specified rate constant. The SOA formed in the SIMPLE model is non-volatile and does not partition to the gas-phase, consistent with the low volatility observed for aged SOA in field studies (e.g., Cappa and Jimenez, 2010).

We replaced the SOA parameterizations discussed above with the SIMPLE parameterization just described, and ran the box model for a large number of possible parameter value combinations (i.e. emission ratio of VOC*/CO and •OH rate constant). Figure 24A shows the difference between model and measurement over that parameter space. The diurnal cycle predicted by the SIMPLE parameterization with the optimum parameters for Pasadena is shown in Figure 24B. The SIMPLE model with the optimized parameters performs comparably to the more complex parameterizations used in this work. At the same time, the SIMPLE parameterization is unable to capture perfectly the location of the peak in time because it depends

solely on CO and photochemical age. The CO concentration at the site peaks at 12:00 and photochemical age peaks at 13:00 (Figure 6A) while the measured SOA has a broad peak between 14:00 – 16:00. The fact that SOA does not peak at the same time as CO and photochemical age indicates the assumption in SIMPLE that VOC*/CO does not vary in time is probably not completely accurate. Still, the performance of the SIMPLE parameterization for urban SOA is sufficient for many applications and certainly far better than many models currently used.

Figure 24. ***(A)*** *Image plot of the root mean square error between the SIMPLE urban SOA parameterization concentration and the measured SV-OOA as a function of both the lumped precursor emission ratio and the oxidation rate constant. The gray stars indicate the parameter pairs that result in the minimum errors for Pasadena (this study) and Mexico City (Hodzic and Jimenez, 2011). The dashed box approximately indicates the range of possible optimal parameter combinations. For reference an emission ratio of 80 μg m^{-3} ppmv^{-1} equals 0.069 g g^{-1}.* ***(B)*** *Diurnal cycle of SV-OOA with corresponding uncertainty (grey dashed lines). The diurnal cycle of SOA predicted by the SIMPLE model is shown as well.*

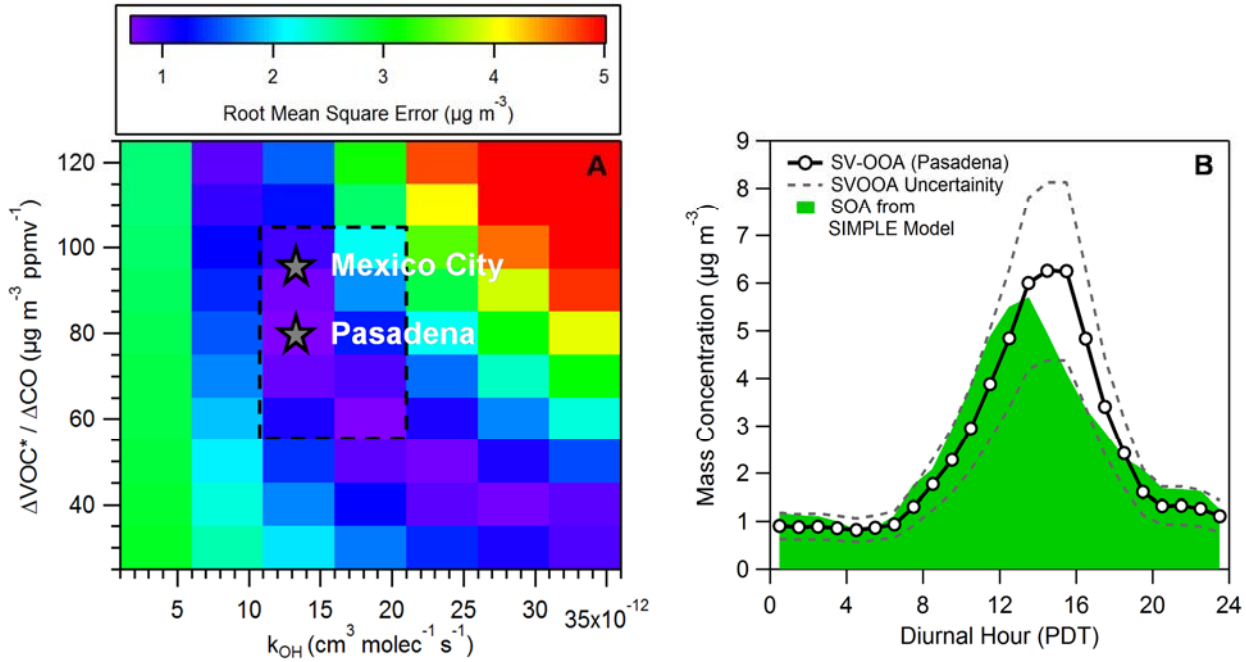

Interestingly, the optimal model parameters for Mexico City and Pasadena are very similar. In other words, when tuning the model separately for each city, the parameters obtained are identical within the estimated uncertainties. This result suggests SIMPLE, with the parameters reported for Mexico City or Pasadena, can be applied to other polluted urban regions as well. In addition, the optimal parameters for Pasadena (and Mexico City) are consistent with the OA/ΔCO ratios observed for highly aged air masses by Bahreini et al. (2012) from the NOAA P3 aircraft in the LA basin outflow, as well as for other urban areas as summarized by de Gouw and Jimenez (2009) and shown in Figure 16. However, it should be noted that a range of SIMPLE parameter combinations still remains in which the different combinations perform similarly in the model/measurement comparison, and this range is indicated by the dashed box in Figure 24A. While the SIMPLE model is promising, additional work should be carried out to verify the optimal SIMPLE model parameters including analysis of data for a broad range of ages, e.g., by utilizing

results from ambient air processed by oxidation flow reactors (Ortega et al., 2013). Also, the accuracy of the SIMPLE model for predicting urban SOA under a variety of atmospheric conditions should be explored (e.g. VOC/NOx or relative amounts of gasoline versus diesel emissions.) Finally, we note that the SIMPLE model parameterizes urban SOA, and is not applicable to biogenic SOA.

Hodzic and Jimenez (2011) also proposed an approach for predicting the oxygen content of SOA that utilized the equation O:C = 1 – 0.6exp(-*A*/1.5), where *A* is the photochemical age in days. (Note: the photochemical age was calculated using a reference •OH concentration of 1.5×10^6 molec cm^{-3}.) As shown in Figure 25, this parameterization compares well with the O:C from measurements. However, the parameterization of Hodzic and Jimenez does not take into account the new AMS O:C calibrations factors, as described in the preceding section. In order to account for this change, the equation proposed by Hodzic and Jimenez must be multiplied by a factor of 1.28. Thus, the updated parameterization is O:C = 1.28(1 – 0.6exp(-A/1.5)), and the corresponding O:C values are shown in Figure 25. The updated simple parameterization also exhibits good agreement with measurements. (Note: The O:C predicted by the updated model does not increase by a factor 1.28 relative to the original version because the SOA from the Hodzic and Jimenez parameterization is mixed with HOA, CIOA, and BG-SOA to determine the total OA O:C shown in Figure 25.)

Figure 25*. Model/measurement comparison of O:C of OA versus time of day for the SIMPLE urban SOA parameterization. The original parameterization proposed by Hodzic and Jimenez (2011) is O:C = 1 – 0.6exp(-A/1.5), where A is the photochemical age. The updated SIMPLE parameterization is O:C = 1.28(1 – 0.6exp(-A/1.5)), which accounts for the updated AMS O:C calibration factors.*

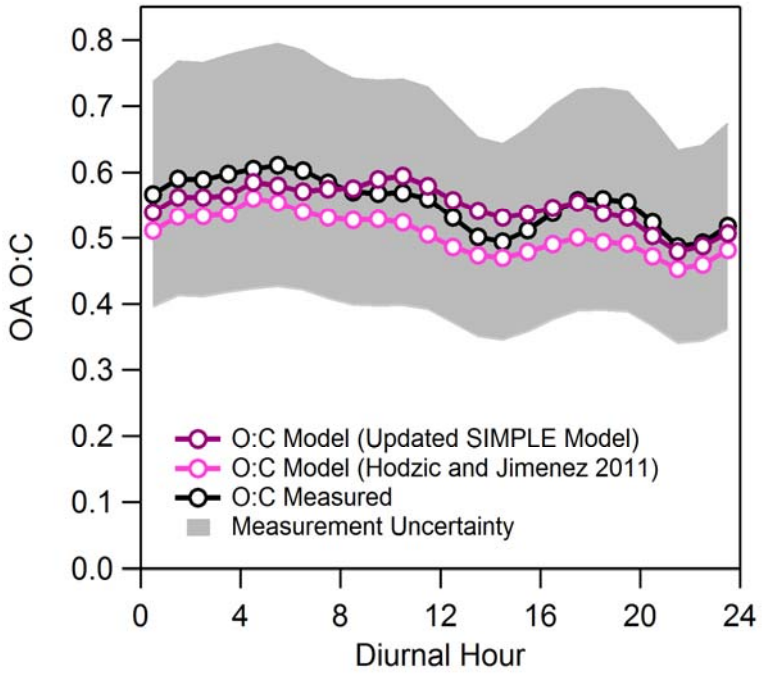

3.4. Update of the U.S. and Global Urban SOA budgets

As shown in Figure 16, the SIMPLE parameterization asymptotically approaches a SOA/ΔCO value of 80 μg m^{-3} ppm^{-1}, which can be used to estimate an urban SOA budget. The SIMPLE parameterization is better for estimating this budget than the more complex parameterizations, because the SIMPLE parameterization is consistent with the observations of de Gouw and Jimenez (2009) that were made at multiple locations. For the ROB+TSI, GRI+TSI, PYE+TSI, and ROB+4xV model variants, values of SOA/ΔCO between 150 and 220 μg m^{-3} ppm^{-1} are predicted at long photochemical ages, and such high values have never been observed, to our knowledge, downwind of anthropogenic-dominated sources. These four more complex parameterizations are based on laboratory data at short photochemical ages, and thus, applying them to long photochemical ages is an extrapolation. The SIMPLE parameterization is imperfect, but based on the available evidence it appears that the SIMPLE model is the most accurate at long photochemical ages and better suited for estimating the urban SOA budget.

For the U.S., the annual urban CO emissions reported in the 2011 NEI are 44 Tg yr^{-1} (EPA, 2013), which when multiplied by SOA/ΔCO gives a national urban SOA source of 3.1 Tg yr^{-1}. The same estimate can be performed for global urban SOA, since similar ratios of SOA/ΔCO have been observed in other countries such as downwind of Mexico City and China (DeCarlo et al., 2010; Hu et al., 2013). Using the EDGAR v4.2 inventory of 371 Tg yr^{-1} of urban/industrial CO for 2008 (JRC, 2011), we estimate a global pollution SOA source of 26 Tg yr^{-1}, or about 17% of the estimated global SOA source of 150 Tg yr^{-1} (Hallquist et al., 2009; Heald et al., 2010; Heald et al., 2011; Spracklen et al., 2011). We note that 1/3 of that SOA would be non-fossil, if a similar cooking fraction is observed globally as in this study, which is expected given the identification of similar fractions of cooking POA in many field studies globally (Wang et al., 2009; Mohr et al., 2011; Sun et al., 2011).

3.5. Oxidation Flow Reactor Observations

The time series of the reactor sample period is shown in Fig. 26a. The ambient aerosol during the first third (30 May–3 June 2010) of the measurement period is characterized by OA dominance, while the remaining two-thirds of the period (3–11 June 2010) is characterized by high concentrations of OA and nitrate, moderate sulfate and ammonium, and low chloride, with a marked diurnal cycle. This second period was strongly affected by in-basin pollution and is the most useful in terms of studying urban SOA formation (Hayes et al., 2013).

A 24-hour snapshot of the time series of ambient and reactor data is shown in Fig. 26b. This period is representative of the diurnal profiles observed from 3–9 June 2010. The oscillations (zig-zag pattern) in reactor output concentrations are due to OH_{exp} stepping as shown in Fig. 9. Day and night periods are highlighted to indicate the period of inactive (20:00–8:00) and active ambient photochemistry (8:00–20:00) in Fig. 26b. Ambient nitrate and ammonium concentrations peak in early morning hours before sunrise, while OA peaks in the late afternoon, during the most photochemically active part of the day. Hayes et al. (2013) attributes this organic aerosol temporal pattern to the formation of fresh urban SOA as the LA-plume undergoes ~0.3 days of photochemical aging during transport to our field location, which is considered a receptor site as it experienced a strong impact from aged urban emissions. However, OA enhancement in the reactor peaked during night, ~12 h before the ambient OA peak. The nighttime reactor-aged OA mass peaks at approximately the same concentration as the following

day's ambient OA concentration, suggesting the reactor's potential for estimating the next day's OA concentrations. Daytime reactor-aged OA mass shows very limited enhancement above the ambient OA mass, indicating that the precursors for SOA formation have been mostly depleted in ambient air. At the peak of the ambient photochemical age during daytime, only small amounts of precursors are available to contribute to further SOA formation from oxidation in the reactor, likely due to previous removal by photochemical oxidation and condensation. Figure 26c shows the average speciated contribution to total aerosol for ambient and the reactor (excluding dark reactor periods, where OH_{exp} = ambient), indicating overall enhancement of all species from reactor aging with very similar composition to ambient aerosol.

Figure 26. *(a) Time series of reactor and ambient species mass concentrations during the sampling period. (b) Zoom on the time series of the species mass concentrations for one representative day. Daytime and nighttime are marked. (c) Average fraction contribution from organic, nitrate, sulfate, ammonium, and chloride to total AMS aerosol measurements for ambient and reactor (excluding dark reactor, "lights off" periods).*

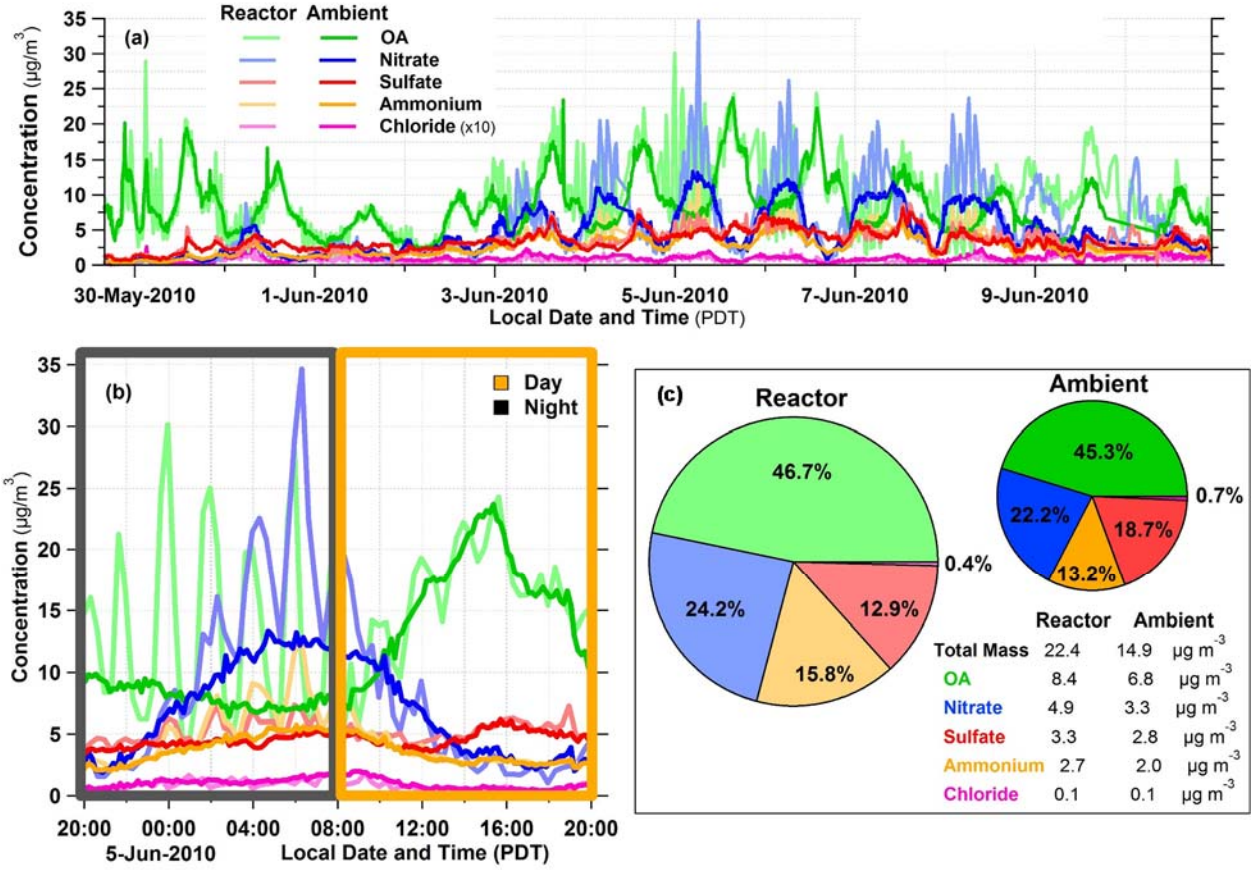

Observations of the OA size distributions indicate reactor aging does not significantly shift the size of the accumulation mode for the average of nighttime ambient and three different reactor age ranges (age ~ ambient, 3.7 days, and 23.5 days), from 2–9 June 2010 (Fig. 27). The reactor size distribution changes in intensity and shape are most pronounced during low ages (~3.7 days and lower), with an enhanced smaller size mode (dva ~80 nm). While many daytime/nighttime average size distributions and age ranges were explored, only ages at or below a few days at nighttime showed significant enhancement of small particle sizes. Highest ages

(>14 days) show overall decrease in concentration across all size bins with the size of the accumulation mode unchanged from ambient within the uncertainty of the measurement. Given the high concentrations of large particles in this urban environment, we expect aging to enhance organic aerosol by condensation of semi- and low-volatile compounds on existing particles to dominate over new particle formation and growth. Reactor results are indicative of this process, although they also indicate the effect of new particle formation and/or of nanoparticle growth at lower OH exposures.

Figure 27. *AMS mass size distribution (vs. vacuum aerodynamic diameter, dva) for reactor and ambient OA, averaged from 20:00 on 2 June 2010 – 00:20 on 9 June 2010 for average nighttime ambient and reactor with no internal* OH_{exp} *(dark reactor), and for ~3.7 days and ~23.5 days aging.*

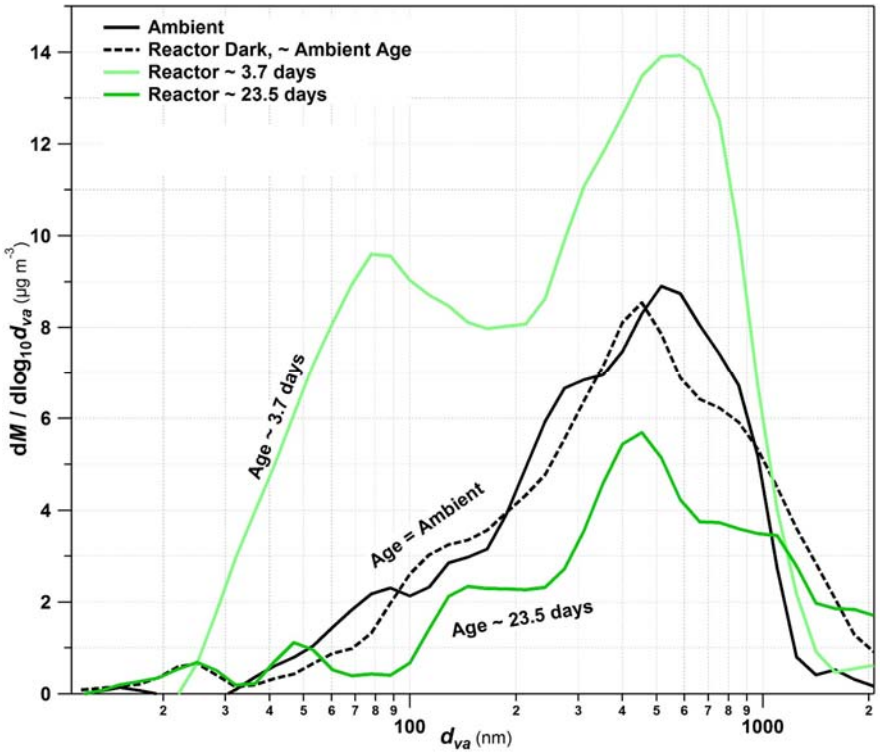

3.6. Aerosol Enhancements

Investigating reactor perturbation of ambient OA allows quantification of both relative and absolute OA changes vs. OH_{exp}. The relative OA enhancement ratio, ER_{OA} = reactor OA / ambient OA, and the absolute OA enhancement factor, ΔOA Mass = reactor OA – ambient OA, are plotted vs. OH_{exp} in Fig. 28a and Fig. 28b respectively for the sample period. OA mass is enhanced up to four times from ambient OA, with the majority of maximum ER_{OA} peaking around a factor of two increase. OA enhancement peaks and plateaus between 0.8–6 days of OH aging, then decreases at higher aging, eventually showing net OA loss beyond two weeks of aging. When separated into daytime and nighttime ER_{OA} and ΔOA mass (Fig. 28), the qualitative trends are the same in both cases, but OA was more enhanced from reactor aging during nighttime by 5 μg m^{-3}, or a factor of 1.7x of ambient. A smaller enhancement is observed during the day ~2 μg m^{-3}, or a factor of 1.2x of ambient The data for greater than 2 weeks of aging

closely overlaps for day and night, with a decrease up to ~2.5 μg m^{-3}, or a factor of 0.5x of ambient.

Figure 28. (a) *Relative OA enhancement (ER_{OA} = reactor OA / ambient OA) vs.estimated reactor photochemical age for the sampling period.* ***(b)*** *Absolute OA mass concentration enhancement (ΔOA Mass = reactor OA - ambient OA) versus photochemical age. The data has been averaged into 6% quantiles for day and night measurements, with vertical error bars indicating standard errors.*

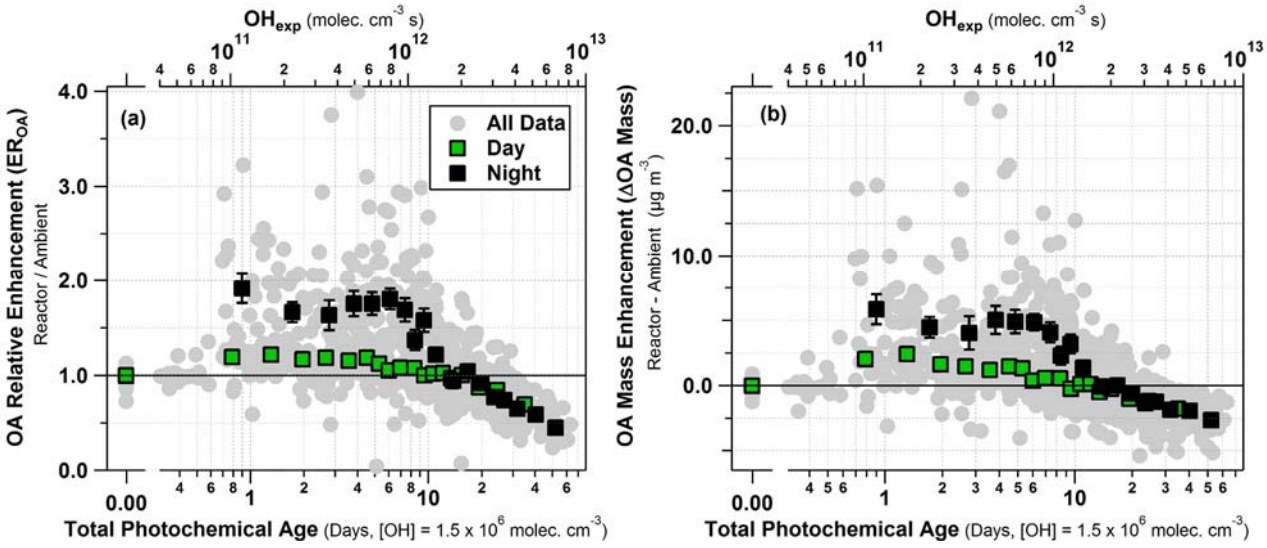

The substantial difference between day- and nighttime enhancements can be explained as during the night the boundary layer is shallow and reactive precursors accumulate due to the absence of ambient photochemistry, with lower ambient photochemical ages of ~0.1 day (Hayes et al., 2015) and minimal loss mechanisms as the dominant urban VOCs do not react with O3 or NO3 (other than a small concentration of monoterpenes). In contrast, during the day reactive precursors in ambient air are depleted due to reaction with OH. Transport times from downtown LA, the dominant precursor source region impacting Pasadena, is ~0.5 days, with ambient photochemical ages reaching ~0.3 days. Thus most of the SOA precursors that can become SOA already have by the time the air was sampled in Pasadena and only about 20% more SOA could be produced from the precursors that remained. The trends in Fig. 28 indicate increased oxidation transitioning from a dominance of functionalization reactions and condensation at low-to-moderate exposures, to fragmentation-dominated reactions and evaporation of reaction products at the highest photochemical ages. Fragmentation can occur in the gas phase by reactions of SVOCs with OH, leading to non-condensable products and decreasing SOA formation. Fragmentation can also be due to heterogeneous oxidation of existing OA, producing more volatile species that may evaporate leading to OA mass loss. Discussion of the relative importance of these processes for this study is presented in Section 3.12 below.

3.7. Gas-Phase Observations

3.7.1. Odd Oxygen (Ox) Relation to SOA Formation

The day-night difference observed in both ER_{OA} and ΔOA mass merits examination of the relationship with ambient odd-oxygen, Ox (O_3 + NO_2). Ambient Ox correlates with freshly produced SOA in urban areas (Herndon et al., 2008; Wood et al., 2010; Hayes et al., 2013; Morino et al., 2014; Zhang et al., 2015), both resulting from recent photochemistry. For the reactor, oxidants are generated internally and are not dependent on ambient Ox. As seen in Fig. 29, there is a steep inverse relationship between ΔOA mass and ambient Ox, at low to moderate aging (<4 days). As daytime ambient photochemical production of oxidants increases (Ox >50 ppbv), the reactor's SOA formation for moderate aging decreases to a near constant OA mass enhancement (2 μg m^{-3}). At high ages (>14 days), OA mass loss is fairly constant with ambient Ox, which is not surprising since the mechanisms responsible for OA depletion at long ages have little dependence on previous photochemical processing in the atmosphere. These results further confirm that as the degree of ambient photochemical processing of the sampled air increases (during daytime), SOA production in the reactor becomes more limited, likely due to the depletion of reactive SOA precursors in ambient air, consistent with the conclusions from Fig. 28.

Figure 29. *Reactor OA mass enhancement vs. ambient Ox, (odd oxygen; O_3+NO_2) for all data in ~3.7 and ~23.5 day reactor age ranges during the sample period, colored by nighttime and daytime. Average for 10% quantiles are shown for ~3.7 days and ~23.5 days of photochemical age.*

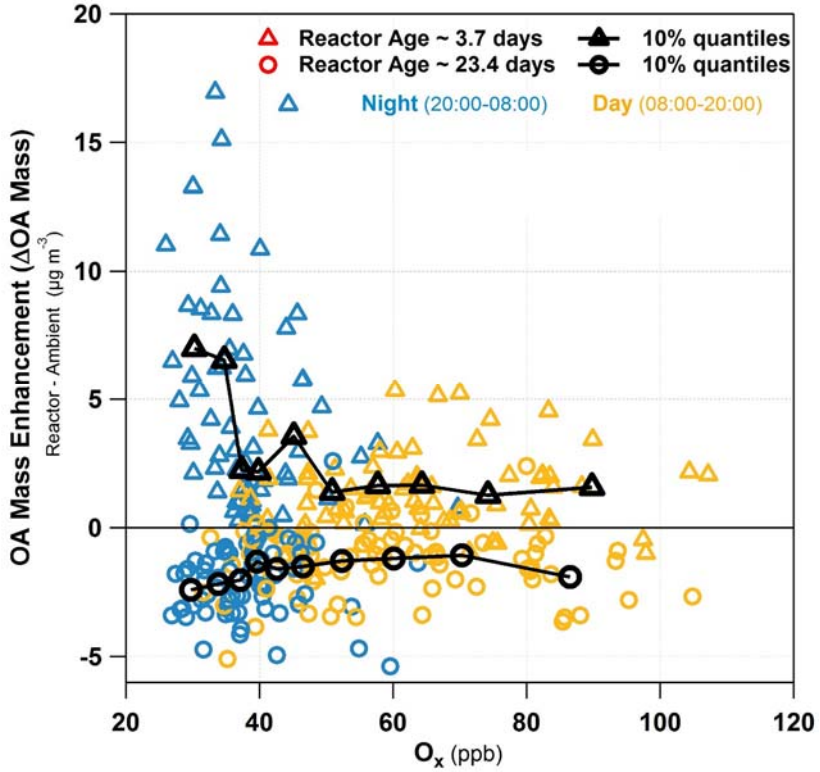

Figure 30. *Times series of benzene, 1,3,5-trimethylbenzene, ambient total oxygenated organic aerosol (OOA), reactor organic mass enhancement, and maximum reactor organic mass enhancement. Inset is a scatter plot of maximum reactor OA mass enhancement (for each OH_{exp} cycle) vs. ambient 1,3,5-trimethylbenzene, with a linear ODR regression fit.*

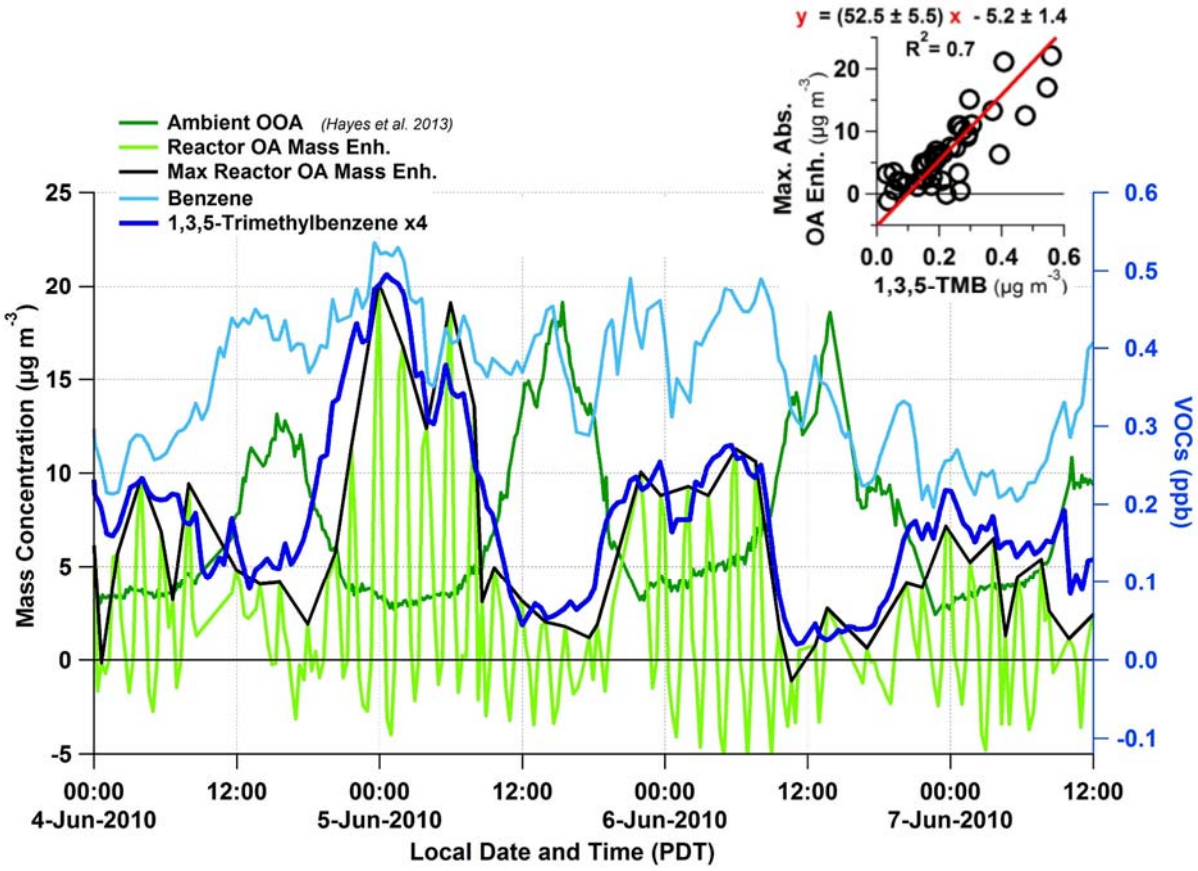

3.7.2. Further Constraints on Urban SOA Formation Timescales from VOC Observations

To further constrain the timescales and precursors of urban SOA formation, ambient and reactor OA data are plotted together with ambient VOCs in Fig. 30. The maximum reactor OA enhancement has a similar diurnal profile to 1,3,5–trimenthylbenzene (TMB). Both TMB and OA enhancement have diurnal profiles that are out of phase with ambient SOA. In contrast, the concentration of benzene shows little correlation with reactor SOA formation in the reactor. The lifetime of TMB by reaction with OH is nearly 2 orders of magnitude shorter, τ_{OH} ~3 hours, kOH = 5.67×10^{-11}, than benzene, τ_{OH} ~6 days, k_{OH} = 1.22×10-12 (Atkinson et al., 2006). The anti-correlation of TMB and reactor enhancement in OA and ambient SOA concentrations suggests that only in the absence of ambient photochemistry, substantial amounts of short-lived SOA precursors are present to produce most of the SOA formed in the reactor. Toluene, a VOC with a lifetime of 1.4 days and $k_{OH} = 5.63\times10^{-12}$ cm^3 $molecule^{-1}$ s^{-1} does not have the same diurnal structure as reactor OA and TMB (Fig. 31). The shape of the diurnal-scale time series in Fig. 30 and 31 can be explained as the sunrises ambient photochemistry begins at sunrise, very short lived precursors, such as TMB, begin decay rapidly due to gas-phase oxidation as well as boundary layer growth. As these gas-phase oxidation products condense, SOA forms and

ambient OA reaches its daytime peak. At the daytime ambient OA peak, most of these short-lived precursors have been consumed, thus the reactor only forms an additional 1–2 μg m^{-3} of SOA as opposed to the greater than 10 μg m^{-3} possible when theses precursors are allowed to build in a shallow boundary layer and in the absence of photochemical sinks. Note that in the afternoon the boundary layer is significantly deeper than at night, and thus the total afternoon SOA formation potential may not be that different than at night, even though the potential per unit volume of air is much smaller.

Figure 31. *Times series of benzene, 1,3,5-trimethylbenzene, and toluene on top panel. Time series of ambient OOA, reactor OA mass enhancement, maximum reactor mass enhancement, and Ox on bottom panel.*

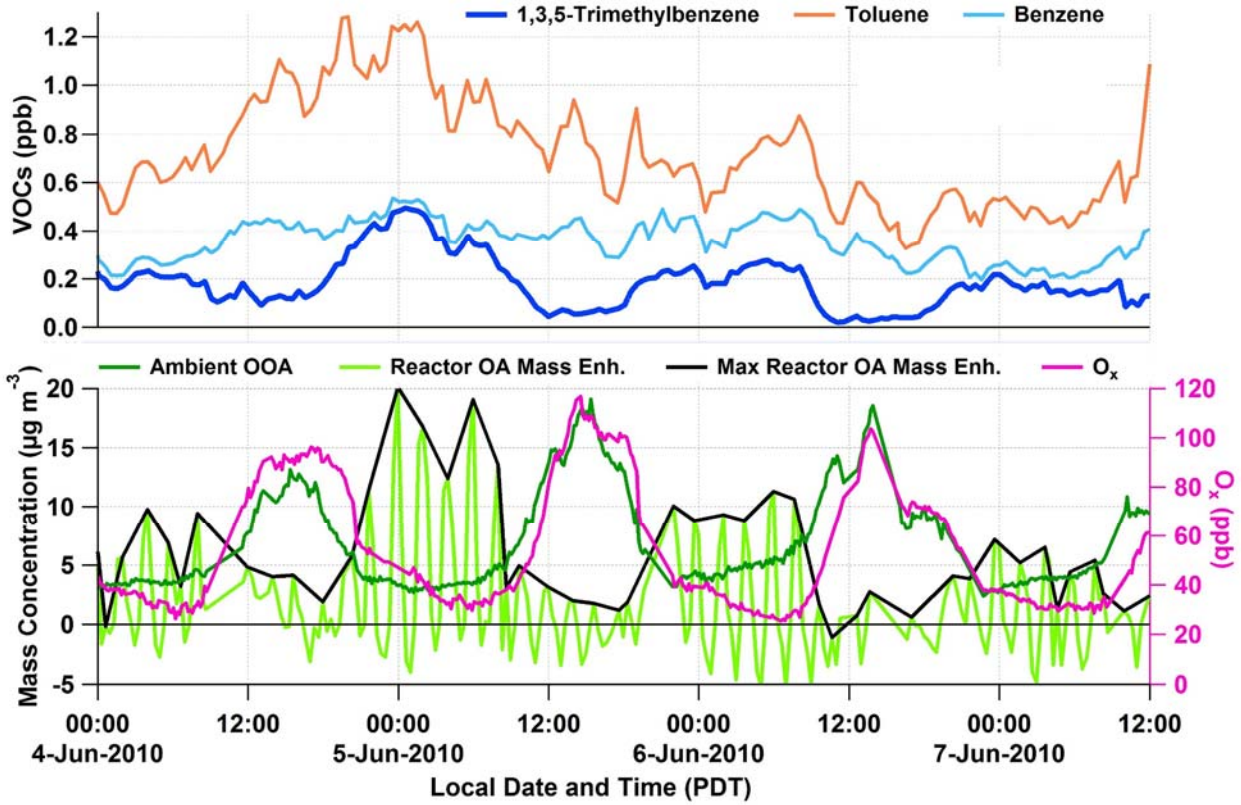

The inset in Fig. 30 is a scatter plot of maximum reactor SOA formation (per OH_{exp} cycle) vs. TMB (slope ~52, R^2=0.7). TMB's SOA yield is on the order of 10% (Cao and Jang, 2007). Thus its concentration is insufficient to explain reactor SOA formation by a factor of ~500, though it is not expected to be the sole SOA precursor. This correlation suggests species with a similar source footprint and lifetime as TMB produce most of the urban SOA. Such species likely include semivolatile and intermediate volatility precursors (S/IVOC) that are rarely measured in ambient air (Dzepina et al., 2009; Zhao et al., 2014; Hayes et al., 2015). A comparison of observed reactor SOA formation with a model that uses all the measured VOCs is discussed below.

3.8. OA Chemical Composition and Evolution with Aging

The evolution of OA chemical composition upon aging has been the subject of several studies, both for ambient (Heald et al., 2010; Ng et al., 2010; Kroll et al., 2011; Ng et al., 2011a) and reactor conditions (Kang et al., 2011; Ortega et al., 2013; Tkacik et al., 2014; Lambe et al., 2015). This evolution results in characteristic trends in specific diagrams: AMS fragments f_{44} vs. f_{43}, and H:C vs. O:C. Both diagrams are shown for the CalNex ambient and reactor data in Fig. 32. f_{44} is a tracer for aged OA (mostly CO_2^+), while f_{43} (mostly $C_2H_3O^+$, due to non-acid oxygenates, with some contribution from $C_3H_7^+$) is a tracer of POA and freshly formed SOA (Ng et al., 2011a). In Figure 32a, ambient and reactor data evolve consistently and move up and to the left with aging, consistent with previous ambient field observations from multiple field campaigns (Ng et al 2010). As expected, reactor data with the highest age has the highest f44. Positive Matrix Factorization (PMF) factors from Hayes et al. (2013) lay within ambient observations and data for lower OH_{exp} in the reactor. Reactor data stays within the boundary of flow reactor results from Lambe et al. (2011a) and below the location of oxalic acid, as expected.

Figure 32: (a) *Fractional contribution of m/z 44 (f_{44}) vs. m/z 43 (f_{43}) to OA for the ambient and reactor data in this work. The region of ambient observations from Ng et al. (2010), and for reactor laboratory observations and oxalic acid from Lambe et al. (2011a) are shown.* ***(b)*** *Van Krevelen diagram for ambient and reactor measurements for the sampling period. Functionalization slopes from Heald et al. (2010), and oxidation state from Kroll et al. (2011) are shown for reference. Elemental analysis has been calculated with the Improved-Ambient method from Canagaratna et al. (2015). Reactor measurements are colored by total photochemical age in days (at OH = 1.5×10^6 molec. cm^{-3}) and ambient PMF-derived HOA, SV- and LV-OOA factors are shown from Hayes et al. (2013).*

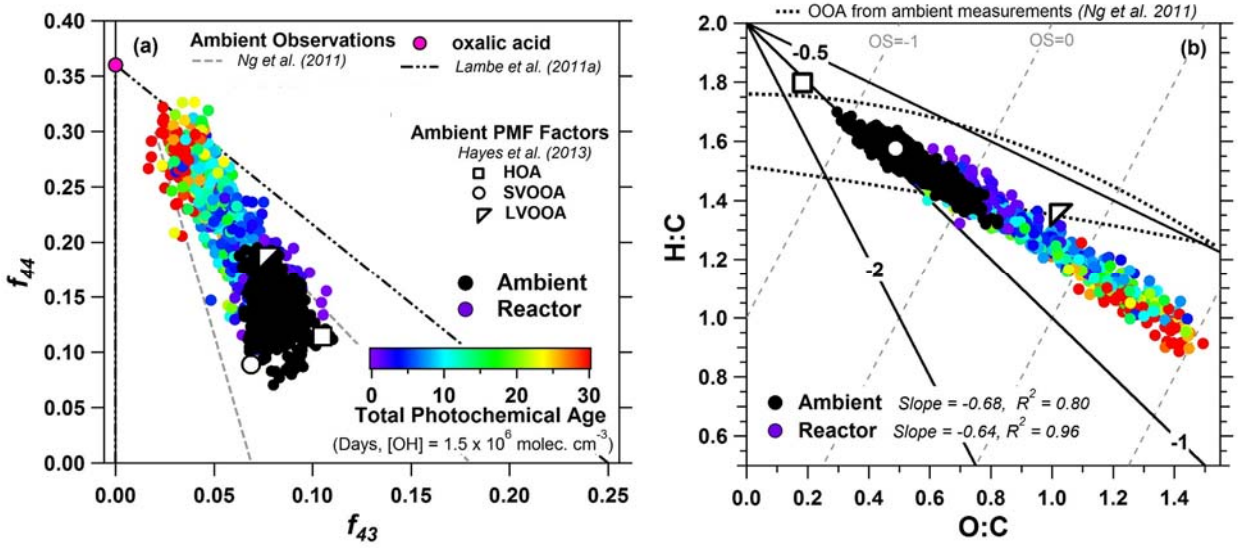

The Van Krevelen diagram (H:C vs. O:C) is shown in Fig.32b and demonstrates results that are very consistent to those of the previous plot. The reactor data follows a similar trend to ambient data, with slopes of -0.64 and -0.68, respectively. A slope between -1 and -0.5 is consistent with the addition of acid and alcohol functional groups without fragmentation or the addition of acid groups with carbon–carbon bond breakage (Ng et al., 2011b). The consistency of

ambient and reactor OA aging suggest that the reactor produces similar SOA composition upon aging to that in the atmosphere within the LA-Basin.

Figure 33: (a) *Oxygen-to-carbon (O:C) and* ***(b)*** *hydrogen-to-carbon (H:C) elemental ratios for OA mass measured from the reactor vs. total photochemical age in days (at OH = 1.5×10^6 molec. cm^{-3}). Results using similar reactors for alkane oxidation from Lambe et al. (2012), and for aging of biomass burning smoke (Ortega et al., 2013) are also shown.* ***(c)*** *Average oxidation state (OS_C = 2O:C – H:C) vs. OH_{exp}. Data are colored by the relative organic enhancement (ER_{OA} = reactor OA / ambient OA).*

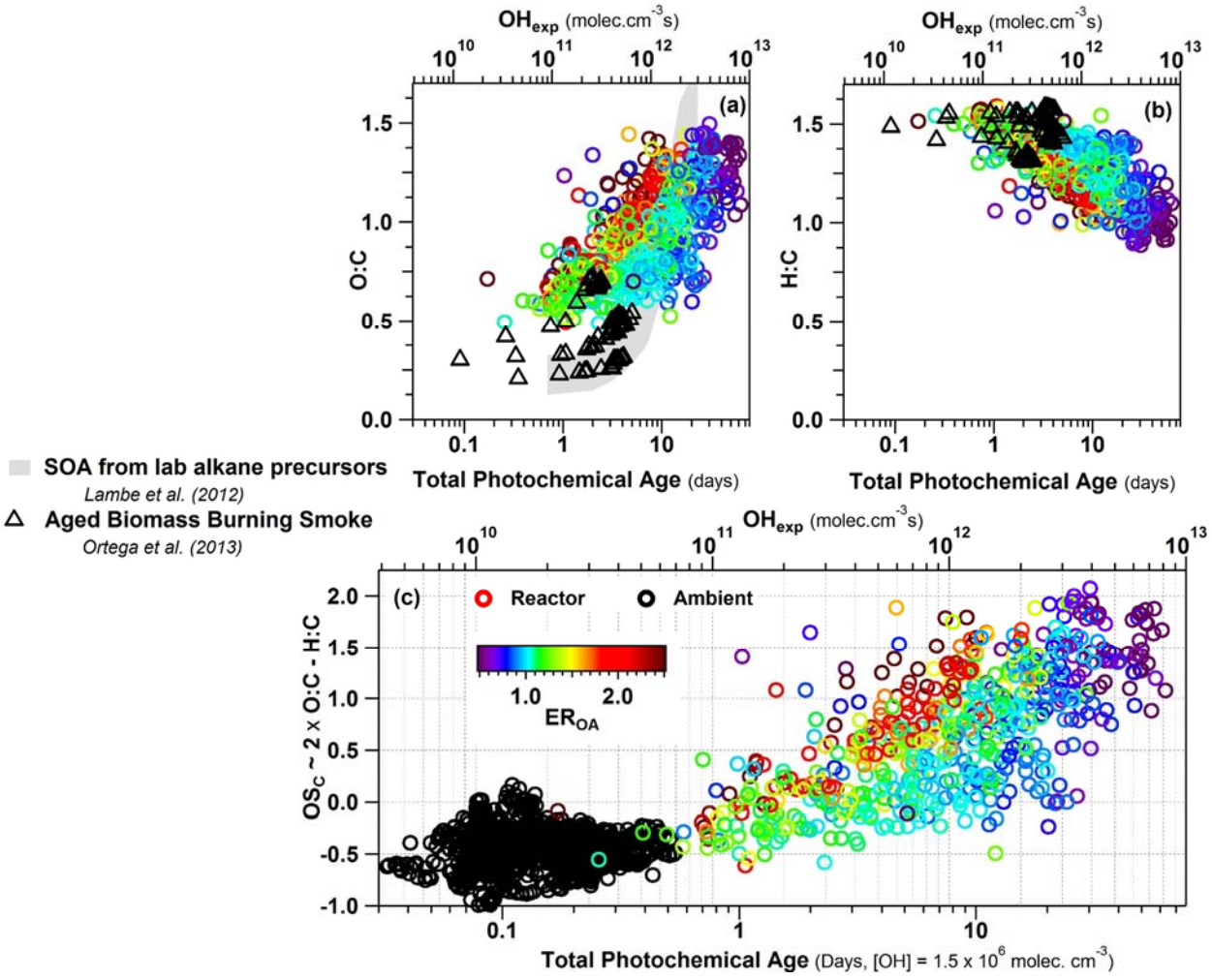

Reactor O:C ratios increase with age and span a wider range than ambient observations (O:C up to 1.4). While O:C (and f44) continually increased with additional OH_{exp}, peak reactor OA enhancement is observed at intermediate exposures and O:C ratios (0.8–6 days and O:C ~1.10–1.25), as seen in Fig. 33a. OA mass loss, i.e. ER_{OA}< 1, is observed together with the highest O:C ratios at the highest ages, which suggests OA fragmentation by heterogeneous oxidation results in the highest oxygen content remaining in the aerosol. With increasing age, H:C decreases continuously with OH_{exp} (Fig. 33b), with H:C ~1.00–1.15 for the periods of maximum reactor OA enhancement. A qualitatively similar trend is observed in the reactor studies of Lambe et al. (2012) for SOA from OH oxidation of alkane precursors (Fig. 33a)

although starting with lower O:C and with a steeper slope at higher ages, and also by Ortega et al. (2013) for aging of biomass burning smoke.

Average carbon oxidation state (OS_C) has been proposed as a metric to characterize the formation and evolution of OA (Kroll et al., 2011). OS_C can be approximated as ~2×O:C–H:C. Figure 33c shows OS_C vs. photochemical age for ambient and reactor data. While ambient OS_C is within the range of previous observed urban/anthropogenic OA, reactor OSC extends this significantly up to +2.0, consistent with ambient low-volatility OA observations up to +1.9 (Kroll et al., 2011). At the same OH exposure, higher OS_C is observed for conditions of high reactor SOA production at intermediate ages. The highest values of OS_C are observed for the highest ages, where heterogeneous oxidation leading to OA mass loss dominates. This indicates that heterogeneous oxidation adds substantial oxygen and reduces hydrogen from molecules to the particles to increase OS_C despite overall mass loss.

Figure 34. *Ratio of OA to excess carbon monoxide (above background levels) vs. total photochemical age in days (at OH = 1.5 × 10^6 molec. cm^{-3}) for ambient and reactor data. Also shown in the value for LA Basin outflow from aircraft measurements from the NOAA WP-3D during CalNex (Bahreini et al., 2012b). See Hayes et al. (2013) for a discussion of the determination of CO background levels. Averages for quantiles of ambient (7%), reactor (7%), reactor dark (25%, internal OH_{exp}= 0) and reactor vapor loss-corrected (12%) data are shown. A fit to reactor data is also shown (see text for details). Results from field studies in the northeastern US and Mexico City are shown in the background (DeCarlo et al., 2010).*

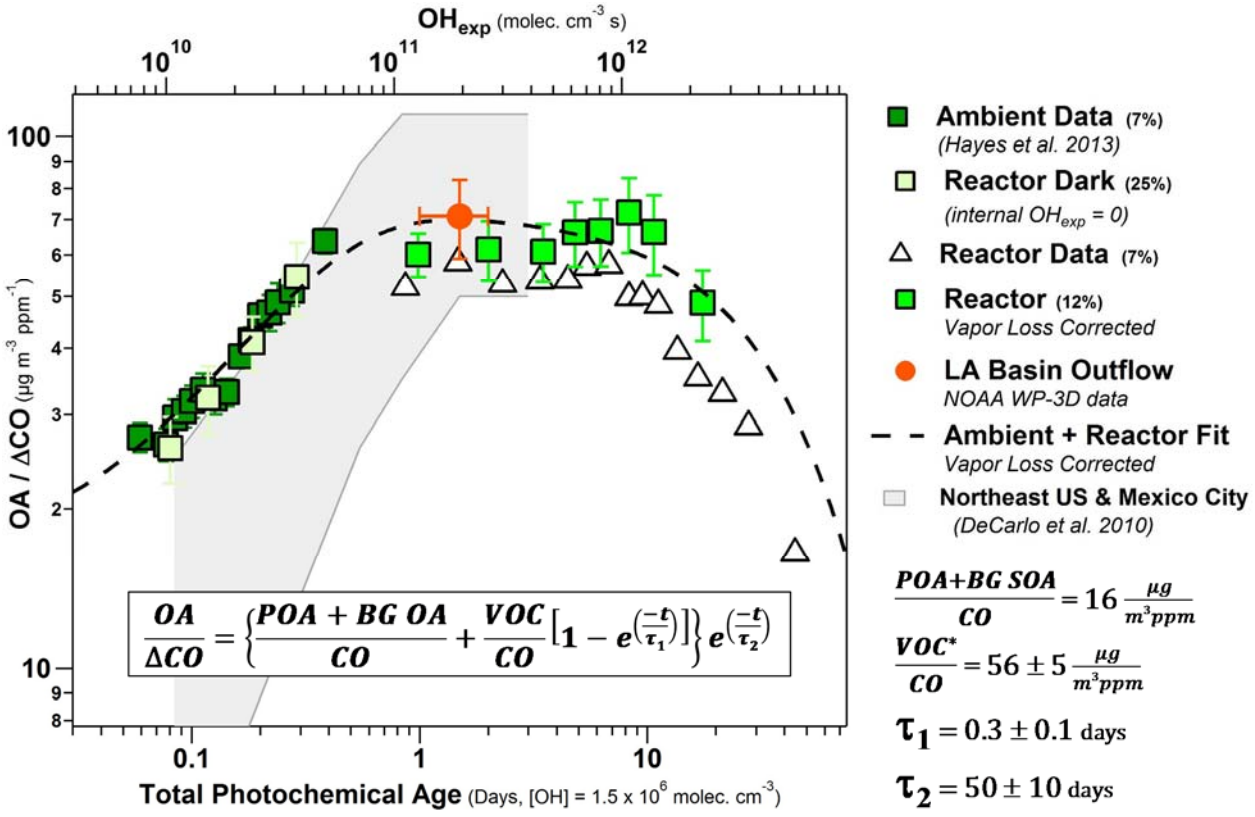

3.9. Evolution of Net Urban OA with Photochemical Age

The identity of the SOA precursors responsible for urban SOA formation remains unclear. Combustion emissions such as those from vehicles are thought to be a major source of urban SOA (e.g. Hayes et al., 2015), and urban non-combustion sources of SOA precursors, if important, are finely spatially intermingled with combustion sources. CO is often used as a tracer of the initial concentration of urban SOA precursors in an airmass and thus allow an implicit correction for dilution occurring in parallel with aging. For this reason, the ratio of OA to CO concentration (above background level) vs. photochemical age is often used to investigate the evolution of urban SOA (de Gouw et al., 2005; DeCarlo et al., 2010).

Fig. 34 shows the results of this analysis for our reactor and ambient measurements. Background CO during CalNex-LA is on average ~105 ppb (ranging from 85—125 ppb, Hayes et al., 2013). A range of ± 20 ppb uncertainty in background CO, results in an average ± 6 μg m^{-3} ppm^{-1} uncertainty in OA/ΔCO. Ambient photochemical age is calculated from the VOC ratio method as in Hayes et al. (2013). Reactor total photochemical age is the sum of ambient photochemical age (of the air ingested into the reactor at each time) and reactor age. The range observed in previous field campaigns in the Northeastern US and Mexico City are shown for reference (DeCarlo et al., 2010). LA Basin outflow data are also shown, from aircraft measurements aboard the NOAA WP-3D during CalNex (Bahreini et al., 2012b), averaged for 1–2 days of photochemical age, falling in the middle of the range of previous ambient observations.

Fig. 34 shows the data averages for 7% quantiles of total photochemical age, to better illustrate the average trends of the observations without the higher noise level of 2.5 min. measurements. All data points for the sample period are shown for ambient and reactor measurements in Fig. 35 for reference. An increase in OA/ΔCO with aging is observed for ambient and reactor dark data (where reactor age = ambient photochemical age in the absence of internal reactor OH_{exp}), consistent with previous studies and as discussed in Hayes et al. (2013; 2015). Reactor data are shown without and with the vapor loss-correction applied (see Sect. 2.3). The reactor data is consistent with SOA formation being dominated by shorter-lived precursors, as little increase in OA/ΔCO is observed after about a day of total age, consistent with the SIMPLE parameterization of urban SOA (Hodzic and Jimenez, 2011; Hayes et al., 2015).

To further illustrate the lifetimes of important urban SOA precursors, OH-decay curves of gas-phase benzene, toluene, and 1,3,5-trimenthylbenzene (TMB) are overlaid in Fig. 35a with data from Fig. 34. The timescale of SOA formation is in between those of TMB and toluene decays, mostly shorter than toluene decay and definitely shorter than benzene decay, again consistent with the previous discussion.

We note that in Fig. 34 aging of CO (decay of CO from reacting with OH in the reactor or atmosphere) was not included in the evolution of OA/ΔCO analysis, as the purpose of ΔCO is to serve as an inert tracer of the urban SOA precursors emitted into each airmass. However, when comparing with aged pollution observed in the field after e.g. a week of transport, the aging to the urban CO needs to be taken into account. This is shown in Fig. 35b, and indicates that ambient observations of very aged pollution would not show a decrease in OA/ΔCO due to photochemistry since the decreases in OA and CO at long photochemical ages have similar timescales. We note that a decrease in the OA/ΔCO ratio for ambient aged pollution may still be observed for other reasons such as wet deposition (Dunlea et al., 2009). Production of CO from

urban VOCs is expected to be less than 1/10 of the directly emitted CO (Hallquist et al., 2009) and is neglected here.

Figure 35: *Ratio of organic aerosol to excess carbon monoxide (above background) vs. total photochemical age in days (at OH = 1.5×10^6 molec. cm^{-3}) for* ***(a)*** *the same data as Fig. 9, showing all data used to produce averages for quantiles of ambient and reactor vapor-loss corrected data. Also shown are the expected decays of benzene, toluene, and 1,3,5-trimethylbenzene in the reactor vs. total photochemical age in days (at OH = 1.5×10^6 molec. cm^{-3}), using reaction rates from Atkinson et al. (2006).* ***(b)*** *The same data as Fig. 9, showing reactor vapor loss-corrected data, but where excess CO is decreased by reaction with OH in the reactor, including means for 12% quantiles. Results from field studies in the northeastern US and Mexico City are shown for comparison to previous observations (DeCarlo et al., 2010). A fit to the data when CO is assumed to react with OH is shown. Since CO and OA are consumed at similar rates at long ages, no second timescale is required to fit the data.*

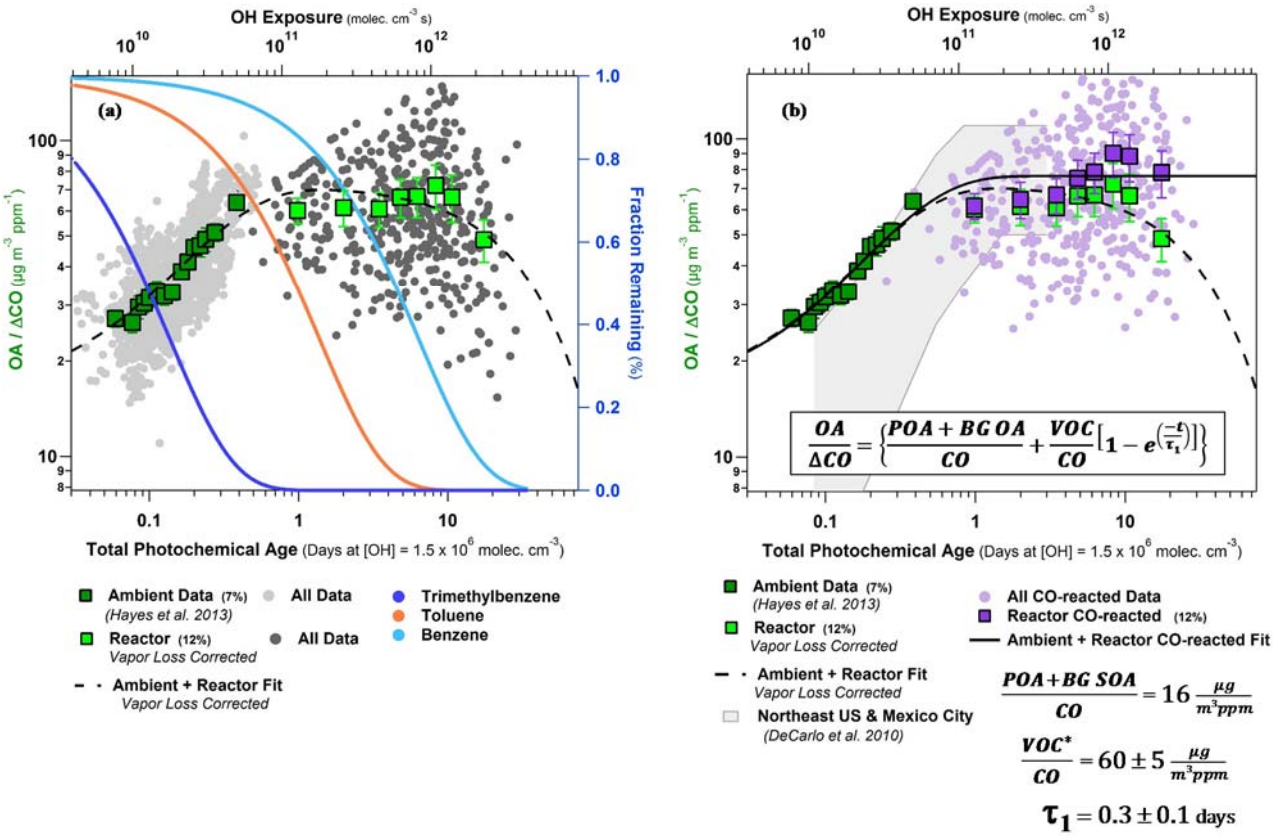

3.10. Fit to the Observed Ambient and Reactor Evolution

The evolution of urban SOA vs. photochemical age follows a similar trend in different field studies with a rapid increase in the first day followed by a plateau at longer ages. Previously, this evolution has been fit with the SIMPLE parameterization, a 2-parameter model in which a single VOC precursor (VOC*) is oxidized with a single rate constant with OH to produce non-volatile SOA. This parameterization has been shown to fit ambient data as well or better than more complex models (Hodzic and Jimenez, 2011; Hayes et al., 2015). However, the evolution past the initial ~2 days is almost completely unconstrained by ambient observations,

due to the difficulty of identifying urban pollution-dominated air masses after advection for several days, and of determining ΔCO when it is of the order of the uncertainties in the CO background. The reactor data from our study offer a unique opportunity to extend the model fit to much longer photochemical ages. The fit in Eqn. 4 was modified from Hayes et al. (2015)'s 2-parameter model for this purpose, where (POA+BGSOA)/CO is the primary OA plus background SOA, constrained at 16 μg m^{-3} ppm^{-1} (Hayes et al., 2015), VOC*/CO is the VOC* emission ratio, and t is photochemical age, using measurements at local temperature and pressure.

$$\frac{OA}{\Delta CO} = \left\{\frac{POA + BGSOA}{CO} + \frac{VOC^*}{CO}\left[1 - e^{\left(\frac{-t}{\tau_1}\right)}\right]\right\} e^{\left(\frac{-t}{\tau_2}\right)} \qquad (4)$$

Fitting the reactor data in this way requires the addition of a 2nd timescale to account for loss of OA at long ages, as done in Eqn. 1. Fitting all ambient plus vapor loss-corrected data results in VOC*/CO = 56±5 μg m^{-3} ppm^{-1}, τ_1 = 0.3±0.1 days, and τ_2 = 50±10 days (Fig. 34, all data points, i.e. before averaged into quantiles is in Fig. 35a). In this parameterization, τ_1 is the timescale for urban SOA formation and τ_2 is the timescale for net OA mass loss due to fragmentation, likely dominated by heterogeneous oxidation.

3.11. Comparison of Reactor output to Urban SOA Model Results

It is of interest to compare the SOA formation constrained from our reactor and ambient data to SOA models used in 3D modeling studies, as those models remain poorly constrained (e.g. Hayes et al., 2015). Here we used two of the model variants described earlier in this report and in Hayes et al. (2015), and compare to our data in Fig. 36. The first model variant is a "traditional model" with SOA formation from VOCs using pre-2007 yields (Koo et al., 2003), which has been shown before to underpredict urban SOA formation by over an order-of-magnitude (Dzepina et al., 2009; Morino et al., 2014; Hayes et al., 2015). This comparison is still of interest as several SOA models still use this approach (e.g. Morino et al., 2014; Baker et al., 2015; Hayes et al., 2015).

The second model variant represents SOA formation from VOCs and primary semivolatile and intermediate volatility precursors (P-S/IVOC; Robinson et al., 2007), and has been shown to predict SOA formation adequately at short timescales (<1 day) but to overpredict at long ages (Dzepina et al., 2011; Hayes et al., 2015). SOA formation from VOCs uses the Tsimpidi et al. (2010) formulation, including "aging" of the SOA, and using the high NOx yields since the observed SOA formation mostly occurs in the urban environment where RO2 react mainly with NO (Hayes et al., 2015). SOA from P-S/IVOCs is represented using the Robinson et al. (2007) parameterization. Recent results suggest that P-S/IVOC are needed to explain SOA formation observed in ambient air during CalNex (Zhao et al., 2014; Hayes et al., 2015), consistent with other locations (Dzepina et al., 2009; Hodzic et al., 2010).

Figure 36a shows the comparison of the SOA models against our ambient and reactor results. The traditional model predicts SOA a factor of 10 lower than our observations, consistent with previous studies. The updated model performance is mixed: the magnitude of SOA formation at short times (<1 day) is somewhat slower but similar to the ambient data. SOA formation at long ages (>1 day) is significantly overpredicted by a factor of ~3. This model does

not include heterogeneous oxidation reactions leading to fragmentation which could decrease predicted OA at high photochemical ages, resulting in a wider discrepancy at very long ages (>10 days). Figure 36b shows the same comparison using lower IVOCs as suggested from field measurements (Zhao et al., 2014). The same model was used, but with the initial concentrations of primary IVOCs decreased by one-half to better match the ambient observations of Zhao et al. (2014), as described by Hayes et al. (2015). Decreasing IVOCs brings down overall SOA predictions, increasing the discrepancy at shorter ages and still overestimating SOA concentrations compared to reactor measurements at the longest ages. This result suggests that the reduced IVOC concentrations cannot account for all model discrepancies. It is of interest to compare the reactor results with those of other SOA mechanisms in the future.

Figure 36. *Comparison of reactor data with model results for evolution of OA/ΔCO vs. total photochemical age in days (at OH = 1.5×10^6 molec. cm^{-3}) with* ***(a)*** *traditional SOA formation model, high NO_x Robinson + Tsimpidi model from Hayes et al. (2014). Also shown is the summary of urban aged ratios from de Gouw and Jimenez (2009).* ***(b)*** *High NO_x Robinson + Tsimpidi model from Hayes et al. (2015) run with one-half IVOCs per the results of Zhao et al. (2014). (POA+BGSOA)/ΔCO is 21 μg m^{-3} ppm^{-1}, which somewhat is higher than the value of 16 μg m^{-3} ppm^{-1} previously reported by Hayes et al. (2013). This difference is due to the different methods used to estimate the background SOA. Briefly, in this work as well as in Hayes et al. (2015), the background SOA is estimated to be equal to the minimum low-volatility oxygenated organic aerosol (LV-OOA) concentration in the diurnal cycle. Whereas in Hayes et al. (2013), the background SOA was estimated to be equal to the mean LV-OOA concentration for photochemical ages less than 1.2 h.*

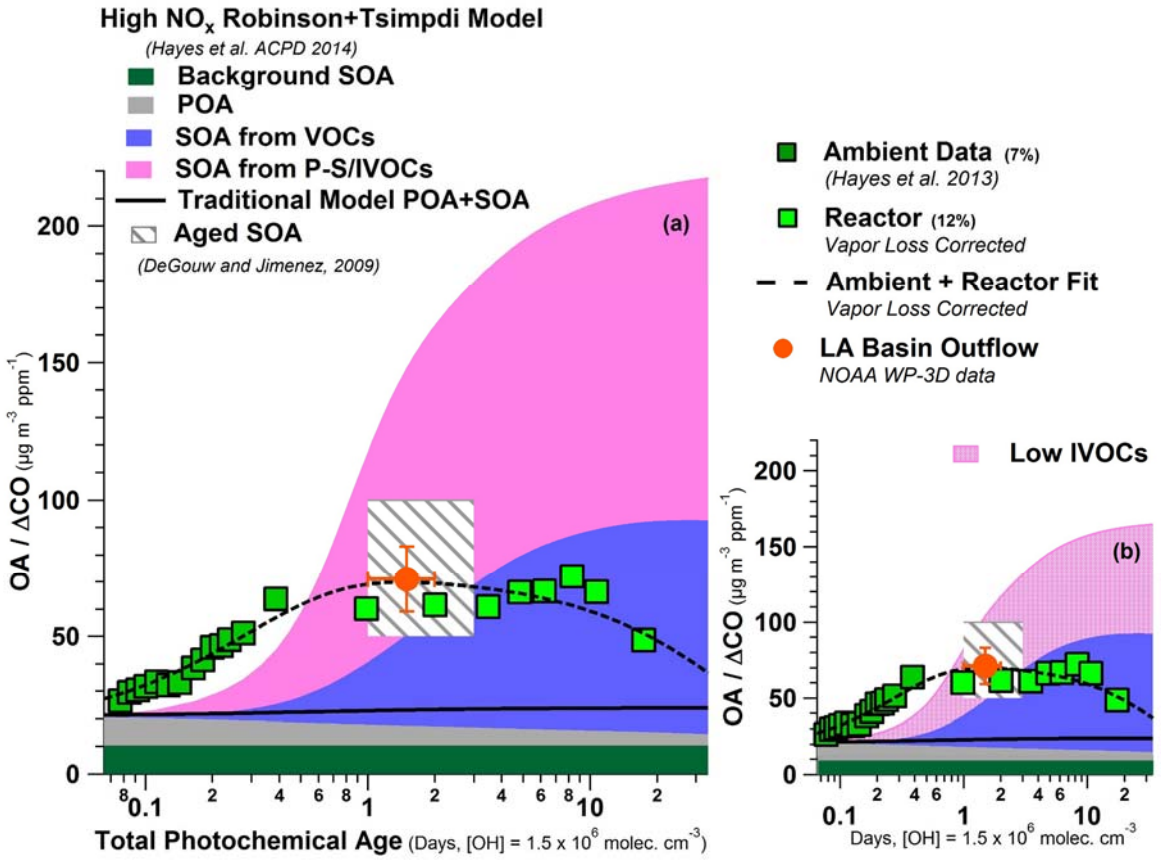

3.12. Evolution at High Photochemical Ages

The photochemical evolution of OA at long ages is of high interest as it partially controls the background of OA at remote locations where it may influence climate more strongly, due to the higher sensitivity of clouds to aerosols at low aerosol concentrations (Reutter et al., 2009). Heald et al. (2011) noted that a process that consumed OA with a timescale of ~10 days was needed in order to avoid overpredictions of OA in remote air. Heterogeneous oxidation is thought to play an important role for long photochemical ages, while being too slow to compete at timescales of a day or so (DeCarlo et al., 2008; George and Abbatt, 2010). Fig. 37a compares our CalNex results to heterogeneous OH oxidation of ambient air from George and Abbatt (2010) using a similar oxidation flow reactor (TPOT), but with gas-phase SOA precursors removed by a denuder. Note that no SOA formation is observed for the George and Abbatt case due to the use of a denuder, and thus only the data for $ER_{OA} < 1$ can be approximately compared. The two datasets show a similar trend with the start of a net decrease around 2 weeks of oxidation and a similar evolution. A decrease in SOA yields at high ages (>7 days) was also observed by Lambe et al. (2012), in experiments where SOA was formed from gaseous precursors. However it is likely that the decrease in that study is dominated by gas-phase fragmentation of condensable species leading to lack of SOA formation, rather than by SOA formation followed by its heterogeneous oxidation (e.g. Fig. 10).

To evaluate directly whether heterogeneous oxidation could explain the gain of oxygen observed in the aerosol, we follow the method outlined in appendix A of DeCarlo et al. (2008). Fig. 38 shows an estimate of the total number of OH collisions with OA in the reactor vs. total photochemical age. Heterogeneous oxidation calculations use volume equivalent diameter (dve) of 285 nm as calculated using the peak of the mass distribution and estimated particle density from AMS components, assume every collision results in reaction ($\gamma = 1$). The measured net oxygen added (ΔOxygen in OA = $O_{atoms,reactor} - O_{atoms,ambient}$) vs. OH_{exp}, is also shown. If it is assumed that each OH collision with OA results in one O atom addition, the number of O atoms added is underpredicted by a factor of 10 at ages ~ 1 day, decreasing to a factor of 2 at ~10 days, and lower values at high ages (>10 days). This analysis supports that heterogeneous oxidation is not dominant in forming SOA at low-to-intermediate ages, but it likely plays a role in OA evolution at the highest photochemical ages in the reactor.

An alternative explanation for the loss of OA at high photochemical ages is that the reaction of semivolatile gas species with OH (leading to fragmentation and thus non-condensing species) can lead to OA evaporation as the semivolatile species in the particles evaporate to re-establish equilibrium partitioning. However, most of OA has too low volatility to evaporate in response to the removal of semivolatile species from the gas phase. Fig. 39 shows the volatility distribution estimated for CalNex OA using concurrent thermal denuder measurements (Huffman et al., 2008; Faulhaber et al., 2009). As observed in other locations (Cappa and Jimenez, 2010), only ~20% of the OA is susceptible of evaporation upon removal of the gas phase. Losing ~60% of the OA would be the equivalent of heating to 100˚C in a thermal denuder. Thus, there is not enough semivolatile material available to account for that degree of loss observed in our reactor measurements. We note that some models predict SOA that is too volatile (Dzepina et al., 2009), and if applied in a flow reactor context they may wrongly predict a large effect from semivolatile evaporation. Additionally, timescales for ambient OA evaporation upon removal of gas-phase organics from field measurements has been shown to be slow and size dependent, with fast evaporation up to only ~20% of OA mass happening on the order of ~100 min, followed by

much slower evaporation of the order of days (Vaden et al., 2011). Given the short residence time utilized in the reactor during this study (< 5 minutes), there is not significant time to allow for substantial repartitioning of OA in equilibrium with semivolatile gas-phase organics.

Figure 37: (a) *Relative organic aerosol enhancement (ER_{OA}) from all reactor data in this study (including 6% quantiles) and from a heterogeneous oxidation study (George and Abbatt, 2010) plotted vs. total photochemical age in days (at OH = 1.5×10^6 molec. cm^{-3}).* ***(b)*** *SOA/ΔCO vs. photochemical age for our study and for aging of vehicle exhaust with a similar reactor at a tunnel near Pittsburgh, PA (Tkacik et al., 2014). Results from field studies in the northeastern US and Mexico City are shown in the background (DeCarlo et al., 2010).*

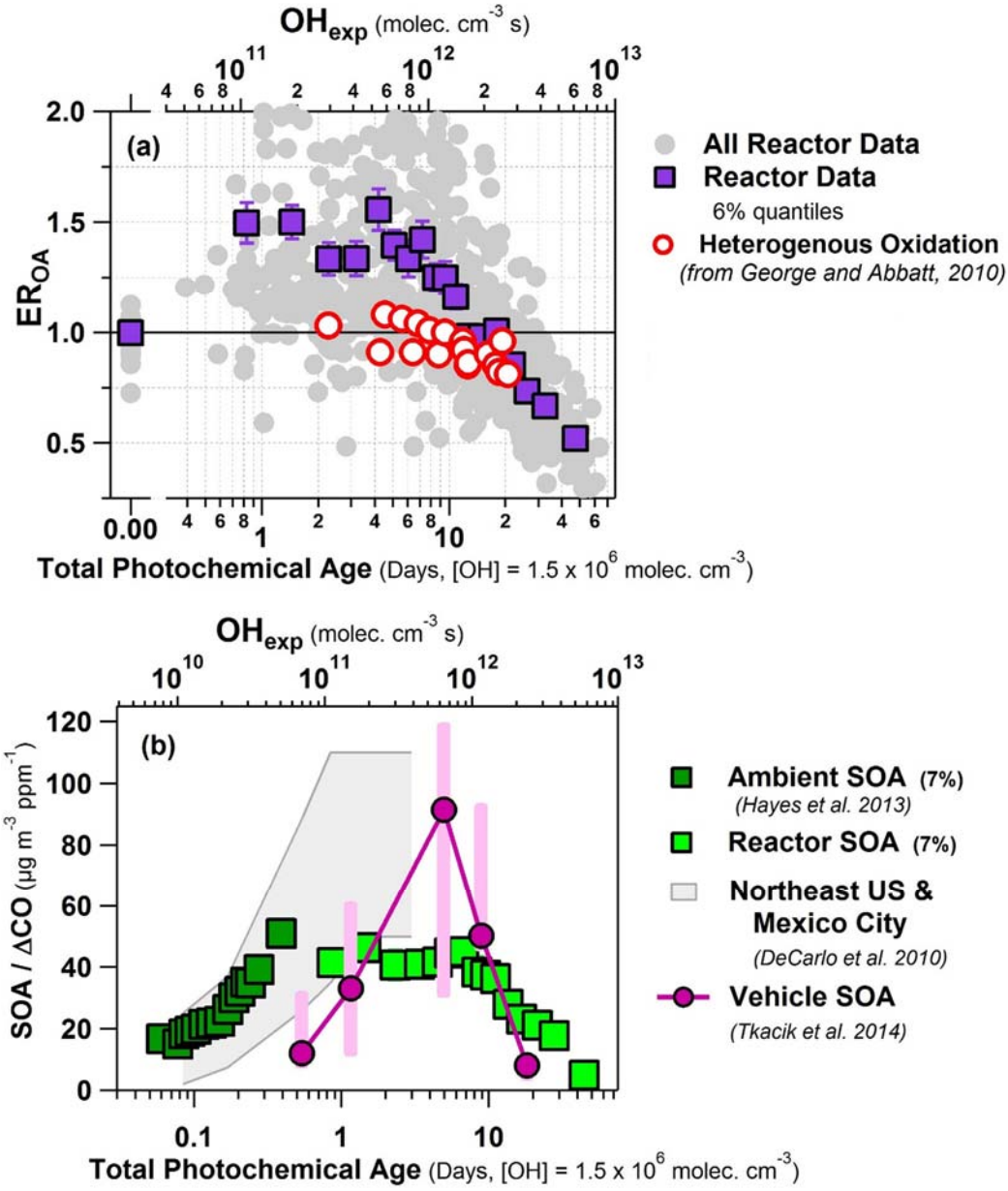

3.13. Comparison to a recent Reactor Study in a Tunnel

It is of interest to compare the evolution of urban SOA vs. photochemical age determined in this work with a recently published study with a similar flow reactor in a vehicle tunnel in Pittsburgh, PA (Tkacik et al., 2014). Whether urban SOA is formed predominantly from vehicle emissions has been the subject of recent debate (Ensberg et al., 2014). The data are compared in Fig. 37b as SOA/ΔCO, where ambient POA and background OA have been subtracted from our reactor data to compare to Tkacik et al. (2014)'s SOA-only measurement. Since the tunnel data has not been corrected for vapor losses in the reactor, we only show uncorrected CalNex reactor data for this comparison.

The tunnel experiment shows qualitatively similar results, with an initial increase to a peak of the same order, followed by a decrease in SOA/ΔCO at high ages. The initial SOA rise and peak occur at higher OH_{exp} than observed in CalNex ambient data and in previous ambient urban studies, as well as our flow reactor data. The difference at low ages between the tunnel and the other studies may be due to several reasons:

(1) Possible OH_{exp} overestimation in the tunnel study. OH_{exp} in flow reactors can be reduced by 1-2 orders of magnitude by high levels of OH reactivity from high concentrations of very fresh emissions, such as those present in the tunnel environment (Li et al., 2015; Peng et al., 2015). OH_{exp} was corrected for OH suppression in the tunnel study using laboratory experiments with NO levels similar to the tunnel. However, the OH reactivity of NOx is expected to decay much faster than that of VOCs and their reaction products. Thus the OH suppression in the tunnel study was likely underestimated (Peng et al., 2015) as OH suppression from VOCs was not considered. Since OH suppression is largest at low OH_{exp} that effect may account for the deviation observed at low ages while having a much smaller effect on the tunnel data at high ages.

(2) There may be substantial losses of semivolatiles in the inlet of the tunnel study. In contrast, our flow reactor was operated without an inlet to minimize the loss of semivolatiles, based on an observation in a previous study of a substantial reduction in SOA formation when any inlet or an inlet plate was used (Ortega et al., 2013). Since semivolatile primary species are larger molecules with faster OH rate constants (Ziemann and Atkinson, 2012), that could explain the lack of SOA formation at ages below a day, compared to the large amount of SOA formed for those ages in the ambient CalNex observations (Hayes et al., 2013; 2015). However the fact that the magnitude of eventual SOA formation is larger in the tunnel study argues against this possibility. Thus it is most likely that the observed difference between the tunnel and our study is due to overestimation of OH_{exp} at lower ages in the tunnel study.

A recent study examining the ambient SOA results from CalNex concluded that either vehicle emissions are not the dominant source of SOA in the LA Basin, or that the ambient SOA mass yields are much larger than what has been derived experimentally (Ensberg et al., 2014). Given the similar magnitude of SOA formation in the tunnel vs. ambient data and the fact that most urban CO arises from motor vehicles, as well as the likely overestimation of OH_{exp} at low ages in the tunnel study, the combination of both studies strongly suggests that motor vehicles are the dominant source of urban SOA, and that the SOA yields from vehicle emissions are much larger than estimated from measured VOCs as by Ensberg et al. (2014). The contribution of typically unmeasured S/IVOCs to SOA may explain the missing vehicle SOA, as discussed above.

Figure 38. *Measured oxygen added to OA in the reactor vs. total photochemical age in days (at OH = 1.5×10^6 molec. cm^{-3}), along with a log normal fit to the ΔOxygen data. Reactor data is colored by OA mass enhancement. The estimated number of OH collisions with OA is shown, based on the methodology outlined in appendix A of DeCarlo et al. (2008).*

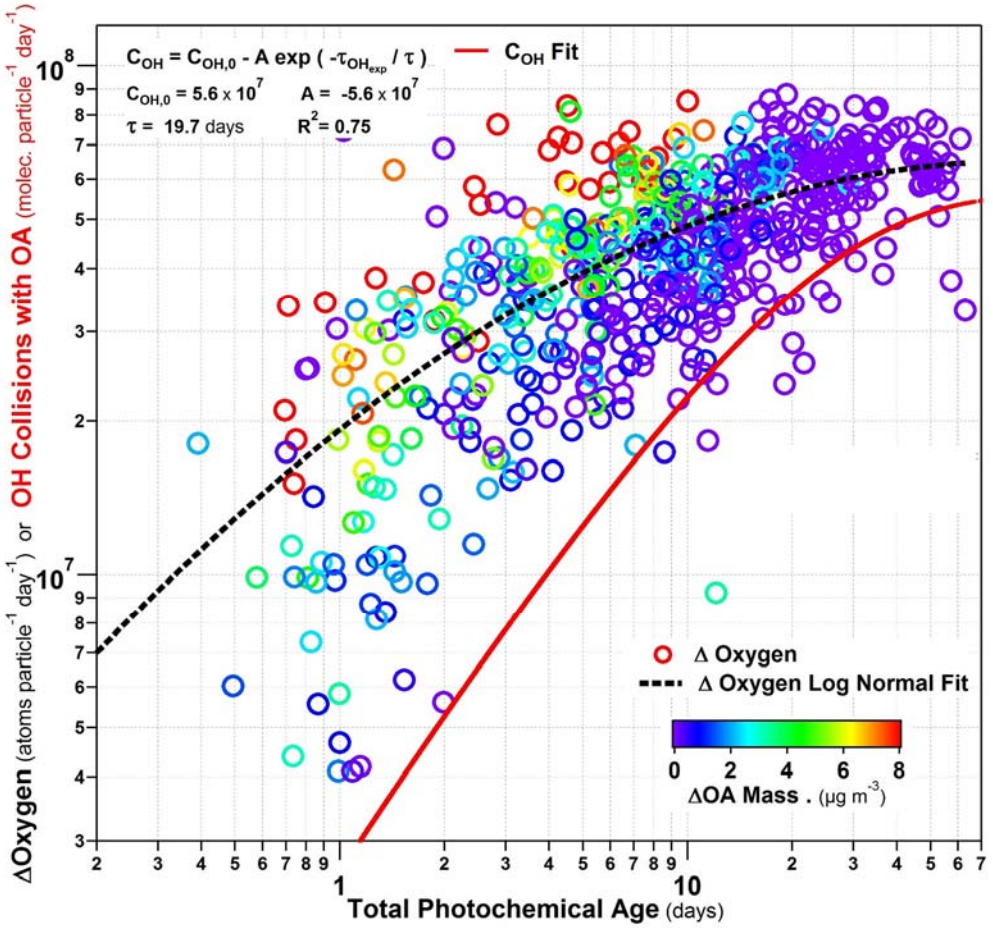

Figure 39. *Top panel: Mass fraction remaining (MFR) for OA vs. thermal denuder temperature for this CalNex-LA dataset, using the methods described in Huffman et al. (2008; 2009). Bottom panel: estimated volatility distribution of particle- and gas-phase species, calculated from the thermal denuder profile using the method of Faulhaber et al. (2009), on bottom panel.*

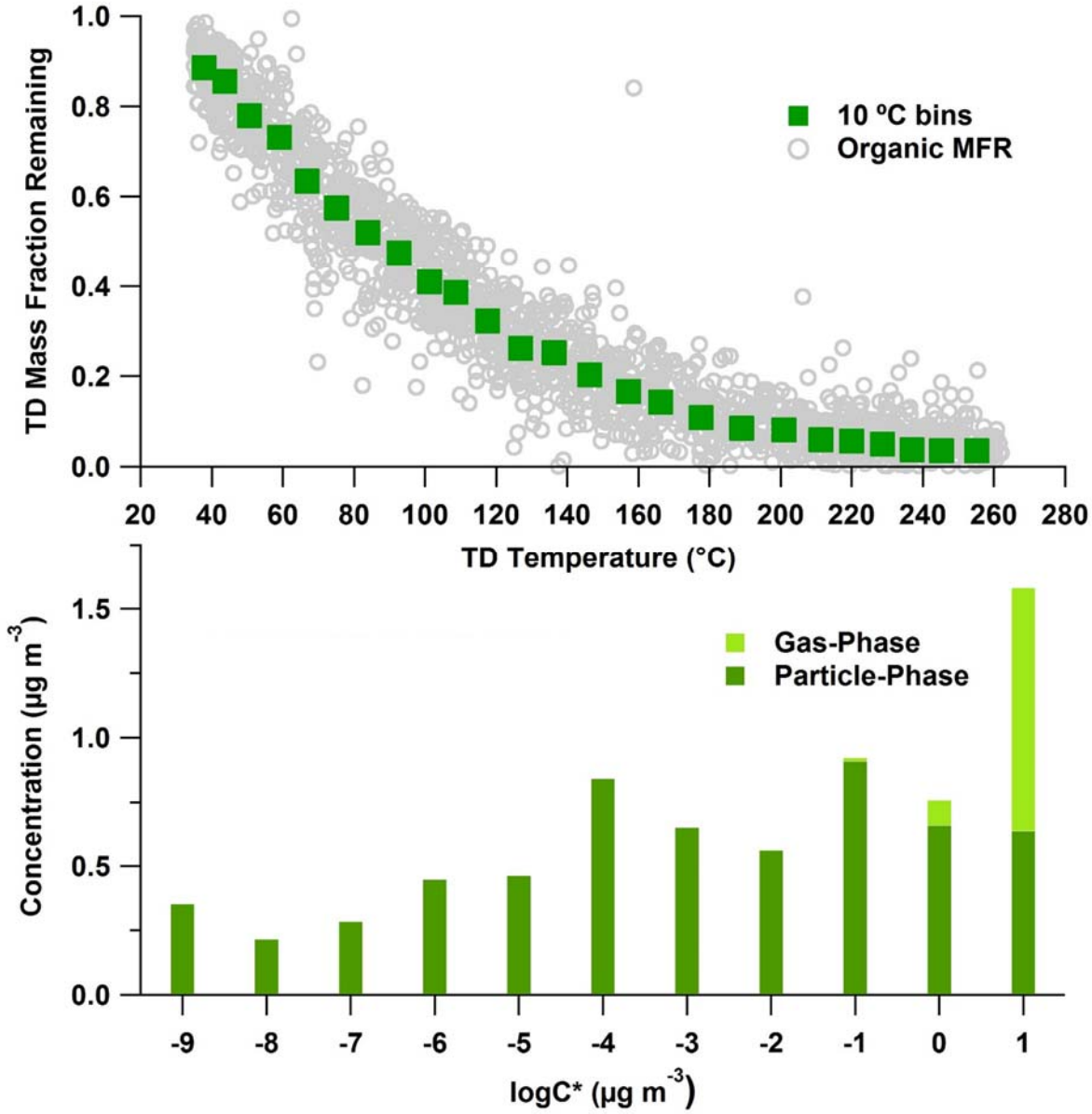

4. Conclusions

SOA in Pasadena during CalNex has been modeled using three different methods: (1) a box model, (2) a 3-D dimensional model, namely, WRF-CMAQ, and (3) a simple two-parameter model. Model/measurement comparisons clearly indicate that SOA formed from P-S/IVOCs, or a similar source, must be included in the models to accurately predict SOA concentrations in Pasadena. In other words, SOA from VOC oxidation is not sufficient to explain the observed concentrations, even when the highest SOA yields are used. Specifically, the parameterizations utilized were the Tsimpidi et al. (2010) parameterization with aging or a modified version of that parameterization in which the SOA yields for aromatic VOCs were multiplied by four as recently suggested by Zhang et al. (2014).

Three parameterizations for SOA formation from P-S/IVOCs were tested. It was found that the parameterization reported by Grieshop et al. (2009) best predicts SOA concentration at the urban site. In contrast, the parameterization of Robinson et al. (2007) predicts too little SOA. These results contrast earlier modeling studies of Mexico City that showed the Robinson parameterization performed better when compared against the measured SOA concentration. The reason for the difference is not clear. Both the Mexico City and Pasadena studies suggest that the Grieshop parameterization more accurately predicts SOA oxygen content, but this conclusion is also dependent on model parameters that are not well-constrained. Additionally, we tested the parameterization proposed in Pye and Seinfeld (2010) for the formation of SOA from P-S/IVOCs, which produces similar results but tends to overpredict SOA concentrations especially at nighttime and in the morning for this case study. The relative importance of VOCs and P-S/IVOCs as contributors to urban SOA over different time and length scales remains unclear. Depending on the parameterization used in the box model, the amount of urban SOA from VOCs can range between 15 – 53% of the total predicted SOA for the Pasadena ground site. This range is 16 – 58% in a sensitivity study in which the IVOC emissions are reduced by one-half. All the parameterizations used in the box model overpredict urban SOA at photochemical ages larger than one day when compared to field observations, which has implications for their use in regional and global models. However, when the IVOC emissions in the box model are reduced by one-half to better match the measurements of Zhao et al. (2014) the predictions of SOA at long photochemical ages are improved although still too high, while the model/measurement comparison at short photochemical ages is still within the measurement uncertainties for the GRI+TSI and ROB+4xV variations.

This work represents the first chemically explicit evaluation of WRF-CMAQ SOA mass predictions in the Western U.S. or California. This model provides excellent predictions of secondary inorganic particle species but underestimates the observed SOA mass by a factor of about 25. The discrepancy is likely attributable to the VOC-only parameterization used that has relatively low yields and does not include SOA from P-S/IVOCs or a similar source.

SOA source apportionment was also carried out using the box model results. Among the explicitly modeled VOCs, the precursor compounds that contribute the most SOA mass are all methylbenzenes. In contrast, measured PAHs including naphthalene, 1-methylnaphthalene, and 2-methylnaphthalene are relatively minor precursors and contribute 0.7% of the SOA mass. In addition, the amount of urban SOA from diesel vehicles, gasoline vehicles, and cooking-related emissions is estimated to be 16 – 27%, 35 – 61%, and 19 – 35%, respectively, with an almost factor of 2 difference in the estimated contribution depending on the box model variant used. A

significant amount of background SOA appears to be formed outside the Los Angeles Basin and transported to the Pasadena site. The percentage estimated from diesel in the model is in agreement with our previous study that estimated the diesel contribution to be 0 – 36% by analyzing the weekly cycle of OOA concentrations (Hayes et al., 2013). The fraction of fossil and non-fossil urban SOA from the different models is generally consistent with the measurements. Importantly, a large source of urban non-fossil SOA most likely due to cooking is identified, while biogenic SOA formed from urban-scale emissions makes a small contribution.

The final portion of this work adapts the SIMPLE two parameter model of Hodzic and Jimenez (2011) to predict SOA properties for Pasadena. The simple model successfully predicts SOA concentration and oxygen content with accuracy similar to the more complex parameterizations. Furthermore, the optimal parameters for the SIMPLE model are very similar in both Mexico City and Pasadena, which indicates that this computationally inexpensive approach may be useful for predicting pollution SOA in global and climate models. Pollution SOA is estimated to account for 17% of global SOA, and we note that ~1/3 of urban SOA may be non-fossil mainly due to the impact of cooking and other sources.

Real-time measurement of SOA formation and OA aging was carried out with a photochemical oxidation flow reactor coupled to an AMS and SMPS during the CalNex field campaign and targeted urban emissions. This work represents the first applications of an oxidation flow reactor to ambient urban air, to our knowledge. Continuous ambient air sampling through the reactor provides complementary information to the analysis of ambient data at the site, and provides constraints on the evolution of urban SOA at long ages that are very difficult to observe with ambient measurements. Additionally, these uninterrupted reactor measurements over a two-week period allowed for observations over a prolonged period of stagnant air accumulating urban emissions.

OA enhancement peaked between 0.8–6 days of atmospheric equivalent aging (OH_{exp} = 1.0–5.2×10^{11} molec. cm^{-3} s). Reactor OA mass showed net destruction decreasing below ambient concentrations after two weeks of atmospheric equivalent aging (OH_{exp} above 2×10^{12} molec. cm^{-3} s) suggesting a shift from chemistry dominated by functionalization/condensation to one dominated by heterogeneous oxidation leading to fragmentation/evaporation, but with functionalization still occurring. Comparison to reactor experiments of heterogeneous oxidation of ambient air shows similar trends to those observed for high ages in this study. High OA enhancement was observed at night (ER_{OA} ~2, delta OA ~5 μg m^{-3}) with reactor-aged OA mass peaking at concentrations similar to peak daytime ambient OA mass. Reactor-derived OA mass enhancement correlates with 1,3,5-trimethylbenzene, and has an inverse relationship with Ox and ambient OOA, suggesting that short-lived precursors (τ_{OH} ~ few hours) dominate SOA formation in the LA-Basin.

The chemical evolution of OA in the reactor was examined with a Van Krevelen diagram (H:C vs. O:C). Reactor-aged OA produces a similar slope (~ -0.65) to that observed in ambient OA, thus is consistent with the reactor producing similar functionalization to ambient oxidation. While total OA mass was observed to decrease at very high OH exposures, O:C continued to increase. Oxidation state of carbon peaked at high values (OSC ~2 at highest OH_{exp}), similar to ambient observations of low volatility OA.

Modeling results indicate predicted maximum SOA from traditional models is a factor of 10 less than the maximum OA mass enhancement observed from aging ambient air in the reactor,

consistent with previous comparisons using ambient data. Updated VBS-based models including both VOC and S/IVOC overpredict SOA formation by a factor of 2–3 at intermediate to high ages. If the IVOC emissions are reduced by a factor of 2 in the updated model to fit recent CalNex observations, the discrepancy between model and observation is reduced but these models cannot capture the reduction of SOA mass concentration that is observed with the OFR at longer OH exposures.

Evolution of the ratio of OA/ΔCO vs. photochemical age shows the reactor produces results consistent with the ambient data. At ages beyond those reliably observed for ambient OA, the reactor observations show a leveling and then decrease in OA/ΔCO. A fit of this data results in a timescale of SOA formation ~0.3 days and fragmentation-dominated heterogeneous oxidation and net mass loss with a timescale of ~50 days. The fit derived in this work may be useful in future studies, e.g. as a check on proposed model-parameterizations of urban SOA formation. Comparison to a similar reactor experiment aging vehicular emissions in a tunnel shows consistent results with our study, especially if a likely overestimation of OH_{exp} at low ages in the tunnel is taken into account. The combination of both studies strongly suggests that vehicle emissions do dominate urban SOA formation and their SOA formation potential is higher than when only VOCs are considered.

This study shows that oxidation flow reactors are useful tools as part of ambient field studies, as they allow real-time measurement of SOA formation potential and oxidation across a wide range of photochemical ages. These results help constrain SOA models not only for the growth phase of the SOA but also for the decay phase, when further aging removes SOA mass. Future studies should apply this technique in other cities and other environments such as forested regions and the outflow from polluted continents, in order to further constrain the SOA formation potential and timescales for different sources and regions.

5. Recommendations

1) Substantial progress in understanding the sources and processes involved in urban SOA formation has been achieved in this project, as well as from research carried out in parallel by our collaborators and others. However the SOA problem remains very difficult due to its complexity and the limitations of the measurements available at the time of CalNex and earlier studies. It should be recognized that substantial continued investment in SOA research for the next decade is needed to reduce the uncertainty in SOA model predictions to a level where policymaking options can be chosen for the right reasons and with high confidence that they will work.

2) The extensive CalNex dataset should continue to be used to further clarify pending questions in urban SOA formation, in particular the relative importance of VOC and S/IVOC and of different sources as SOA precursors (diesel, gasoline, cooking, biogenic etc.). An enormous investment has been made in collecting and analyzing data and performing many types of modeling. It would be very efficient to apply additional tools currently available to those research questions.

3) Further investigation of SOA formation from vehicle emissions and from cooking emissions should be conducted, using a combination of field, laboratory, modeling and studies.

4) Comprehensive measurements of aerosols, their precursors, oxidants, and transport, similar in scope to CalNex, should be conducted periodically (at least every 10 years) in key areas of California to better characterize and understand trends in emissions and the resulting impact on secondary species, as well as to take advantage of rapidly improving instrumentation that can be used to greatly advance additional research questions.

5) Increased scope and sophistication of air quality monitoring programs is highly desirable, for instance, through the deployment of Aerodyne Aerosol Chemical Speciation Monitors (ACSM) or similar instrumentation, as well as by time-resolved monitoring of anthropogenic and biogenic VOCs. This type of data will also allow a more detailed study of weekday / weekend effects that have provided very useful information in the past.

6) Deployment of oxidation flow reactors (OFRs) for extended periods of time, and co-located with routine monitoring networks should be considered. However due to the complexity of OFR operation, the need for collocated advanced VOC data, and especially data interpretation this task is only appropriate at present for research groups, in our opinion.

7) The chemical nature and sources of the rapidly-reacting SOA precursors that dominate SOA formation should be further investigated.

8) Collaboration of SOA modeling groups should be strongly encouraged, as this field can be rather fragmented. While on the surface some conclusions appear contradictory, each method has strengths and weaknesses and provides strong conclusions in some areas and weaker conclusions in others. A mechanism to elicit a discussion and to achieve consensus where possible within the research community may be very useful to CARB and the wider community. For example, writing of a review paper collaboratively across all active groups should be encouraged (maybe required for funded groups) as that will force debate and clarification on some confusion in the current literature. Funding a small project shared by several key groups whose outcome is such a review would make certain that it would be produced.

9) Standard versions of air quality models (e.g. used for regulatory compliance) should be updated including recent findings on urban SOA formation. As shown in this study, errors of more than an order-of-magnitude remain on models that have not been updated such as CMAQ v.5.0.1. The SIMPLE parameterization should be used to obtain reasonable urban SOA concentrations when their study is not the main goal of the study (as done successfully by the Jacob group at Harvard in e.g. Kim et al., *Atmos. Chem. Phys.*, 2015).

References

Ahmadov, R., McKeen, S.A., Robinson, A.L., Bahreini, R., Middlebrook, A.M., de Gouw, J.A., Meagher, J., Hsie, E.Y., Edgerton, E., Shaw, S. and Trainer, M. (2012) A volatility basis set model for summertime secondary organic aerosols over the eastern United States in 2006. J. Geophys. Res.-Atmos. 117, D06301.

Aiken, A.C., DeCarlo, P.F. and Jimenez, J.L. (2007) Elemental analysis of organic species with electron ionization high-resolution mass spectrometry. Anal. Chem. 79, 8350-8358.

Aiken, A. C., DeCarlo, P. F., Kroll, J. H., Worsnop, D. R., Huffman, J. A., Docherty, K. S., Ulbrich, I. M., Mohr, C., Kimmel, J. R., Sueper, D., Sun, Y., Zhang, Q., Trimborn, A., Northway, M., Ziemann, P. J., Canagaratna, M. R., Onasch, T. B., Alfarra, M. R., Prevot, A. S. H., Dommen, J., Duplissy, J., Metzger, A., Baltensperger, U., and Jimenez, J. L.: O/C and OM/OC Ratios of Primary, Secondary, and Ambient Organic Aerosols with High-Resolution Time-of-Flight Aerosol Mass Spectrometry, Environmental Science & Technology, 42, 4478-4485, 10.1021/es703009q, 2008.

Atkinson, R. and Arey, J. (2003) Atmospheric degradation of volatile organic compounds. Chem. Rev. 103, 4605-4638.

Atkinson, R., Baulch, D. L., Cox, R. A., Crowley, J. N., Hampson, R. F., Hynes, R. G., Jenkin, M. E., Rossi, M. J., Troe, J., and Subcommittee, I.: Evaluated kinetic and photochemical data for atmospheric chemistry: Volume II: gas phase reactions of organic species, Atmos. Chem. Phys., 6, 3625-4055, 10.5194/acp-6-3625-2006, 2006.

Bahreini, R., Middlebrook, A. M., Brock, C. A., de Gouw, J. A., McKeen, S. A., Williams, L. R., Daumit, K. E., Lambe, A. T., Massoli, P., Canagaratna, M. R., Ahmadov, R., Carrasquillo, A. J., Cross, E. S., Ervens, B., Holloway, J. S., Hunter, J. F., Onasch, T. B., Pollack, I. B., Roberts, J. M., Ryerson, T. B., Warneke, C., Davidovits, P., Worsnop, D. R., and Kroll, J. H.: Mass Spectral Analysis of Organic Aerosol Formed Downwind of the Deepwater Horizon Oil Spill: Field Studies and Laboratory Confirmations, Environmental Science & Technology, 46, 8025-8034, 10.1021/es301691k, 2012a.

Bahreini, R., Middlebrook, A. M., de Gouw, J. A., Warneke, C., Trainer, M., Brock, C. A., Stark, H., Brown, S. S., Dube, W. P., Gilman, J. B., Hall, K., Holloway, J. S., Kuster, W. C., Perring, A. E., Prevot, A. S. H., Schwarz, J. P., Spackman, J. R., Szidat, S., Wagner, N. L., Weber, R. J., Zotter, P., and Parrish, D. D.: Gasoline emissions dominate over diesel in formation of secondary organic aerosol mass, Geophysical Research Letters, 39, 10.1029/2011gl050718, 2012b.

Baker, K.R., Misenis, C., Obland, M.D., Ferrare, R.A., Scarino, A.J. and Kelly, J.T. (2013) Evaluation of surface and upper air fine scale WRF meteorological modeling of the May and June 2010 CalNex period in California. Atmos. Environ. 80, 299-309.

Baker, K. R., Carlton, A. G., Kleindienst, T. E., Offenberg, J. H., Beaver, M. R., Gentner, D. R., Goldstein, A. H., Hayes, P. L., Jimenez, J. L., Gilman, J. B., de Gouw, J. A., Woody, M. C., Pye, H. O. T., Kelly, J. T., Lewandowski, M., Jaoui, M., Stevens, P. S., Brune, W. H., Lin, Y. H., Rubitschun, C. L., and Surratt, J. D.: Gas and aerosol carbon in California: comparison of

measurements and model predictions in Pasadena and Bakersfield, Atmos. Chem. Phys., 15, 5243-5258, 10.5194/acp-15-5243-2015, 2015.

Bertram, A.K., Martin, S.T., Hanna, S.J., Smith, M.L., Bodsworth, A., Chen, Q., Kuwata, M., Liu, A., You, Y. and Zorn, S.R. (2011) Predicting the relative humidities of liquid-liquid phase separation, efflorescence, and deliquescence of mixed particles of ammonium sulfate, organic material, and water using the organic-to-sulfate mass ratio of the particle and the oxygen-to-carbon elemental ratio of the organic component. Atmos. Chem. Phys. 11, 10995-11006.

Borbon, A., Gilman, J. B., Kuster, W. C., Grand, N., Chevaillier, S., Colomb, A., Dolgorouky, C., Gros, V., Lopez, M., Sarda-Esteve, R., Holloway, J., Stutz, J., Petetin, H., McKeen, S., Beekmann, M., Warneke, C., Parrish, D. D., and de Gouw, J. A.: Emission ratios of anthropogenic volatile organic compounds in northern mid-latitude megacities: Observations versus emission inventories in Los Angeles and Paris, Journal of Geophysical Research: Atmospheres, 118, 2041-2057, 10.1002/jgrd.50059, 2013.

Bruns, E. A., El Haddad, I., Keller, A., Klein, F., Kumar, N. K., Pieber, S. M., Corbin, J. C., Slowik, J. G., Brune, W. H., Baltensperger, U., and Prévôt, A. S. H.: Inter-comparison of laboratory smog chamber and flow reactor systems on organic aerosol yield and composition, Atmos. Meas. Tech., 8, 2315-2332, doi:10.5194/amt-8-2315-2015, 2015.

Canagaratna, M. R., Jayne, J. T., Jimenez, J. L., Allan, J. D., Alfarra, M. R., Zhang, Q., Onasch, T. B., Drewnick, F., Coe, H., Middlebrook, A., Delia, A., Williams, L. R., Trimborn, A. M., Northway, M. J., DeCarlo, P. F., Kolb, C. E., Davidovits, P., and Worsnop, D. R.: Chemical and microphysical characterization of ambient aerosols with the aerodyne aerosol mass spectrometer, Mass Spectrometry Reviews, 26, 185-222, 10.1002/mas.20115, 2007.

Canagaratna, M. R., Jimenez, J. L., Kroll, J. H., Chen, Q., Kessler, S. H., Massoli, P., Hildebrandt Ruiz, L., Fortner, E., Williams, L. R., Wilson, K. R., Surratt, J. D., Donahue, N. M., Jayne, J. T., and Worsnop, D. R.: Elemental ratio measurements of organic compounds using aerosol mass spectrometry: characterization, improved calibration, and implications, Atmos. Chem. Phys., 15, 253-272, 10.5194/acp-15-253-2015, 2015.

Cao, G., and Jang, M.: Effects of particle acidity and UV light on secondary organic aerosol formation from oxidation of aromatics in the absence of NOx, Atmospheric Environment, 41, 7603-7613, http://dx.doi.org/10.1016/j.atmosenv.2007.05.034, 2007.

Cappa, C. D., and Jimenez, J. L.: Quantitative estimates of the volatility of ambient organic aerosol, Atmos. Chem. Phys., 10, 5409-5424, 10.5194/acp-10-5409-2010, 2010.

Cappa, C.D. and Wilson, K.R. (2011) Evolution of organic aerosol mass spectra upon heating: implications for OA phase and partitioning behavior. Atmos. Chem. Phys. 11, 1895-1911.

Cappa, C.D., Onasch, T.B., Massoli, P., Worsnop, D.R., Bates, T.S., Cross, E.S., Davidovits, P., Hakala, J., Hayden, K.L., Jobson, B.T., Kolesar, K.R., Lack, D.A., Lerner, B.M., Li, S.M., Mellon, D., Nuaaman, I., Olfert, J.S., Petaja, T., Quinn, P.K., Song, C., Subramanian, R., Williams, E.J. and Zaveri, R.A. (2012) Radiative Absorption Enhancements Due to the Mixing State of Atmospheric Black Carbon. Science 337, 1078-1081.

Carlton, A.G. and Baker, K.R. (2011) Photochemical Modeling of the Ozark Isoprene Volcano: MEGAN, BEIS, and Their Impacts on Air Quality Predictions. Environ. Sci. Technol. 45, 4438-4445.

Carlton, A.G., Bhave, P.V., Napelenok, S.L., Edney, E.D., Sarwar, G., Pinder, R.W., Pouliot, G.A. and Houyoux, M. (2010) Model Representation of Secondary Organic Aerosol in CMAQv4.7. Environ. Sci. Technol. 44, 8553-8560.

Carlton, A.G., Turpin, B.J., Altieri, K.E., Seitzinger, S.P., Mathur, R., Roselle, S.J. and Weber, R.J. (2008) CMAQ model performance enhanced when in-cloud SOA is included: comparisons of OC predictions with measurements. Environ. Sci. Technol. 42, 8798-8802.

Carter, W.P.L. (2010) Development of the SAPRC-07 chemical mechanism. Atmos. Environ. 44, 5324-5335.

Chan, A.W.H., Kautzman, K.E., Chhabra, P.S., Surratt, J.D., Chan, M.N., Crounse, J.D., Kürten, A., Wennberg, P.O., Flagan, R.C. and Seinfeld, J.H. (2009) Secondary organic aerosol formation from photooxidation of naphthalene and alkylnaphthalenes: implications for oxidation of intermediate volatility organic compounds (IVOCs). Atmos. Chem. Phys. 9, 3049-3060.

Chen, Q., Farmer, D.K., Schneider, J., Zorn, S.R., Heald, C.L., Karl, T.G., Guenther, A., Allan, J.D., Robinson, N., Coe, H., Kimmel, J.R., Pauliquevis, T., Borrmann, S., Poschl, U., Andreae, M.O., Artaxo, P., Jimenez, J.L. and Martin, S.T. (2009) Mass spectral characterization of submicron biogenic organic particles in the Amazon Basin. Geophys. Res. Lett. 36, L20806.

Claeys, M., Szmigielski, R., Kourtchev, I., Van der Veken, P., Vermeylen, R., Maenhaut, W., Jaoui, M., Kleindienst, T.E., Lewandowski, M., Offenberg, J.H. and Edney, E.O. (2007) Hydroxydicarboxylic Acids: Markers for Secondary Organic Aerosol from the Photooxidation of α-Pinene. Environ. Sci. Technol. 41, 1628-1634.

Cubison, M. J., Ortega, A. M., Hayes, P. L., Farmer, D. K., Day, D., Lechner, M. J., Brune, W. H., Apel, E., Diskin, G. S., Fisher, J. A., Fuelberg, H. E., Hecobian, A., Knapp, D. J., Mikoviny, T., Riemer, D., Sachse, G. W., Sessions, W., Weber, R. J., Weinheimer, A. J., Wisthaler, A., and Jimenez, J. L.: Effects of aging on organic aerosol from open biomass burning smoke in aircraft and laboratory studies, Atmos Chem Phys, 11, 12049-12064, DOI 10.5194/acp-11-12049-2011, 2011.

de Gouw, J., and Jimenez, J. L.: Organic Aerosols in the Earth's Atmosphere, Environmental Science & Technology, 43, 7614-7618, 10.1021/es9006004, 2009.

de Gouw, J. A., Middlebrook, A. M., Warneke, C., Goldan, P. D., Kuster, W. C., Roberts, J. M., Fehsenfeld, F. C., Worsnop, D. R., Canagaratna, M. R., Pszenny, A. A. P., Keene, W. C., Marchewka, M., Bertman, S. B., and Bates, T. S.: Budget of organic carbon in a polluted atmosphere: Results from the New England Air Quality Study in 2002, J. Geophys. Res., 110, D16305, 10.1029/2004jd005623, 2005.

de Gouw, J.A., Gilman, J.B., Borbon, A., Warneke, C., Kuster, W.C., Goldan, P.D., Holloway, J.S., Peischl, J., Ryerson, T.B., Parrish, D.D., Gentner, D.R., Goldstein, A.H. and Harley, R.A. (2012) Increasing atmospheric burden of ethanol in the United States. Geophys. Res. Lett. 39, L15803.

DeCarlo, P. F., Kimmel, J. R., Trimborn, A., Northway, M. J., Jayne, J. T., Aiken, A. C., Gonin, M., Fuhrer, K., Horvath, T., Docherty, K., Worsnop, D. R., and Jimenez, J. L.: Field-Deployable, High-Resolution, Time-of-Flight Aerosol Mass Spectrometer, Analytical Chemistry, 78, 8281-8289, 2006.

DeCarlo, P. F., Dunlea, E. J., Kimmel, J. R., Aiken, A. C., Sueper, D., Crounse, J., Wennberg, P. O., Emmons, L., Shinozuka, Y., Clarke, A., Zhou, J., Tomlinson, J., Collins, D. R., Knapp, D., Weinheimer, A. J., Montzka, D. D., Campos, T., and Jimenez, J. L.: Fast airborne aerosol size and chemistry measurements above Mexico City and Central Mexico during the MILAGRO campaign, Atmos. Chem. Phys., 8, 4027-4048, 10.5194/acp-8-4027-2008, 2008.

DeCarlo, P. F., Ulbrich, I. M., Crounse, J., de Foy, B., Dunlea, E. J., Aiken, A. C., Knapp, D., Weinheimer, A. J., Campos, T., Wennberg, P. O., and Jimenez, J. L.: Investigation of the sources and processing of organic aerosol over the Central Mexican Plateau from aircraft measurements during MILAGRO, Atmos. Chem. Phys., 10, 5257-5280, 10.5194/acp-10-5257-2010, 2010.

Docherty, K. S., Stone, E. A., Ulbrich, I. M., DeCarlo, P. F., Snyder, D. C., Schauer, J. J., Peltier, R. E., Weber, R. J., Murphy, S. M., Seinfeld, J. H., Grover, B. D., Eatough, D. J., and Jimenez, J. L.: Apportionment of Primary and Secondary Organic Aerosols in Southern California during the 2005 Study of Organic Aerosols in Riverside (SOAR-1), Environmental Science & Technology, 42, 7655-7662, 10.1021/es8008166, 2008.

Docherty, K. S., Aiken, A. C., Huffman, J. A., Ulbrich, I. M., DeCarlo, P. F., Sueper, D., Worsnop, D. R., Snyder, D. C., Peltier, R. E., Weber, R. J., Grover, B. D., Eatough, D. J., Williams, B. J., Goldstein, A. H., Ziemann, P. J., and Jimenez, J. L.: The 2005 Study of Organic Aerosols at Riverside (SOAR-1): instrumental intercomparisons and fine particle composition, Atmos. Chem. Phys., 11, 12387-12420, 10.5194/acp-11-12387-2011, 2011.

Dockery, D.W. and Pope, C.A. (1994) Acute respiratory effects of particulate air-pollution. Annu. Rev. Publ. Health 15, 107-132.

Donahue, N. M., Robinson, A. L., Stanier, C. O., and Pandis, S. N.: Coupled Partitioning, Dilution, and Chemical Aging of Semivolatile Organics, Environmental Science & Technology, 40, 2635-2643, 10.1021/es052297c, 2006.

Donahue, N. M., Chuang, W., Epstein, S. A., Kroll, J. H., Worsnop, D. R., Robinson, A. L., Adams, P. J., and Pandis, S. N.: Why do organic aerosols exist? Understanding aerosol lifetimes using the two-dimensional volatility basis set, Environ. Chem., 10, 151-157, 10.1071/en13022, 2013.

Drewnick, F., Hings, S. S., DeCarlo, P., Jayne, J. T., Gonin, M., Fuhrer, K., Weimer, S., Jimenez, J. L., Demerjian, K. L., Borrmann, S., and Worsnop, D. R.: A New Time-of-Flight Aerosol Mass Spectrometer (TOF-AMS)—Instrument Description and First Field Deployment, Aerosol Science and Technology, 39, 637-658, 10.1080/02786820500182040, 2005.

Dunlea, E. J., DeCarlo, P. F., Aiken, A. C., Kimmel, J. R., Peltier, R. E., Weber, R. J., Tomlinson, J., Collins, D. R., Shinozuka, Y., McNaughton, C. S., Howell, S. G., Clarke, A. D., Emmons, L. K., Apel, E. C., Pfister, G. G., van Donkelaar, A., Martin, R. V., Millet, D. B., Heald, C. L., and Jimenez, J. L.: Evolution of Asian aerosols during transpacific transport in INTEX-B, Atmos. Chem. Phys., 9, 7257-7287, 10.5194/acp-9-7257-2009, 2009.

Dzepina, K., Volkamer, R. M., Madronich, S., Tulet, P., Ulbrich, I. M., Zhang, Q., Cappa, C. D., Ziemann, P. J., and Jimenez, J. L.: Evaluation of recently-proposed secondary organic aerosol models for a case study in Mexico City, Atmos. Chem. Phys., 9, 5681-5709, 10.5194/acp-9-5681-2009, 2009.

Dzepina, K., Cappa, C. D., Volkamer, R. M., Madronich, S., DeCarlo, P. F., Zaveri, R. A., and Jimenez, J. L.: Modeling the Multiday Evolution and Aging of Secondary Organic Aerosol During MILAGRO 2006, Environmental Science & Technology, 45, 3496-3503, 10.1021/es103186f, 2011.

Edney, E.O., Kleindienst, T.E., Jaoui, M., Lewandowski, M., Offenberg, J.H., Wang, W. and Claeys, M. (2005) Formation of 2-methyl tetrols and 2-methylglyceric acid in secondary organic aerosol from laboratory irradiated isoprene/NOX/SO2/air mixtures and their detection in ambient PM2.5 samples collected in the eastern United States. Atmos. Environ. 39, 5281-5289.

El Haddad, I., Platt, S., Slowik, J.G., Mohr, C., Crippa, M., Temime-Roussel, B., Detournay, A., Marchand, N., Baltensperger, U. and Prevot, A.S.H. (2012) Contributions of Cooking Emissions to Primary and Secondary Organic Aerosol in Urban Atmospheres, American Association for Aerosol Research 31st Annual Conference, Minneapolis, Minnesota http://aaarabstracts.com/2012/AbstractBook.pdf

Ensberg, J. J., Hayes, P. L., Jimenez, J. L., Gilman, J. B., Kuster, W. C., de Gouw, J. A., Holloway, J. S., Gordon, T. D., Jathar, S., Robinson, A. L., and Seinfeld, J. H.: Emission factor ratios, SOA mass yields, and the impact of vehicular emissions on SOA formation, Atmos. Chem. Phys., 14, 2383-2397, 10.5194/acp-14-2383-2014, 2014.

EPA (2013) National Emissions Inventory. Environmental Protection Agency http://www.epa.gov/ttn/chief/net/2011inventory.html

Ervens, B. and Volkamer, R. (2010) Glyoxal processing by aerosol multiphase chemistry: towards a kinetic modeling framework of secondary organic aerosol formation in aqueous particles. Atmos. Chem. Phys. 10, 8219-8244.

Ervens, B., Turpin, B. J., and Weber, R. J.: Secondary organic aerosol formation in cloud droplets and aqueous particles (aqSOA): a review of laboratory, field and model studies, Atmos. Chem. Phys., 11, 11069-11102, 10.5194/acp-11-11069-2011, 2011.

Faulhaber, A. E., Thomas, B. M., Jimenez, J. L., Jayne, J. T., Worsnop, D. R., and Ziemann, P. J.: Characterization of a thermodenuder-particle beam mass spectrometer system for the study of organic aerosol volatility and composition, Atmos. Meas. Tech., 2, 15-31, 10.5194/amt-2-15-2009, 2009.

Fountoukis, C. and Nenes, A. (2007) ISORROPIA II: a computationally efficient thermodynamic equilibrium model for K+-Ca2+-Mg2+-Nh(4)(+)-Na+-SO42--NO3--Cl--H2O aerosols. Atmos. Chem. Phys. 7, 4639-4659.

Gentner, D.R., Isaacman, G., Worton, D.R., Chan, A.W.H., Dallmann, T.R., Davis, L., Liu, S., Day, D.A., Russell, L.M., Wilson, K.R., Weber, R., Guha, A., Harley, R.A. and Goldstein, A.H. (2012) Elucidating secondary organic aerosol from diesel and gasoline vehicles through detailed characterization of organic carbon emissions. Proc. Natl. Acad. Sci. U. S. A. 109, 18318-18323.

George, I.J. and Abbatt, J.P.D. (2010) Chemical evolution of secondary organic aerosol from OH-initiated heterogeneous oxidation. Atmos. Chem. Phys. 10, 5551-5563.

George, I. J., and Abbatt, J. P. D.: Heterogeneous oxidation of atmospheric aerosol particles by gas-phase radicals, Nat Chem, 2, 713-722, 2010.

Grieshop, A.P., Logue, J.M., Donahue, N.M. and Robinson, A.L. (2009) Laboratory investigation of photochemical oxidation of organic aerosol from wood fires 1: measurement and simulation of organic aerosol evolution. Atmos. Chem. Phys. 9, 1263-1277.

Griffin, R.J., Chen, J.J., Carmody, K., Vutukuru, S. and Dabdub, D. (2007) Contribution of gas phase oxidation of volatile organic compounds to atmospheric carbon monoxide levels in two areas of the United States. J. Geophys. Res.-Atmos. 112, D10S17.

Guzman-Morales, J., Frossard, A.A., Corrigan, A.L., Russell, L.M., Liu, S., Takahama, S., Taylor, J.W., Allan, J., Coe, H., Zhao, Y. and Goldstein, A.H. (2014) Estimated contributions of primary and secondary organic aerosol from fossil fuel combustion during the CalNex and Cal-Mex campaigns. Atmos. Environ. 88, 330-340.

Hallquist, M., Wenger, J. C., Baltensperger, U., Rudich, Y., Simpson, D., Claeys, M., Dommen, J., Donahue, N. M., George, C., Goldstein, A. H., Hamilton, J. F., Herrmann, H., Hoffmann, T., Iinuma, Y., Jang, M., Jenkin, M. E., Jimenez, J. L., Kiendler-Scharr, A., Maenhaut, W., Mcfiggans, G., Mentel, T. F., Monod, A., Prévôt, A. S. H., Seinfeld, J. H., Surratt, J. D., Szmigielski, R., and Wildt, J.: The formation, properties and impact of secondary organic aerosol: current and emerging issues, Atmos. Chem. Phys., 9, 5155-5236, 10.5194/acp-9-5155-2009, 2009.

Hayes, P. L., Ortega, A. M., Cubison, M. J., Froyd, K. D., Zhao, Y., Cliff, S. S., Hu, W. W., Toohey, D. W., Flynn, J. H., Lefer, B. L., Grossberg, N., Alvarez, S., Rappenglück, B., Taylor, J. W., Allan, J. D., Holloway, J. S., Gilman, J. B., Kuster, W. C., de Gouw, J. A., Massoli, P., Zhang, X., Liu, J., Weber, R. J., Corrigan, A. L., Russell, L. M., Isaacman, G., Worton, D. R., Kreisberg, N. M., Goldstein, A. H., Thalman, R., Waxman, E. M., Volkamer, R., Lin, Y. H., Surratt, J. D., Kleindienst, T. E., Offenberg, J. H., Dusanter, S., Griffith, S., Stevens, P. S., Brioude, J., Angevine, W. M., and Jimenez, J. L.: Organic aerosol composition and sources in Pasadena, California, during the 2010 CalNex campaign, Journal of Geophysical Research: Atmospheres, 118, 9233-9257, 10.1002/jgrd.50530, 2013.

Hayes, P. L., Carlton, A. G., Baker, K. R., Ahmadov, R., Washenfelder, R. A., Alvarez, S., Rappenglück, B., Gilman, J. B., Kuster, W. C., de Gouw, J. A., Zotter, P., Prévôt, A. S. H., Szidat, S., Kleindienst, T. E., Offenberg, J. H., Ma, P. K., and Jimenez, J. L.: Modeling the formation and aging of secondary organic aerosols in Los Angeles during CalNex 2010, Atmos. Chem. Phys., 15, 5773-5801, 10.5194/acp-15-5773-2015, 2015.

Heald, C. L., Kroll, J. H., Jimenez, J. L., Docherty, K. S., DeCarlo, P. F., Aiken, A. C., Chen, Q., Martin, S. T., Farmer, D. K., and Artaxo, P.: A simplified description of the evolution of organic aerosol composition in the atmosphere, Geophys. Res. Lett., 37, L08803, 10.1029/2010gl042737, 2010.

Heald, C. L., Coe, H., Jimenez, J. L., Weber, R. J., Bahreini, R., Middlebrook, A. M., Russell, L. M., Jolleys, M., Fu, T. M., Allan, J. D., Bower, K. N., Capes, G., Crosier, J., Morgan, W. T., Robinson, N. H., Williams, P. I., Cubison, M. J., DeCarlo, P. F., and Dunlea, E. J.:

Exploring the vertical profile of atmospheric organic aerosol: comparing 17 aircraft field campaigns with a global model, Atmos. Chem. Phys., 11, 12673-12696, 10.5194/acp-11-12673-2011, 2011.

Heald, C.L., Ridley, D.A., Kreidenweis, S.M. and Drury, E.E. (2010) Satellite observations cap the atmospheric organic aerosol budget. Geophys. Res. Lett. 37, L24808.

Heo, J., de Foy, B., Olson, M.R., Pakbin, P., Sioutas, C. and Schauer, J.J. (2015) Impact of regional transport on the anthropogenic and biogenic secondary organic aerosols in the Los Angeles Basin. Atmos. Environ. 103, 171-179.

Herndon, S. C., Onasch, T. B., Wood, E. C., Kroll, J. H., Canagaratna, M. R., Jayne, J. T., Zavala, M. A., Knighton, W. B., Mazzoleni, C., Dubey, M. K., Ulbrich, I. M., Jimenez, J. L., Seila, R., de Gouw, J. A., de Foy, B., Fast, J., Molina, L. T., Kolb, C. E., and Worsnop, D. R.: Correlation of secondary organic aerosol with odd oxygen in Mexico City, Geophysical Research Letters, 35, L15804, 10.1029/2008gl034058, 2008.

Hersey, S. P., Craven, J. S., Schilling, K. A., Metcalf, A. R., Sorooshian, A., Chan, M. N., Flagan, R. C., and Seinfeld, J. H.: The Pasadena Aerosol Characterization Observatory (PACO): chemical and physical analysis of the Western Los Angeles basin aerosol, Atmos. Chem. Phys., 11, 7417-7443, 10.5194/acp-11-7417-2011, 2011.

Hodzic, A., Jimenez, J.L., Madronich, S., Aiken, A.C., Bessagnet, B., Curci, G., Fast, J., Lamarque, J.F., Onasch, T.B., Roux, G., Schauer, J.J., Stone, E.A. and Ulbrich, I.M. (2009) Modeling organic aerosols during MILAGRO: importance of biogenic secondary organic aerosols. Atmos. Chem. Phys. 9, 6949-6981.

Hodzic, A., Jimenez, J. L., Madronich, S., Canagaratna, M. R., DeCarlo, P. F., Kleinman, L., and Fast, J.: Modeling organic aerosols in a megacity: potential contribution of semi-volatile and intermediate volatility primary organic compounds to secondary organic aerosol formation, Atmos. Chem. Phys., 10, 5491-5514, 10.5194/acp-10-5491-2010, 2010.

Hodzic, A., Jimenez, J.L., Prevot, A.S.H., Szidat, S., Fast, J.D. and Madronich, S. (2010b) Can 3-D models explain the observed fractions of fossil and non-fossil carbon in and near Mexico City? Atmos. Chem. Phys. 10, 10997-11016.

Hodzic, A., and Jimenez, J. L.: Modeling anthropogenically controlled secondary organic aerosols in a megacity: a simplified framework for global and climate models, Geosci. Model Dev., 4, 901-917, 10.5194/gmd-4-901-2011, 2011.

Hu, W.W., Hu, M., Yuan, B., Jimenez, J.L., Tang, Q., Peng, J.F., Hu, W., Shao, M., Wang, M., Zeng, L.M., Wu, Y.S., Gong, Z.H., Huang, X.F. and He, L.Y. (2013) Insights on organic aerosol aging and the influence of coal combustion at a regional receptor site of central eastern China. Atmos. Chem. Phys. 13, 10095-10112.

Huffman, J. A., Ziemann, P. J., Jayne, J. T., Worsnop, D. R., and Jimenez, J. L.: Development and Characterization of a Fast-Stepping/Scanning Thermodenuder for Chemically-Resolved Aerosol Volatility Measurements, Aerosol Science and Technology, 42, 395-407, 10.1080/02786820802104981, 2008.

Huffman, J. A., Docherty, K. S., Aiken, A. C., Cubison, M. J., Ulbrich, I. M., DeCarlo, P. F., Sueper, D., Jayne, J. T., Worsnop, D. R., Ziemann, P. J., and Jimenez, J. L.: Chemically-

resolved aerosol volatility measurements from two megacity field studies, Atmos. Chem. Phys., 9, 7161-7182, 10.5194/acp-9-7161-2009, 2009.

IPCC (2013) Climate Change 2013: The Physical Scientific Basis. Intergovernmental Panel on Climate Change: Working Group I, Geneva Switzerland

Jaoui, M., Kleindienst, T.E., Lewandowski, M., Offenberg, J.H. and Edney, E.O. (2005) Identification and Quantification of Aerosol Polar Oxygenated Compounds Bearing Carboxylic or Hydroxyl Groups. 2. Organic Tracer Compounds from Monoterpenes. Environ. Sci. Technol. 39, 5661-5673.

Jathar, S.H., Gordon, T.D., Hennigan, C.J., Pye, H.O.T., Pouliot, G., Adams, P.J., Donahue, N.M. and Robinson, A.L. (2014) Unspeciated organic emissions from combustion sources and their influence on the secondary organic aerosol budget in the United States. Proc. Natl. Acad. Sci. U. S. A. 111, 10473-10478.

Jathar, S.H., Miracolo, M.A., Tkacik, D.S., Donahue, N.M., Adams, P.J. and Robinson, A.L. (2013) Secondary Organic Aerosol Formation from Photo-Oxidation of Unburned Fuel: Experimental Results and Implications for Aerosol Formation from Combustion Emissions. Environ. Sci. Technol. 47, 12886-12893.

Jimenez, J. L., Jayne, J. T., Shi, Q., Kolb, C. E., Worsnop, D. R., Yourshaw, I., Seinfeld, J. H., Flagan, R. C., Zhang, X. F., Smith, K. A., Morris, J. W., and Davidovits, P.: Ambient aerosol sampling using the Aerodyne Aerosol Mass Spectrometer, Journal of Geophysical Research-Atmospheres, 108, 8425, 10.1029/2001jd001213, 2003.

Jimenez, J. L., Canagaratna, M. R., Donahue, N. M., Prevot, A. S. H., Zhang, Q., Kroll, J. H., DeCarlo, P. F., Allan, J. D., Coe, H., Ng, N. L., Aiken, A. C., Docherty, K. S., Ulbrich, I. M., Grieshop, A. P., Robinson, A. L., Duplissy, J., Smith, J. D., Wilson, K. R., Lanz, V. A., Hueglin, C., Sun, Y. L., Tian, J., Laaksonen, A., Raatikainen, T., Rautiainen, J., Vaattovaara, P., Ehn, M., Kulmala, M., Tomlinson, J. M., Collins, D. R., Cubison, M. J., Dunlea, E. J., Huffman, J. A., Onasch, T. B., Alfarra, M. R., Williams, P. I., Bower, K., Kondo, Y., Schneider, J., Drewnick, F., Borrmann, S., Weimer, S., Demerjian, K., Salcedo, D., Cottrell, L., Griffin, R., Takami, A., Miyoshi, T., Hatakeyama, S., Shimono, A., Sun, J. Y., Zhang, Y. M., Dzepina, K., Kimmel, J. R., Sueper, D., Jayne, J. T., Herndon, S. C., Trimborn, A. M., Williams, L. R., Wood, E. C., Middlebrook, A. M., Kolb, C. E., Baltensperger, U., and Worsnop, D. R.: Evolution of Organic Aerosols in the Atmosphere, Science, 326, 1525-1529, 10.1126/science.1180353, 2009.

JRC (2011) Emission Database for Global Atmospheric Research. European Commission's Joint Research Centre http://edgar.jrc.ec.europa.eu/overview.php?v=42

Kang, E., Root, M. J., Toohey, D. W., and Brune, W. H.: Introducing the concept of Potential Aerosol Mass (PAM), Atmos. Chem. Phys., 7, 5727-5744, 10.5194/acp-7-5727-2007, 2007.

Kang, E., Toohey, D. W., and Brune, W. H.: Dependence of SOA oxidation on organic aerosol mass concentration and OH exposure: experimental PAM chamber studies, Atmos. Chem. Phys., 11, 1837-1852, 10.5194/acp-11-1837-2011, 2011.

Kelly, J.T., Baker, K.R., Nowak, J.B., Murphy, J.G., Markovic, M.Z., VandenBoer, T.C., Ellis, R.A., Neuman, J.A., Weber, R.J. and Roberts, J.M. (2014) Fine-scale simulation of

ammonium and nitrate over the South Coast Air Basin and San Joaquin Valley of California during CalNex-2010. J. Geophys. Res.-Atmos. 119, 3600-3614.

Kleindienst, T.E., Jaoui, M., Lewandowski, M., Offenberg, J.H. and Docherty, K.S. (2012) The formation of SOA and chemical tracer compounds from the photooxidation of naphthalene and its methyl analogs in the presence and absence of nitrogen oxides. Atmos. Chem. Phys. 12, 8711-8726.

Kleinman, L.I., Daum, P.H., Lee, Y.N., Senum, G.I., Springston, S.R., Wang, J., Berkowitz, C., Hubbe, J., Zaveri, R.A., Brechtel, F.J., Jayne, J., Onasch, T.B. and Worsnop, D. (2007) Aircraft observations of aerosol composition and ageing in New England and Mid-Atlantic States during the summer 2002 New England Air Quality Study field campaign. J. Geophys. Res.-Atmos. 112, D09310.

Knote, C., Brunner, D., Vogel, H., Allan, J., Asmi, A., Äijälä, M., Carbone, S., van der Gon, H. D., Jimenez, J. L., Kiendler-Scharr, A., Mohr, C., Poulain, L., Prévôt, A. S. H., Swietlicki, E., and Vogel, B.: Towards an online-coupled chemistry-climate model: evaluation of trace gases and aerosols in COSMO-ART, Geosci. Model Dev., 4, 1077-1102, 10.5194/gmd-4-1077-2011, 2011.

Knote, C., Hodzic, A., Jimenez, J.L., Volkamer, R., Orlando, J.J., Baidar, S., Brioude, J., Fast, J., Gentner, D.R., Goldstein, A.H., Hayes, P.L., Knighton, W.B., Oetjen, H., Setyan, A., Stark, H., Thalman, R., Tyndall, G., Washenfelder, R., Waxman, E. and Zhang, Q. (2014b) Simulation of semi-explicit mechanisms of SOA formation from glyoxal in aerosol in a 3-D model. Atmos. Chem. Phys. 14, 6213-6239.

Knote, C., Hodzic, A., and Jimenez, J. L.: The effect of dry and wet deposition of condensable vapors on secondary organic aerosols concentrations over the continental US, Atmos. Chem. Phys., 15, 1-18, 10.5194/acp-15-1-2015, 2015.

Koo, B.Y., Ansari, A.S. and Pandis, S.N. (2003) Integrated approaches to modeling the organic and inorganic atmospheric aerosol components. Atmos. Environ. 37, 4757-4768.

Kroll, J.H., Ng, N.L., Murphy, S.M., Flagan, R.C. and Seinfeld, J.H. (2006) Secondary organic aerosol formation from isoprene photooxidation. Environ. Sci. Technol. 40, 1869-1877.

Kroll, J. H., Donahue, N. M., Jimenez, J. L., Kessler, S. H., Canagaratna, M. R., Wilson, K. R., Altieri, K. E., Mazzoleni, L. R., Wozniak, A. S., Bluhm, H., Mysak, E. R., Smith, J. D., Kolb, C. E., and Worsnop, D. R.: Carbon oxidation state as a metric for describing the chemistry of atmospheric organic aerosol, Nature Chemistry, 3, 133-139, 10.1038/nchem.948, 2011.

Lambe, A. T., Ahern, A. T., Williams, L. R., Slowik, J. G., Wong, J. P. S., Abbatt, J. P. D., Brune, W. H., Ng, N. L., Wright, J. P., Croasdale, D. R., Worsnop, D. R., Davidovits, P., and Onasch, T. B.: Characterization of aerosol photooxidation flow reactors: heterogeneous oxidation, secondary organic aerosol formation and cloud condensation nuclei activity measurements, Atmos. Meas. Tech., 4, 445-461, 10.5194/amt-4-445-2011, 2011a.

Lambe, A. T., Onasch, T. B., Massoli, P., Croasdale, D. R., Wright, J. P., Ahern, A. T., Williams, L. R., Worsnop, D. R., Brune, W. H., and Davidovits, P.: Laboratory studies of the chemical composition and cloud condensation nuclei (CCN) activity of secondary organic aerosol (SOA) and oxidized primary organic aerosol (OPOA), Atmos. Chem. Phys., 11, 8913-8928, 10.5194/acp-11-8913-2011, 2011b.

Lambe, A. T., Onasch, T. B., Croasdale, D. R., Wright, J. P., Martin, A. T., Franklin, J. P., Massoli, P., Kroll, J. H., Canagaratna, M. R., Brune, W. H., Worsnop, D. R., and Davidovits, P.: Transitions from Functionalization to Fragmentation Reactions of Laboratory Secondary Organic Aerosol (SOA) Generated from the OH Oxidation of Alkane Precursors, Environmental Science & Technology, 46, 5430–5437, 10.1021/es300274t, 2012.

Lambe, A. T., Chhabra, P. S., Onasch, T. B., Brune, W. H., Hunter, J. F., Kroll, J. H., Cummings, M. J., Brogan, J. F., Parmar, Y., Worsnop, D. R., Kolb, C. E., and Davidovits, P.: Effect of oxidant concentration, exposure time, and seed particles on secondary organic aerosol chemical composition and yield, Atmos. Chem. Phys., 15, 3063-3075, 10.5194/acp-15-3063-2015, 2015.

Lewis, C.W., Volckens, J., Braddock, J.N., Crews, W.S., Lonneman, W.A. and McNichol, A.P. (2006) Absence of 14C in PM2.5 Emissions from Gasohol Combustion in Small Engines. Aerosol Sci. Technol. 40, 657-663.

Li, R., Palm, B. B., Borbon, A., Graus, M., Warneke, C., Ortega, A. M., Day, D. A., Brune, W. H., Jimenez, J. L., and de Gouw, J. A.: Laboratory Studies on Secondary Organic Aerosol Formation from Crude Oil Vapors, Environmental Science & Technology, 47, 12566-12574, 10.1021/es402265y, 2013.

Li, R., Palm, B. B., Ortega, A. M., Hlywiak, J. A., Hu, W., Peng, Z., Day, D. A., Knote, C., Brune, W. H., de Gouw, J. A., and Jimenez, J. L.: Modeling the Radical Chemistry in an Oxidation Flow Reactor: Radical Formation and Recycling, Sensitivities, and OH Exposure Estimation Equation, The Journal of Physical Chemistry A, 10.1021/jp509534k, 2015.

Lim, H.J., Carlton, A.G. and Turpin, B.J. (2005) Isoprene forms secondary organic aerosol through cloud processing: Model simulations. Environ. Sci. Technol. 39, 4441-4446.

Loza, C.L., Craven, J.S., Yee, L.D., Coggon, M.M., Schwantes, R.H., Shiraiwa, M., Zhang, X., Schilling, K.A., Ng, N.L., Canagaratna, M.R., Ziemann, P.J., Flagan, R.C. and Seinfeld, J.H. (2014) Secondary organic aerosol yields of 12-carbon alkanes. Atmos. Chem. Phys. 14, 1423-1439.

Martin-Reviejo, M. and Wirtz, K. (2005) Is benzene a precursor for secondary organic aerosol? Environ. Sci. Technol. 39, 1045-1054.

Mao, J., Ren, X., Brune, W. H., Olson, J. R., Crawford, J. H., Fried, A., Huey, L. G., Cohen, R. C., Heikes, B., Singh, H. B., Blake, D. R., Sachse, G. W., Diskin, G. S., Hall, S. R., and Shetter, R. E.: Airborne measurement of OH reactivity during INTEX-B, Atmos. Chem. Phys., 9, 163-173, 10.5194/acp-9-163-2009, 2009.

Massoli, P., Lambe, A. T., Ahern, A. T., Williams, L. R., Ehn, M., Mikkilä, J., Canagaratna, M. R., Brune, W. H., Onasch, T. B., Jayne, J. T., Petäjä, T., Kulmala, M., Laaksonen, A., Kolb, C. E., Davidovits, P., and Worsnop, D. R.: Relationship between aerosol oxidation level and hygroscopic properties of laboratory generated secondary organic aerosol (SOA) particles, Geophys. Res. Lett., 37, L24801, 10.1029/2010gl045258, 2010.

Matsunaga, A. and Ziemann, P.J. (2010) Gas-Wall Partitioning of Organic Compounds in a Teflon Film Chamber and Potential Effects on Reaction Product and Aerosol Yield Measurements. Aerosol Sci. Technol. 44, 881-892.

McKeen, S., Chung, S.H., Wilczak, J., Grell, G., Djalalova, I., Peckham, S., Gong, W., Bouchet, V., Moffet, R., Tang, Y., Carmichael, G.R., Mathur, R. and Yu, S. (2007) Evaluation of several PM(2.5) forecast models using data collected during the ICARTT/NEAQS 2004 field study. J. Geophys. Res.-Atmos. 112.

McMurry, P. H., and Grosjean, D.: Gas and aerosol wall losses in Teflon film smog chambers, Environmental Science & Technology, 19, 1176-1182, 10.1021/es00142a006, 1985.

Middlebrook, A.M., Bahreini, R., Jimenez, J.L. and Canagaratna, M.R. (2012) Evaluation of Composition-Dependent Collection Efficiencies for the Aerodyne Aerosol Mass Spectrometer using Field Data. Aerosol Sci. Technol. 46, 258-271.

Mohr, C., DeCarlo, P.F., Heringa, M.F., Chirico, R., Slowik, J.G., Richter, R., Reche, C., Alastuey, A., Querol, X., Seco, R., Peñuelas, J., Jiménez, J.L., Crippa, M., Zimmermann, R., Baltensperger, U. and Prévôt, A.S.H. (2011) Identification and quantification of organic aerosol from cooking and other sources in Barcelona using aerosol mass spectrometer data. Atmos. Chem. Phys. 11, 1649-1665.

Morino, Y., Tanabe, K., Sato, K., and Ohara, T.: Secondary organic aerosol model intercomparison based on secondary organic aerosol to odd oxygen ratio in Tokyo, Journal of Geophysical Research: Atmospheres, 119, 2014JD021937, 10.1002/2014jd021937, 2014.

Murphy, B.N., Donahue, N.M., Fountoukis, C. and Pandis, S.N. (2011) Simulating the oxygen content of ambient organic aerosol with the 2D volatility basis set. Atmos. Chem. Phys. 11, 7859-7873.

Murphy, D. M., Cziczo, D. J., Froyd, K. D., Hudson, P. K., Matthew, B. M., Middlebrook, A. M., Peltier, R. E., Sullivan, A., Thomson, D. S., and Weber, R. J.: Single-particle mass spectrometry of tropospheric aerosol particles, Journal of Geophysical Research: Atmospheres, 111, D23S32, 10.1029/2006jd007340, 2006.

Myhre, G., Shindell, D., Bréon, F.-M., Collins, W., Fuglestvedt, J., Huang, J., Koch, D., Lamarque, J.-F., Lee, D., Mendoza, B., Nakajima, T., Robock, A., Stephens, G., Takemura, T., and Zhang, H.: Anthropogenic and Natural Radiative Forcing, in Climate Change 2013: The Physical Science Basis. Contribution of Working Group I to the Fifth Assessment Report of the Intergovernmental Panel on Climate Change, edited by V. B. and P. M. M. Stocker, T.F., D. Qin, G.-K. Plattner, M. Tignor, S.K. Allen, J. Boschung, A. Nauels, Y. Xia, Cambridge University Press, Cambridge, United Kingdom and New York, NY, USA., 2013.

Ng, N.L., Kroll, J.H., Chan, A.W.H., Chhabra, P.S., Flagan, R.C. and Seinfeld, J.H. (2007) Secondary organic aerosol formation from m-xylene, toluene, and benzene. Atmos. Chem. Phys. 7, 3909-3922.

Ng, N. L., Canagaratna, M. R., Jimenez, J. L., Chhabra, P. S., Seinfeld, J. H., and Worsnop, D. R.: Changes in organic aerosol composition with aging inferred from aerosol mass spectra, Atmos Chem Phys, 11, 6465-6474, 10.5194/acp-11-6465-2011, 2011a.

Ng, N. L., Canagaratna, M. R., Jimenez, J. L., Zhang, Q., Ulbrich, I. M., and Worsnop, D. R.: Real-Time Methods for Estimating Organic Component Mass Concentrations from Aerosol Mass Spectrometer Data, Environmental Science & Technology, 45, 910-916, 10.1021/es102951k, 2011b.

Ortega, A. M., Day, D. A., Cubison, M. J., Brune, W. H., Bon, D., de Gouw, J. A., and Jimenez, J. L.: Secondary organic aerosol formation and primary organic aerosol oxidation from biomass-burning smoke in a flow reactor during FLAME-3, Atmos. Chem. Phys., 13, 11551-11571, 10.5194/acp-13-11551-2013, 2013.

Palm, B. B., Campuzano-Jost, P., Ortega, A. M., Day, D. A., Karl, T., Kaser, L., Jud, W., Hansel, A., Hunter, J. F., Kroll, J. H., Brune, W. H., and Jimenez, J. L.: In-situ Secondary Organic Aerosol Formation in ambient pine forest air using an oxidation flow reactor. , Atmos. Chem. Phys. Discuss., 15, 30409-30471, doi:10.5194/acpd-15-30409-2015, 2015.

Pankow, J. F.: An absorption model of gas/particle partitioning of organic compounds in the atmosphere, Atmospheric Environment, 28, 185-188, http://dx.doi.org/10.1016/1352-2310(94)90093-0, 1994.

Parrish, D.D., Stohl, A., Forster, C., Atlas, E.L., Blake, D.R., Goldan, P.D., Kuster, W.C. and de Gouw, J.A. (2007) Effects of mixing on evolution of hydrocarbon ratios in the troposphere. J. Geophys. Res.-Atmos. 112, D10S34.

Peng, Z., Day, D. A., Stark, H., Li, R., Palm, B. B., Brune, W. H., and Jimenez, J. L.: HOx radical chemistry in oxidation flow reactors with low-pressure mercury lamps systematically examined by modeling, Atmospheric Measurement Techniques, 8, 4863-4890, doi:10.5194/amt-8-4863-2015, 2015.

Perraud, V., Bruns, E.A., Ezell, M.J., Johnson, S.N., Yu, Y., Alexander, M.L., Zelenyuk, A., Imre, D., Chang, W.L., Dabdub, D., Pankow, J.F. and Finlayson-Pitts, B.J. (2012) Nonequilibrium atmospheric secondary organic aerosol formation and growth. Proc. Natl. Acad. Sci. U. S. A. 109, 2836-2841.

Pirjola, L., Kulmala, M., Wilck, M., Bischoff, A., Stratmann, F., and Otto, E.: Formation of Sulphuric Acid Aerosols and Cloud COndensation Nuclei: An Expresion for Significant Nucleation and Model Comprarison, Journal of Aerosol Science, 30, 1079-1094, http://dx.doi.org/10.1016/S0021-8502(98)00776-9, 1999.

Pope, C. A., Burnett, R. T., Thun, M. J., Calle, E. E., Krewski, D., Ito, K., and Thurston, G. D.: Lung cancer, cardiopulmonary mortality, and long-term exposure to fine particulate air pollution, Jama-Journal of the American Medical Association, 287, 1132-1141, 10.1001/jama.287.9.1132, 2002.

Presto, A.A., Hennigan, C.J., Nguyen, N.T. and Robinson, A.L. (2012) Determination of Volatility Distributions of Primary Organic Aerosol Emissions from Internal Combustion Engines Using Thermal Desorption Gas Chromatography Mass Spectrometry. Aerosol Sci. Technol. 46, 1129-1139.

Presto, A.A., Nguyen, N.T., Ranjan, M., Reeder, A.J., Lipsky, E.M., Hennigan, C.J., Miracolo, M.A., Riemer, D.D. and Robinson, A.L. (2011) Fine particle and organic vapor emissions from staged tests of an in-use aircraft engine. Atmos. Environ. 45, 3603-3612.

Pye, H.O.T. and Seinfeld, J.H. (2010) A global perspective on aerosol from low-volatility organic compounds. Atmos. Chem. Phys. 10, 4377-4401.

Renbaum-Wolff, L., Grayson, J.W., Bateman, A.P., Kuwata, M., Sellier, M., Murray, B.J., Shilling, J.E., Martin, S.T. and Bertram, A.K. (2013) Viscosity of alpha-pinene secondary

organic material and implications for particle growth and reactivity. Proc. Natl. Acad. Sci. U. S. A. 110, 8014-8019.

Reutter, P., Su, H., Trentmann, J., Simmel, M., Rose, D., Gunthe, S. S., Wernli, H., Andreae, M. O., and Pöschl, U.: Aerosol- and updraft-limited regimes of cloud droplet formation: influence of particle number, size and hygroscopicity on the activation of cloud condensation nuclei (CCN), Atmos. Chem. Phys., 9, 7067-7080, 10.5194/acp-9-7067-2009, 2009.

Robinson, A.L., Subramanian, R., Donahue, N.M., Bernardo-Bricker, A. and Rogge, W.F. (2006) Source apportionment of molecular markers and organic aerosol. 3. Food cooking emissions. Environ. Sci. Technol. 40, 7820-7827.

Robinson, A. L., Donahue, N. M., Shrivastava, M. K., Weitkamp, E. A., Sage, A. M., Grieshop, A. P., Lane, T. E., Pierce, J. R., and Pandis, S. N.: Rethinking Organic Aerosols: Semivolatile Emissions and Photochemical Aging, Science, 315, 1259-1262, 10.1126/science.1133061, 2007.

Ryerson, T. B., Andrews, A. E., Angevine, W. M., Bates, T. S., Brock, C. A., Cairns, B., Cohen, R. C., Cooper, O. R., de Gouw, J. A., Fehsenfeld, F. C., Ferrare, R. A., Fischer, M. L., Flagan, R. C., Goldstein, A. H., Hair, J. W., Hardesty, R. M., Hostetler, C. A., Jimenez, J. L., Langford, A. O., McCauley, E., McKeen, S. A., Molina, L. T., Nenes, A., Oltmans, S. J., Parrish, D. D., Pederson, J. R., Pierce, R. B., Prather, K., Quinn, P. K., Seinfeld, J. H., Senff, C. J., Sorooshian, A., Stutz, J., Surratt, J. D., Trainer, M., Volkamer, R., Williams, E. J., and Wofsy, S. C.: The 2010 California Research at the Nexus of Air Quality and Climate Change (CalNex) field study, Journal of Geophysical Research: Atmospheres, 118, 5830-5866, 10.1002/jgrd.50331, 2013.

Sarwar, G., Fahey, K., Kwok, R., Gilliam, R.C., Roselle, S.J., Mathur, R., Xue, J., Yu, J. and Carter, W.P.L. (2013) Potential impacts of two SO2 oxidation pathways on regional sulfate concentrations: Aqueous-phase oxidation by NO2 and gas-phase oxidation by Stabilized Criegee Intermediates. Atmos. Environ. 68, 186-197.

Schauer, J.J., Kleeman, M.J., Cass, G.R. and Simoneit, B.R.T. (1999) Measurement of emissions from air pollution sources. 1. C-1 through C-29 organic compounds from meat charbroiling. Environ. Sci. Technol. 33, 1566-1577.

Schauer, J.J., Kleeman, M.J., Cass, G.R. and Simoneit, B.R.T. (2002) Measurement of emissions from air pollution sources. 4. C-1-C-27 organic compounds from cooking with seed oils. Environ. Sci. Technol. 36, 567-575.

Skamarock, W.C., Klemp, J.B., Dudhia, J., Gill, D.O., Barker, D.M., Duda, M.G., Huang, X., Wang, W. and Powers, J.G. (2008) A description of the Advanced Reserch WRF version 3. NCAR Technical Note NCAR/TN-475+STR.

Slowik, J.G., Stroud, C., Bottenheim, J.W., Brickell, P.C., Chang, R.Y.W., Liggio, J., Makar, P.A., Martin, R.V., Moran, M.D., Shantz, N.C., Sjostedt, S.J., van Donkelaar, A., Vlasenko, A., Wiebe, H.A., Xia, A.G., Zhang, J., Leaitch, W.R. and Abbatt, J.P.D. (2010) Characterization of a large biogenic secondary organic aerosol event from eastern Canadian forests. Atmos. Chem. Phys. 10, 2825-2845.

Spracklen, D.V., Jimenez, J.L., Carslaw, K.S., Worsnop, D.R., Evans, M.J., Mann, G.W., Zhang, Q., Canagaratna, M.R., Allan, J., Coe, H., Mcfiggans, G., Rap, A. and Forster, P. (2011) Aerosol mass spectrometer constraint on the global secondary organic aerosol budget. Atmos. Chem. Phys. 11, 12109-12136.

Sun, Y.L., Zhang, Q., Schwab, J.J., Demerjian, K.L., Chen, W.N., Bae, M.S., Hung, H.M., Hogrefe, O., Frank, B., Rattigan, O.V. and Lin, Y.C. (2011) Characterization of the sources and processes of organic and inorganic aerosols in New York city with a high-resolution time-of-flight aerosol mass apectrometer. Atmos. Chem. Phys. 11, 1581-1602.

Szmigielski, R., Surratt, J.D., Gómez-González, Y., Van der Veken, P., Kourtchev, I., Vermeylen, R., Blockhuys, F., Jaoui, M., Kleindienst, T.E., Lewandowski, M., Offenberg, J.H., Edney, E.O., Seinfeld, J.H., Maenhaut, W. and Claeys, M. (2007) 3-methyl-1,2,3-butanetricarboxylic acid: An atmospheric tracer for terpene secondary organic aerosol. Geophys. Res. Lett. 34, L24811.

Tkacik, D. S., Lambe, A. T., Jathar, S., Li, X., Presto, A. A., Zhao, Y., Blake, D., Meinardi, S., Jayne, J. T., Croteau, P. L., and Robinson, A. L.: Secondary Organic Aerosol Formation from in-Use Motor Vehicle Emissions Using a Potential Aerosol Mass Reactor, Environmental Science & Technology, 48, 11235-11242, 10.1021/es502239v, 2014.

Tsimpidi, A. P., Karydis, V. A., Zavala, M., Lei, W., Molina, L., Ulbrich, I. M., Jimenez, J. L., and Pandis, S. N.: Evaluation of the volatility basis-set approach for the simulation of organic aerosol formation in the Mexico City metropolitan area, Atmos. Chem. Phys., 10, 525-546, 10.5194/acp-10-525-2010, 2010.

Tunved, P., Hansson, H.C., Kerminen, V.M., Strom, J., Dal Maso, M., Lihavainen, H., Viisanen, Y., Aalto, P.P., Komppula, M. and Kulmala, M. (2006) High natural aerosol loading over boreal forests. Science 312, 261-263.

Vaden, T. D., Imre, D., Beránek, J., Shrivastava, M., and Zelenyuk, A.: Evaporation kinetics and phase of laboratory and ambient secondary organic aerosol, Proceedings of the National Academy of Sciences, 108, 2190-2195, 10.1073/pnas.1013391108, 2011.

Volkamer, R., Jimenez, J. L., San Martini, F., Dzepina, K., Zhang, Q., Salcedo, D., Molina, L. T., Worsnop, D. R., and Molina, M. J.: Secondary organic aerosol formation from anthropogenic air pollution: Rapid and higher than expected, Geophys. Res. Lett., 33, L17811, 10.1029/2006gl026899, 2006.

Volkamer, R., San Martini, F., Molina, L.T., Salcedo, D., Jimenez, J.L. and Molina, M.J. (2007) A missing sink for gas-phase glyoxal in Mexico City: Formation of secondary organic aerosol. Geophys. Res. Lett. 34, L19807.

Volkamer, R., Ziemann, P.J. and Molina, M.J. (2009) Secondary Organic Aerosol Formation from Acetylene (C(2)H(2)): seed effect on SOA yields due to organic photochemistry in the aerosol aqueous phase. Atmos. Chem. Phys. 9, 1907-1928.

von der Weiden, S. L., Drewnick, F., and Borrmann, S.: Particle Loss Calculator – a new software tool for the assessment of the performance of aerosol inlet systems, Atmos. Meas. Tech., 2, 479-494, doi:10.5194/amt-2-479-2009, 2009.

Wang, Q., Shao, M., Zhang, Y., Wei, Y., Hu, M. and Guo, S. (2009) Source apportionment of fine organic aerosols in Beijing. Atmos. Chem. Phys. 9, 8573-8585.

Warneke, C., de Gouw, J.A., Holloway, J.S., Peischl, J., Ryerson, T.B., Atlas, E., Blake, D., Trainer, M. and Parrish, D.D. (2012) Multiyear trends in volatile organic compounds in Los Angeles, California: Five decades of decreasing emissions. J. Geophys. Res.-Atmos. 117, D00V17.

Warneke, C., McKeen, S.A., de Gouw, J.A., Goldan, P.D., Kuster, W.C., Holloway, J.S., Williams, E.J., Lerner, B.M., Parrish, D.D., Trainer, M., Fehsenfeld, F.C., Kato, S., Atlas, E.L., Baker, A. and Blake, D.R. (2007) Determination of urban volatile organic compound emission ratios and comparison with an emissions database. J. Geophys. Res.-Atmos. 112, D10S47.

Warneke, C., de Gouw, J. A., Edwards, P. M., Holloway, J. S., Gilman, J. B., Kuster, W. C., Graus, M., Atlas, E., Blake, D., Gentner, D. R., Goldstein, A. H., Harley, R. A., Alvarez, S., Rappenglueck, B., Trainer, M., and Parrish, D. D.: Photochemical aging of volatile organic compounds in the Los Angeles basin: Weekday-weekend effect, Journal of Geophysical Research: Atmospheres, 118, 5018-5028, 10.1002/jgrd.50423, 2013.

Washenfelder, R. A., Young, C. J., Brown, S. S., Angevine, W. M., Atlas, E. L., Blake, D. R., Bon, D. M., Cubison, M. J., de Gouw, J. A., Dusanter, S., Flynn, J., Gilman, J. B., Graus, M., Griffith, S., Grossberg, N., Hayes, P. L., Jimenez, J. L., Kuster, W. C., Lefer, B. L., Pollack, I. B., Ryerson, T. B., Stark, H., Stevens, P. S., and Trainer, M. K.: The glyoxal budget and its contribution to organic aerosol for Los Angeles, California, during CalNex 2010, Journal of Geophysical Research: Atmospheres, 116, D00V02, 10.1029/2011jd016314, 2011.

Watson, J. G.: Visibility: Science and regulation, Journal of the Air & Waste Management Association, 52, 628-713, 2002.

Wood, E. C., Canagaratna, M. R., Herndon, S. C., Onasch, T. B., Kolb, C. E., Worsnop, D. R., Kroll, J. H., Knighton, W. B., Seila, R., Zavala, M., Molina, L. T., DeCarlo, P. F., Jimenez, J. L., Weinheimer, A. J., Knapp, D. J., Jobson, B. T., Stutz, J., Kuster, W. C., and Williams, E. J.: Investigation of the correlation between odd oxygen and secondary organic aerosol in Mexico City and Houston, Atmos. Chem. Phys., 10, 8947-8968, 10.5194/acp-10-8947-2010, 2010.

Yarwood, G., Jung, J., Whitten, G.Z., Heo, G., Mellberg, J., Estes, E. (2010) Updates to the Carbon Bond Mechanism for Version 6 (CB6). Presented at the 9th Annual CMAS Conference, Chapel, Hill, NC. ENVIRON International Corporation, Novato http://www.camx.com/publ/pdfs/CB05_Final_Report_120805.pdf

Yatavelli, R.L.N., Stark, H., Thompson, S.L., Kimmel, J.R., Cubison, M.J., Day, D.A., Campuzano-Jost, P., Palm, B.B., Hodzic, A., Thornton, J.A., Jayne, J.T., Worsnop, D.R. and Jimenez, J.L. (2014) Semicontinuous measurements of gas–particle partitioning of organic acids in a ponderosa pine forest using a MOVI-HRToF-CIMS. Atmos. Chem. Phys. 14, 1527-1546.

Zhang, Q., Jimenez, J. L., Canagaratna, M. R., Allan, J. D., Coe, H., Ulbrich, I., Alfarra, M. R., Takami, A., Middlebrook, A. M., Sun, Y. L., Dzepina, K., Dunlea, E., Docherty, K., DeCarlo, P. F., Salcedo, D., Onasch, T., Jayne, J. T., Miyoshi, T., Shimono, A., Hatakeyama, S., Takegawa, N., Kondo, Y., Schneider, J., Drewnick, F., Borrmann, S., Weimer, S., Demerjian, K., Williams, P., Bower, K., Bahreini, R., Cottrell, L., Griffin, R. J., Rautiainen, J., Sun, J. Y.,

Zhang, Y. M., and Worsnop, D. R.: Ubiquity and dominance of oxygenated species in organic aerosols in anthropogenically-influenced Northern Hemisphere midlatitudes, Geophys. Res. Lett., 34, L13801, 10.1029/2007gl029979, 2007.

Zhang, Q. J., Beekmann, M., Freney, E., Sellegri, K., Pichon, J. M., Schwarzenboeck, A., Colomb, A., Bourrianne, T., Michoud, V., and Borbon, A.: Formation of secondary organic aerosol in the Paris pollution plume and its impact on surrounding regions, Atmos. Chem. Phys., 15, 13973-13992, doi:10.5194/acp-15-13973-2015, 2015.

Zhang, X., Liu, J., Parker, E.T., Hayes, P.L., Jimenez, J.L., de Gouw, J.A., Flynn, J.H., Grossberg, N., Lefer, B.L. and Weber, R.J. (2012) On the gas-particle partitioning of soluble organic aerosol in two urban atmospheres with contrasting emissions: 1. Bulk water-soluble organic carbon. J. Geophys. Res.-Atmos. 117, D00V16.

Zhang, X., Cappa, C. D., Jathar, S. H., McVay, R. C., Ensberg, J. J., Kleeman, M. J., and Seinfeld, J. H.: Influence of vapor wall loss in laboratory chambers on yields of secondary organic aerosol, Proceedings of the National Academy of Sciences, 111, 5802-5807, 10.1073/pnas.1404727111, 2014.

Zhao, Y., Hennigan, C. J., May, A. A., Tkacik, D. S., de Gouw, J. A., Gilman, J. B., Kuster, W. C., Borbon, A., and Robinson, A. L.: Intermediate-Volatility Organic Compounds: A Large Source of Secondary Organic Aerosol, Environmental Science & Technology, 48, 13743-13750, 10.1021/es5035188, 2014.

Ziemann, P. J., and Atkinson, R.: Kinetics, products, and mechanisms of secondary organic aerosol formation, Chemical Society Reviews, 41, 6582-6605, 10.1039/c2cs35122f, 2012.

Zotter, P., El-Haddad, I., Zhang, Y., Hayes, P.L., Zhang, X., Lin, Y.-H., Wacker, L., Schnelle-Kreis, J., Abbaszade, G., Zimmermann, R., Surratt, J.D., Weber, R., Jimenez, J.L., Szidat, S., Baltensperger, U. and Prévôt, A.S.H. (2014) Diurnal cycle of fossil and nonfossil carbon using radiocarbon analyses during CalNex. J. Geophys. Res.-Atmos. 119, 6818-6835.

List of Publications Produced

So far 20 papers have been published that acknowledge support from this contract, either led or with participation from our group. Papers #1, #21, as well as the completion of #2 represent the main output led by our group with support from this contract. Papers #4, #20, and #23 were also led by our group and mainly supported by other grants, and they were critical to the quantitative interpretation of the CalNex Oxidation Flow Reactor data in paper #21. The rest of the papers acknowledge partial support from this contract, in the sense that this contract kept our group actively thinking about and researching further the CalNex datasets, and allowed us to collaborate effectively in multiple papers let by other groups. Of note is that we have collaborated on multiple SOA modeling papers led by others, including an EPA group (#3 and #22), a NCAR group (#6 and #9), a PNNL group (#7), a Caltech group (#10), a Berkeley group (#16), a UC-Davis consortium (#24), and a Swiss group (#25). Our collaboration on those papers has helped ensure the consistent interpretation of the field data and improved the cross-referencing and comparison of results in the literature. Overall and given the high quality of the papers, we consider this an excellent level of productivity that has been uniquely enabled by this contract.

Peer-Reviewed Publications

(1) P.L. Hayes, A.G. Carlton, K.R. Baker, R. Ahmadov, R.A. Washenfelder, S. Alvarez, B. Rappenglück, J.B. Gilman, W.C. Kuster, J.A. de Gouw, P. Zotter, A.S.H. Prévôt, S. Szidat, T.E. Kleindienst, J.H. Offenberg, and J.L. Jimenez. Modeling the formation and aging of secondary organic aerosols in Los Angeles during CalNex 2010. *Atmospheric Chemistry and Physics*, 15, 5773-5801, doi:10.5194/acp-15-5773-2015, 2015.

(2) P.L. Hayes, A.M. Ortega, M.J. Cubison, W.W. Hu, D.W. Toohey, J.H. Flynn, B.L. Lefer, N. Grossberg, S. Alvarez, B. Rappenglück, J.W. Taylor, J.D. Allan, J.S. Holloway, J.B. Gilman, W.C. Kuster, J.A. de Gouw, P. Massoli, X. Zhang, J. Liu, R.J. Weber, A.L. Corrigan, L.M. Russell, Y. Zhao, S.S. Cliff, G. Isaacman, D.R. Worton, N.M. Kreisberg, S.V. Hering, A.H. Goldstein, R. Thalman, E.M. Waxman, R. Volkamer, Y.H. Lin, J.D. Surratt, T.E. Kleindienst, J.H. Offenberg, K.D. Froyd, S. Dusanter, S. Griffith, P.S. Stevens, J. Brioude, W.M. Angevine, and J. L. Jimenez. Aerosol Composition and Sources in Los Angeles During the 2010 CalNex Campaign. *Journal of Geophysical Research-Atmospheres*, 118, 9233–9257, doi:10.1002/jgrd.50530, 2013.

(3) K.R. Baker, A.G. Carlton, T.E. Kleindienst, J.H. Offenberg, M.R. Beaver, D.R. Gentner, A.H. Goldstein, P.L. Hayes, J.L. Jimenez, J.B. Gilman, J.A. de Gouw, M.C. Woody, H.O.T. Pye, J.T. Kelly, M. Lewandowski, M. Jaoui, P.S. Stevens, W.H. Brune, Y.-H. Lin, C.L. Rubitschun, and J.D. Surratt. Gas and aerosol carbon in California: comparison of measurements and model predictions in Pasadena and Bakersfield. *Atmospheric Chemistry and Physics*, 15, 5243-5258, doi:10.5194/acp-15-5243-2015, 2015.

(4) R. Li, W.H. Brune, B.B. Palm, A.M. Ortega, J. Hlywiak, W. Hu, Z. Peng, D.A. Day, C. Knote, J. de Gouw, and J. L. Jimenez. Modeling the radical chemistry in an Oxidation Flow

Reactor: radical formation and recycling, sensitivities, and OH exposure estimation equation. *Journal of Physical Chemistry A*, 119, 4418–4432, doi:10.1021/jp509534k, 2015.

(5) B. Yuan, P.R. Veres, C. Warneke, J.M. Roberts, J.B. Gilman, A. Koss, P.M. Edwards, M. Graus, W.C. Kuster, S.M. Li, R.J. Wild, S.S. Brown, W.P. Dube, B.M. Lerner, E.J. Williams, J. Johnson, P.K. Quinn, T.S. Bates, B. Lefer, P. Hayes, J.L. Jimenez, R.J. Weber, R. Zamora, B. Ervens, D. Millet, B. Rappenglück, and J.A. de Gouw. Investigation of secondary formation of formic acid: urban environment vs. oil and gas producing region. *Atmospheric Chemistry and Physics*, 15, 1975-1993, doi:10.5194/acp-15-1975-2015, 2015.

(6) C. Knote, A. Hodzic, and J.L. Jimenez. The effect of dry and wet deposition of condensable vapors on secondary organic aerosols concentrations over the continental U.S. *Atmospheric Chemistry and Physics*, 15, 1-18, doi:10.5194/acp-15-1-2015, 2015.

(7) J.D. Fast, J. Allan, R. Bahreini, J. Craven, L. Emmons, R. Ferrare, P. L. Hayes, A. Hodzic, J. Holloway, C. Hostetler, J.L. Jimenez, H. Jonsson, S. Liu, Y. Liu, A. Metcalf, A. Middlebrook, J. Nowak, M. Pekour, A. Perring, L. Russell, A. Sedlacek, J. Seinfeld, A. Setyan, J. Shilling, M. Shrivastava, S. Springston, C. Song, R. Subramanian, J.W. Taylor, V. Vinoj, Q. Yang, R.A. Zaveri, and Q. Zhang. Modeling Regional Aerosol Variability over California and Its Sensitivity to Emissions and Long-Range Transport during the 2010 CalNex and CARES Campaigns. *Atmospheric Chemistry and Physics*, 14, 10013-10060, doi:10.5194/acp-14-10013-2014, 2014.

(8) L.E. Hatch, K.A. Pratt, J.A. Huffman, J.L. Jimenez, and K.A. Prather. Impacts of aerosol aging on laser desorption/ionization in single-particle mass spectrometers. *Aerosol Science and Technology*, 48, 1050-1058, doi:10.1080/02786826.2014.955907, 2014.

(9) C. Knote, A. Hodzic, J.L. Jimenez, R.M. Volkamer, J.J. Orlando, S. Baidar, J. Brioude, J. Fast, D.R. Gentner, A. Goldstein, P.L. Hayes, W.B. Knighton, H. Oetjen, A. Setyan, H. Stark, R. Thalman, G. Tyndall, R. Washenfelder, E. Waxman, and Q. Zhang. Simulation of semi-explicit mechanisms of SOA formation from glyoxal in aerosol in a 3D model. *Atmospheric Chemistry and Physics*, 14, 6213-6239, doi:10.5194/acp-14-6213-2014, 2014.

(10) J.J. Ensberg, P.L. Hayes, J.L. Jimenez, J.B. Gilman, W.C. Kuster, J.A. de Gouw, J.S. Holloway, T.D. Gordon, S. Jathar, A.L. Robinson, and J.H. Seinfeld. Emission Factor Ratios, SOA Mass Yields, and the Impact of Vehicular Emissions on SOA Formation. *Atmospheric Chemistry and Physics*, 14, 2383-2397, doi:10.5194/acp-14-2383-2014, 2014.

(11) B.J. Williams, J.T. Jayne, A.T. Lambe, T. Hohaus, J.R. Kimmel, D. Sueper, W. Brooks, L.R. Williams, A.M. Trimborn, P.L. Hayes, J.L. Jimenez, N.M. Kreisberg, S.V. Hering, D.R. Worton, A.H. Goldstein, D.R. Worsnop. The First Combined Thermal Desorption Aerosol Gas Chromatograph - Aerosol Mass Spectrometer (TAG-AMS). *Aerosol Science and Technology,* 48, 358-370, doi:10.1080/02786826.2013.875114, 2014.

(12) P. Zotter, I. El-Haddad, Y. Zhang, P.L. Hayes, X. Zhang, Y.H. Lin, L. Wacker, J. Schnelle-Kreis, G. Abbaszade, R. Zimmermann, J.D. Surratt, R. Weber, J.L. Jimenez, S. Szidat,

U. Baltensperger, A.S.H. Prévôt. Diurnal cycle of fossil and non-fossil carbon using radiocarbon analyses during CalNex. *Journal of Geophysical Research-Atmospheres*, 119, 6818–6835, doi:10.1002/2013JD021114, 2014.

(13) J.S. Craven, A.R. Metcalf, R. Bahreini, A. Middlebrook, P.L. Hayes, H.T. Duong, A. Sorooshian, J.L. Jimenez, R.C. Flagan, and J.H. Seinfeld. Los Angeles Basin Airborne Organic Aerosol Characterization during CalNex. *Journal of Geophysical Research-Atmospheres*, 118, 11453–11467, doi:10.1002/jgrd.50853, 2013.

(14) R. Holzinger, A.H. Goldstein, P.L. Hayes, J.L. Jimenez, and J. Timkovsky Chemical evolution of organic aerosol in Los Angeles during the CalNex 2010 study. *Atmospheric Chemistry and Physics*, 13, 10125-10141, doi:10.5194/acp-13-10125-2013, 2013.

(15) L.H. Mielke, J. Stutz, C. Tsai, S.C. Hurlock, J.M. Roberts, P.R. Veres, K.D. Froyd, P.L. Hayes, M.J. Cubison, J.L. Jimenez, R.A.Washenfelder, C.J. Young, J.B. Gilman, J. de Gouw, J.H. Flynn, N. Grossberg, B.L. Lefer, J. Liu, R.J. Weber, and H.D. Osthoff. Nocturnal NOx reservoir species during Calnex-LA 2010. *Journal of Geophysical Research-Atmospheres*, 118, 10638–10652, doi:10.1002/jgrd.50783, 2013.

(16) A.W.H. Chan, G. Isaacman, K.R. Wilson, D.R. Worton, C.R. Ruehl, T. Nah, D.R. Gentner, T.R. Dallmann, T.W. Kirchstetter, R.A. Harley, J.B. Gilman, W.C. Kuster, J.A. de Gouw, J.H. Offenberg, T.E. Kleindienst, Y.H. Lin, C.L. Rubitschun, J.D. Surratt, P.L. Hayes, J.L. Jimenez, and A.H. Goldstein. Detailed Chemical Characterization of Unresolved Complex Mixtures in Atmospheric Organics: Insights into Emission Sources, Atmospheric Processing and Secondary Organic Aerosol Formation. *Journal of Geophysical Research-Atmospheres*, 118, 6783–6796, doi:10.1002/jgrd.50533, 2013. Abstract

(17) T.B. Ryerson, A.E. Andrews, W.M. Angevine, T.S. Bates, C.A. Brock, B. Cairns, R.C. Cohen, O.R. Cooper, J.A. de Gouw, F.C. Fehsenfeld, R.A. Ferrare, M.L. Fischer, R.C. Flagan, A.H. Goldstein, J.W. Hair, R.M. Hardesty, C.A. Hostetler, J.L. Jimenez, A.O. Langford, E. McCauley, S.A. McKeen, L.T. Molina, A. Nenes, S.J. Oltmans, D.D. Parrish, J.R. Pederson, R.B. Pierce, K. Prather, P.K. Quinn, J.H. Seinfeld, C.J. Senff, A. Sorooshian, J. Stutz, J.D. Surratt, M. Trainer, R. Volkamer, E.J. Williams, and S.C. Wofsy. The 2010 California Research at the Nexus of Air Quality and Climate Change (CalNex) field study. *Journal of Geophysical Research-Atmospheres*, 118, 5830–5866, doi:10.1002/jgrd.50331, 2013.

(18) F. Mei, P.L. Hayes, A. Ortega, J.W. Taylor, J.D. Allan, J. Gilman, W. Kuster, J. de Gouw, J.L. Jimenez, and J. Wang. Droplet activation properties of organic aerosols observed at an urban site during CalNex-LA. *Journal of Geophysical Research-Atmospheres*, 118, 2903–2917, doi:10.1002/jgrd.50285, 2013.

(19) R.E. O'Brien, T.B. Nguyen, A. Laskin, J. Laskin, P.L. Hayes, S. Liu, J.L. Jimenez, L.M. Russell, S.A. Nizkorodov, A.H. Goldstein. Probing Molecular Associations of Field-Collected and Laboratory-Generated SOA with Nano-DESI High-Resolution Mass Spectrometry. *Journal of Geophysical Research-Atmospheres*, 118, 1042–1051, doi:10.1002/jgrd.50119, 2013.

(20) Z. Peng, D.A. Day, H. Stark, R. Li, B.B. Palm, W.H. Brune, and J.L. Jimenez. HOx radical chemistry in oxidation flow reactors with low-pressure mercury lamps systematically examined by modeling. Atmospheric Measurement Techniques Discussions, 8, 3883-3932, doi:10.5194/amtd-8-3883-2015, 2015.

Publications Undergoing Peer-Review

(21) Ortega, A.M., P.L. Hayes, Z. Peng, B.B. Palm, W. Hu, D.A. Day, R. Li, M.J. Cubison, W.H. Brune, M. Graus, C. Warneke, J.B. Gilman, W.C. Kuster, J. de Gouw, and J.L. Jimenez. Real-time Measurements of Secondary Organic Aerosol Formation and Aging from Ambient Air in an Oxidation Flow Reactor in the Los Angeles Area. *Atmospheric Chemistry and Physics Discussions*, 15, 21907-21958, doi:10.5194/acpd-15-21907-2015, 2015.

(22) M.C. Woody, K.R. Baker, P.L. Hayes, J.L. Jimenez, B. Koo, and H.O.T. Pye. Understanding Sources of Organic Aerosol During CalNex-2010 Using the CMAQ-VBS. Atmospheric Chemistry and Physics Discussions, 15, 26745-26793, doi:10.5194/acpd-15-26745-2015, 2015.

(23) Z. Peng, D.A. Day, A.M. Ortega, B.B. Palm, W. Hu, H. Stark, R. Li, K. Tsigaridis, W.H. Brune, and J.L. Jimenez. Non-OH chemistry in oxidation flow reactors for the study of atmospheric chemistry systematically examined by modeling Atmospheric Chemistry and Physics Discussions, 15, 23543-23586, doi:10.5194/acpd-15-23543-2015, 2015.

(24) C.D. Cappa, S. Jathar, M.J. Kleeman, K.S. Docherty, J.L. Jimenez, J.H. Seinfeld, A. Wexler. Simulating Secondary Organic Aerosol in a Regional Air Quality Model Using the Statistical Oxidation Model: 2. Assessing the Influence of Vapor Wall Losses. Atmospheric Chemistry and Physics Discussions, 15, 30081-30126, doi:10.5194/acpd-15-30081-2015, 2015.

Publications To-Be-Submitted Shortly

(25) S.M. Platt, I. El Haddad, S.M. Pieber, A.A. Zardini, R. Suarez-Bertoa, M. Clairotte, K. Dällenbach, R.J. Huang, J.G. Slowik, S. Hellebust, B. Temime-Roussel, J. de Gouw, N. Marchand, C. Astorga, J.L. Jimenez, P.L. Hayes, A.L. Robinson, U. Baltensperger, and A.S.H. Prévôt. Passenger car carbonaceous particulate pollution increasingly dominated by gasoline, not diesel. In preparation, 2015.

Appendix A: Additional Information Used for SOA Modeling

Table A-1. VOC parameters used to model the formation of SOA (Atkinson and Arey, 2003; Carter, 2010; Tsimpidi et al., 2010). All aging of VOCs after the initial oxidation reaction occurs with a gas-phase rate constant of $k_{OH} = 1 \times 10^{-1}$ cm^{-1} molec^{-1} s^{-1}. Note that the aging rate constant was erroneously reported in Tsimpidi et al. All SOA from VOCs has a ΔH_{vap} of 36 kJ mol^{-1} (Volkamer et al., 2006).

Precursor Family Name	**Compounds**	k_{OH} (cm^3 molec^{-1} s^{-1})	**ΔVOC/ΔCO (ppt ppb^{-1})**	**Stoichiometric SOA yield High-NO_X, 298 K, (μg m^{-3})**				M.W. (g mol^{-1})
				1	10	100	1000	
ALK5	Methylcyclopentane	5.68×10^{-12}	0.566	0.000	0.015	0.000	0.000	150
	Cyclohexane	6.97×10^{-12}	0.285					
	Methylcyclohexane	9.64×10^{-12}	0.202					
	n-Heptane	6.76×10^{-12}	0.398					
	2-Methyl Hexane	6.89×10^{-12}	0.385					
	3-Methyl Hexane	7.17×10^{-12}	0.460					
	2,3-Dimethyl Pentane	7.15×10^{-12}	0.252					
	2,4-Dimethyl Pentane	4.77×10^{-12}	0.171					
	2,2,3-Trimethyl Butane	3.81×10^{-12}	0.031					
	N-Octane	8.11×10^{-12}	0.197					
	3-Methyl Heptane	8.59×10^{-12}	0.131					
	2-Methyl Heptane	8.31×10^{-12}	0.171					
	2,2,4-Trimethyl Pentane	3.34×10^{-12}	0.476					
	2,3,4-Trimethyl Pentane	6.60×10^{-12}	0.171					
	2,3,3-Trimethyl Pentane	4.40×10^{-12}	0.194					
	N-Nonane	9.70×10^{-12}	0.220					
	N-Decane	11.0×10^{-12}	0.180					
	Undecane	12.3×10^{-12}	0.290					

Table A-1. (continued).

Precursor Family Name	**Compounds**	k_{OH} **(cm^3 $molec^{-1}$ s^{-1})**	**ΔVOC/ΔCO (ppt ppb^{-1})**	**Stoichiometric SOA yield High-NO_X, 298 K, (μg m^{-3})**				Molecular Weight (g mol^{-1})
				1	10	100	1000	
OLE1	Propene	26.3×10^{-12}	3.740	0.001	0.005	0.038	0.150	120
	1-Butene	31.4×10^{-12}	0.340					
	1-Pentene	31.4×10^{-12}	0.112					
	2-methyl-1-butene	61.0×10^{-12}	0.250					
	3-methyl-1-butene	31.8×10^{-12}	0.058					
OLE2	1,3-Butadiene	66.6×10^{-12}	0.350	0.003	0.026	0.083	0.27	120
	trans-2-Pentene	67.0×10^{-12}	0.097					
	cis-2-Pentene	65.0×10^{-12}	0.050					
	Styrene	58.0×10^{-12}	0.220					
ARO1	Toluene	5.63×10^{-12}	3.180	0.003	0.165	0.300	0.435	150
	Ethylbenzene	7.00×10^{-12}	0.570					
	i-Propylbenzene	6.30×10^{-12}	0.030					
	n-Propylbenzene	5.80×10^{-12}	0.110					
	Benzene	1.22×10^{-12}	1.300					
ARO2	o-Ethyltoluene	9.57×10^{-12}	0.120	0.002	0.195	0.300	0.435	150
	1,2,3-Trimethylbenzene	11.9×10^{-12}	0.240					
	1,2,4-Trimethylbenzene	32.7×10^{-12}	0.620					
	1,3,5-Trimethylbenzene	32.5×10^{-12}	0.310					
	m-xylene	56.7×10^{-12}	1.790					
	p-xylene	23.1×10^{-12}	1.790					

Table A-1. (continued).

Precursor Family Name	**Compounds**	k_{OH} **(cm^3 $molec^{-1}$ s^{-1})**	**ΔVOC/ΔCO (ppt ppb^{-1})**	**Stoichiometric SOA yield High-NO_X, 298 K, (μg m^{-3})**				Molecular Weight ($g\ mol^{-1}$)
				1	10	100	1000	
NAPH	Naphthalene	24.4×10^{-12}	0.065	0.165	0.005	0.516	0.881	150
	1-Methylnaphthalene	40.9×10^{-12}	0.01					
	2-Methylnaphthalene	48.6×10^{-12}	0.021					
ISOP	Isoprene (Anthropogenic)	100×10^{-12}	N/A (see text)	0.001	0.023	0.015	0.000	136
	Isoprene (Biogenic)	100×10^{-12}	N/A (see text)					
TERP	α-Pinene + β-Pinene + Limonene	98.2×10^{-12}	N/A (see text)	0.012	0.122	0.201	0.5	180

Table A-2. Summary of the Robinson et al. (2007) and the Grieshop et al. (2009) parameterizations for P-S/IVOCs.

c^* @ 300 K ($\mu g\ m^{-3}$)	ΔH_{vap} ($kJ\ mol^{-1}$)		Molecular Weight ($g\ mol^{-1}$)		Fraction of total P-S/IVOC (%)
ROB & GRI	ROB	GRI	ROB	GRI	ROB & GRI
0.01	112	77	250	524	1.2
0.1	106	73	250	479	2.4
1	100	69	250	434	3.6
10	94	65	250	389	5.6
100	88	61	250	344	7.2
1,000	82	57	250	299	12
10,000	76	54	250	254	16
100,000	70	50	250	208	20
1,000,000	64	46	250	163	32

	ROB	GRI
k_{OH} at 300 K ($cm^3\ molec^{-1}\ s^{-1}$)	4×10^{-11}	2×10^{-11}
Oxygen gain per oxidation generation (%)	7.5	40
Volatility bin decrease per oxidation generation	1 order of magnitude	2 orders of magnitude

Table A-3. Initial concentrations of primary IVOCs predicted by the box model (ROB parameterization) in comparison with data from Zhao et al. (2014) as a function of the saturation concentration (C*) at 298 K. Note that the corresponding results for the GRI parameterization are very similar with the concentration being 8% higher due to differences in the ΔH_{vap}.

C* (µg m^{-3})	**Estimated Primary IVOCs (µg m^{-3})**	**Estimated Primary IVOCs without cooking emissions (µg m^{-3})**	**Measured Primary IVOCs (µg m^{-3})**
10^3	2.47	1.70	0.21 (± 0.07)
10^4	3.30	2.27	1.39 (± 0.29)
10^5	4.12	2.84	2.64 (± 0.64)
10^6	6.59	4.54	3.82 (± 0.99)

Table A-4. Summary of tracers used by the EPA group to determine the concentration of SOA from a certain precursor.

Tracer Molecule	**Precursors**	**Reference**
2-Methylglyceric acid	Isoprene	Edney et al. *Atmos. Environ.* 2005, 5281-5289.
2-Methylthreitol	Isoprene	Edney et al. *Atmos. Environ.* 2005, 5281-5289.
2-Methylerythritol	Isoprene	Edney et al. *Atmos. Environ.* 2005, 5281-5289.
3-Acetyl pentanedioic acid	Monoterpenes	Jaoui et al. *Environ. Sci. Technol.* 2005, 5661-5673.
3-Acetyl hexanedioic acid	Monoterpenes	Jaoui et al. *Environ. Sci. Technol.* 2005, 5661-5673.
3-Methyl-1,2,3-butanetricarboxylic acid	Monoterpenes	Szmigielski et al. *J. Geophys. Res.-Atmos.* 2007, L24811.
3-Hydroxyglutaric acid	Monoterpenes	Claeys et al. *Environ. Sci. Technol.* 2005, 1628-1634.
3-Hydroxy-4,4-dimethylglutaric acid	Monoterpenes	Claeys et al. *Environ. Sci. Technol.* 2005, 1628-1634.
Pinic acid	Monoterpenes	Claeys et al. *Environ. Sci. Technol.* 2005, 1628-1634.

Appendix B: Quantification of AMS Reactor Data

All aspects of quantification of AMS data are the same as described by Hayes et al. (2013). Here we describe only those aspects where additional analysis or corrections are needed specifically for the reactor output data.

B.1. AMS Collection Efficiency

Quantification of AMS concentration data requires a correction for particle bounce at the vaporizer, referred to as the collection efficiency (CE; Canagaratna et al., 2007). The composition-dependent CE formulation of Middlebrook et al. (2012) was used by Hayes et al. (2013) to estimate CE for the ambient data, leading to good intercomparisons with multiple collocated instruments as documented by that study. The same methodology has also been applied to reactor output measurements.

Fig. B-1a shows the time series of reactor and ambient aerosol concentrations and estimated CE. Ambient CE periodically rises above 0.5 due to larger fractions of ammonium nitrate aerosol, which leads to reduced particle bounce (Middlebrook et al., 2012). The reactor typically formed additional ammonium sulfate and ammonium nitrate beyond ambient concentrations at the same time as ambient levels peak for those compounds, thus the reactor CE profile has a very similar temporal structure to ambient. However, Fig. B-1b shows that the estimated CE increases at the highest reactor OH_{exp}, due to additional ammonium nitrate formation in the reactor with increased photochemical age.

Figure B-1. *(a) Estimated AMS collection efficiency (CE) and corresponding AMS mass concentration time series for ambient and reactor data (after applying CE correction). (b) Estimated CE vs. OH exposure (OH_{exp}) in the reactor for all reactor measurements and averages for 7% quantiles.*

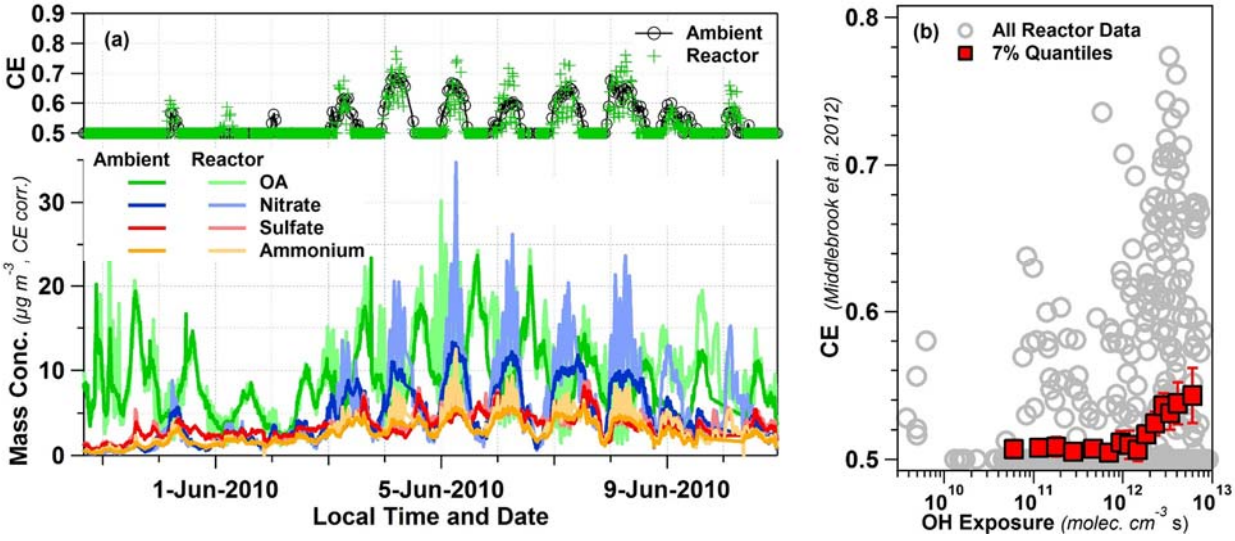

Highly acidic particles, as indicated by the ammonium balance, can also lead to increased CE in the AMS (Middlebrook et al., 2012). The ammonium balance method compares the measured ammonium to that required to fully neutralize observed sulfate, nitrate, and chloride (Zhang et al., 2007), as shown in Fig. B-2. Ambient and reactor results have near identical slopes

that are indistinguishable from the one-to-one line within the uncertainties of the measurements, signifying full neutralization for both. Furthermore, this comparison indicates that the reactor is producing similar inorganic composition to that observed in the atmosphere as nitric acid and sulfuric acid gases are formed in the reactor and fully neutralized by ammonium forming ammonium nitrate and ammonium sulfate. Thus no correction of CE due to the presence of highly acidic particles are needed in this study.

Figure B-2.*Measured vs. predicted ammonium assuming full neutralization ("Ammonium balance") for ambient and reactor data. Linear orthogonal distance regression fit lines, slope and R^2 for each are also shown.*

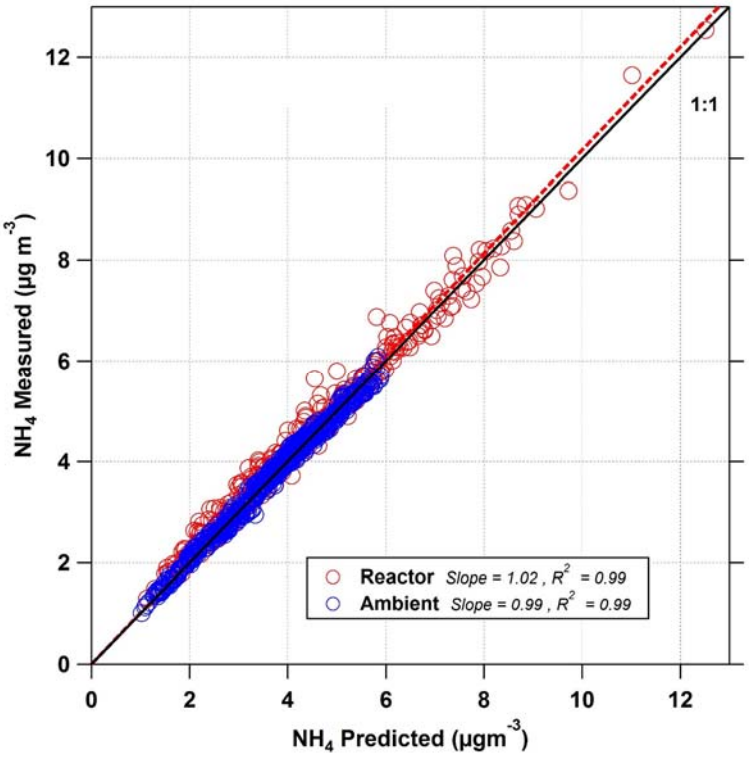

Comparison of AMS and SMPS measurements for ambient and reactor data, shows that ambient data falls along a one-to-one line, indicating both instruments are measuring the same amount of mass within the uncertainties (Fig. B-3a). Reactor output data has a slightly higher slope of 1.14, i.e. the AMS measures ~14% higher mass than the SMPS from the reactor and also shows a cluster of points where SMPS>AMS due to periods where substantial mass is formed at small particle sizes (see below). Both slopes are within the combined uncertainties of the two measurements. Fig. B-3b shows the relative increase in aerosol concentration in the reactor (i.e. ratio of reactor to ambient concentrations) for the SMPS vs. AMS which also compare well, on average (slope = 1.05), but with considerable scatter, most of which is likely due to additional measurement noise introduced from ratioing multiple short measurements. Evaporation of freshly formed NH_4NO_3 in the longer residence times in the SMPS (compared to the faster AMS analysis) where the sheath flow may have reduced NH_3 and HNO_3 gas concentrations, has been observed with this experimental setup, and may be a cause of the slightly larger slope for reactor

output conditions. An small underestimation of AMS CE for the reactor conditions could also result in this observation.

Figure B-3. (a) *Scatter plot of AMS mass vs. mass estimated from SMPS measurements for ambient and reactor data, with linear orthogonal distance regression fit slope and R^2 for each. A one-to-one line and +/-15% region is shown for reference.* ***(b)*** *Relative enhancement ratio from AMS and SMPS data with raw data, 20-minute averaged smooth data, linear orthogonal distance regression, line, fit slope and R^2 for each.*

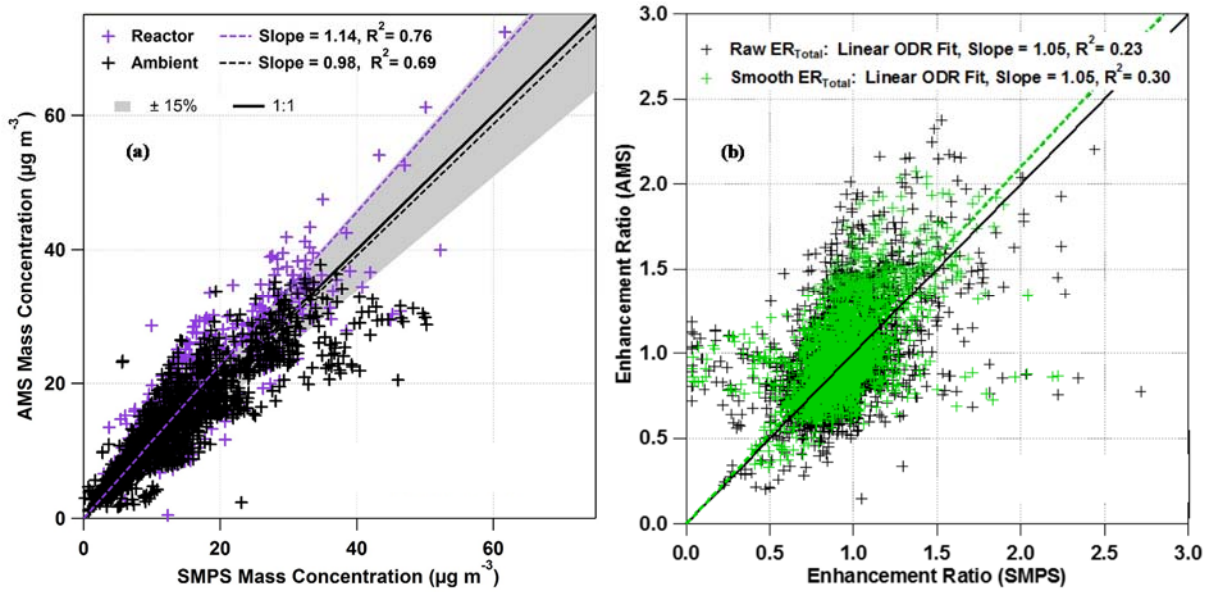

Figure B-4. *Estimated particle transmission of inlet plumbing vs. particle diameter for reactor and ambient sampling lines for both AMS and SMPS measurements, calculated using the particle loss calculator of von der Weiden et al. (2009).*

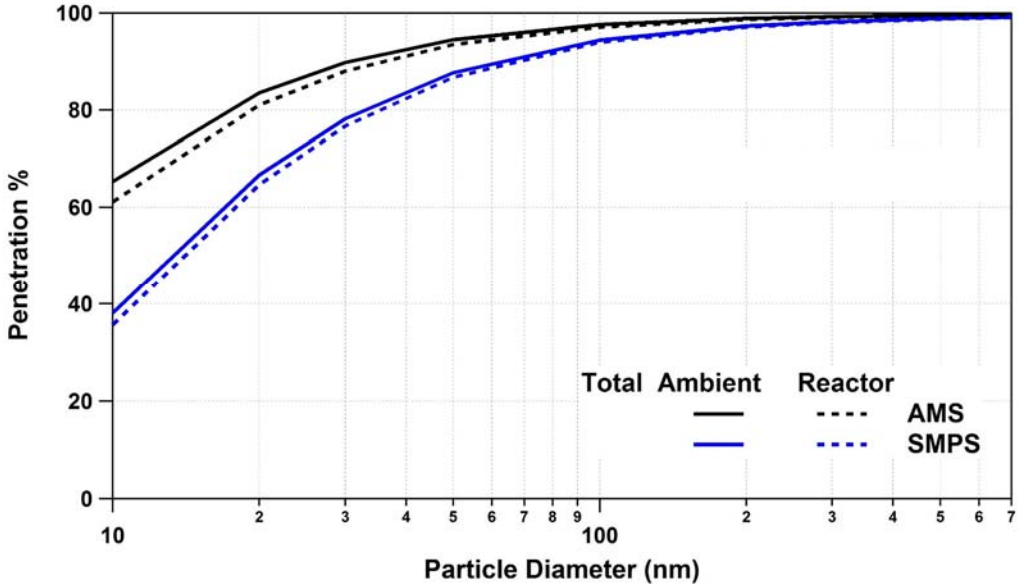

Figure B-5. (a) *Time series of SMPS mass measured below the AMS lens transmission size for ambient and reactor measurements.* ***(b)*** *Percent of estimated mass not measured by AMS, due to on particle losses in sampling lines and the AMS lens transmission at small sizes, for the reactor vs. total photochemical age in days (at OH = 1.5×10^6 molec. cm^{-3}), where all data is colored by ΔOA mass with average 5% quantiles and standard error bars.*

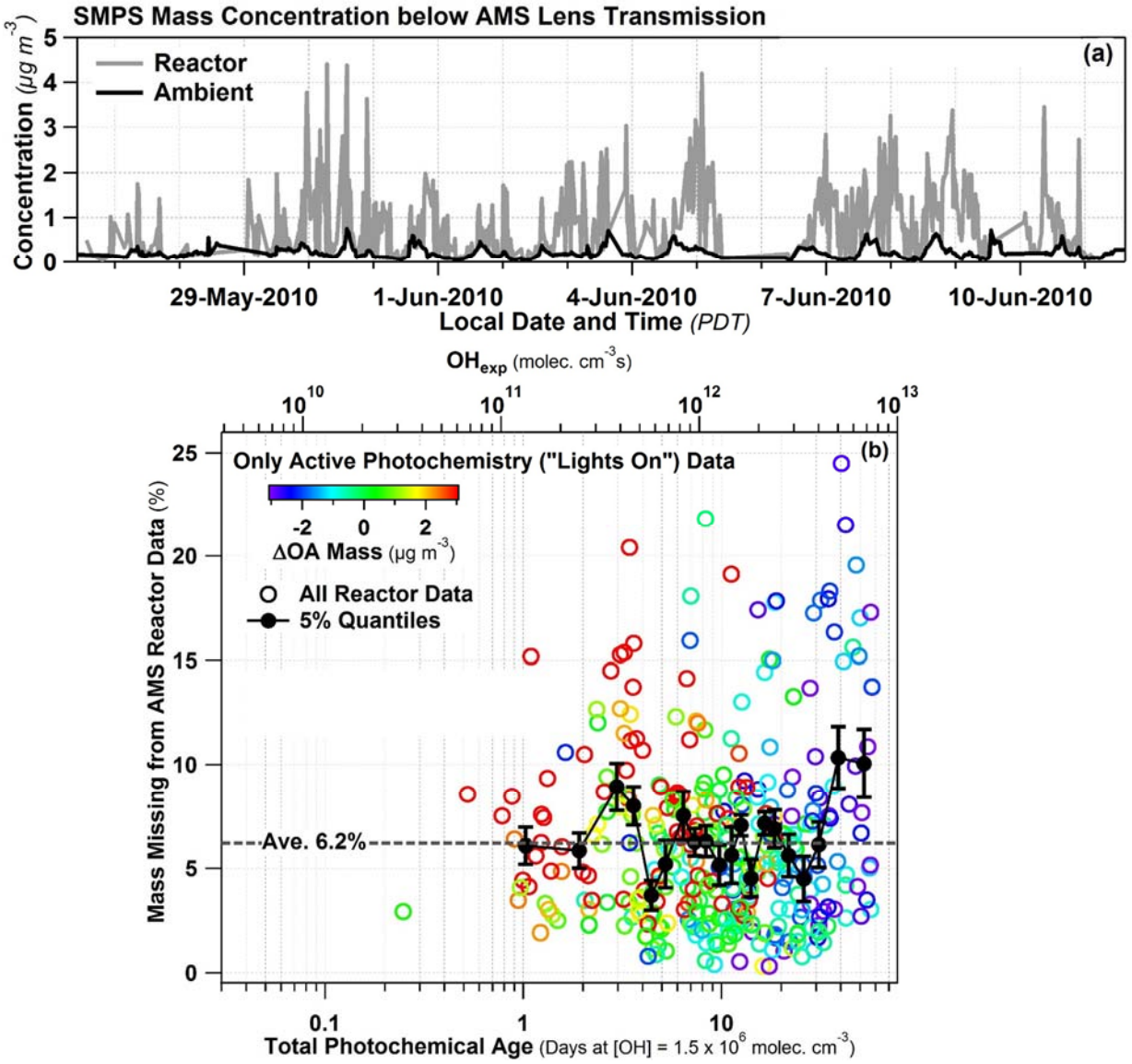

B.2. Accounting for Particle Mass below the AMS Lens Transmission

As the reactor exposed ambient air to high levels of OH and O_3, new particle formation and growth was sometimes observed. To fully account for the mass of all particles formed in the reactor, it is necessary to quantify the mass of small particles below the AMS lens transmission size (Zhang et al., 2004). SMPS data was used to estimate the total mass concentration below the AMS size cut. First, particle transmission from plumbing line losses was corrected using the Particle Loss Calculator (von der Weiden et al., 2009) for this experimental plumbing and flowrate configuration for both reactor and ambient SMPS data, with transmission curves as

shown in Fig. B-4. Second, the measured SMPS mass that is below the AMS transmission curve was estimated using a published AMS lens transmission parameterization (Knote et al., 2011) multiplying the SMPS size-dependent mass by the size-dependent AMS lens fractional loss (1-transmission). Figure B-5a shows a time series of estimated reactor and ambient mass missed by the AMS due to transmission losses. Since corrections needed to account for the contribution of these small sizes to total mass is small for ambient data (on average 1.7%), Hayes et al. (2013) did not apply a correction to AMS ambient data. Fig. B-5b shows the estimated fraction of the reactor output mass that is below the AMS lens transmission size vs. total photochemical age in days (at OH = 1.5×10^6 molec. cm^{-3}). An average of 6.2% of the total reactor output mass is estimated to be below the AMS lens transmission, with no dependence on photochemical age except possibly at the highest values (>20 days of age).

We note that the AMS measurements from the reactor may be biased ~6% low, on average, and sometimes as much as 20%. This non-measured mass likely has a large OA fraction (see Fig. 27). Thus, reactor-reported mass enhancement above ambient may be underestimated by these amounts. Given the 6.2% AMS underestimation from particle transmission of small sizes in the reactor, and the apparent 14% overestimation in the AMS vs SMPS comparison, but overall good agreement in the relative enhancement of total aerosol between both instruments, we have not corrected for these differences as the net correction would be small and within the uncertainties of the measurement, while the correction process would introduce additional noise.